The Thesis Committee for Konstantinos Victor Belivanis
Certifies that this is the approved version of the following thesis:

Assessment of Remaining Fatigue Performance of High Mast Illumination Poles

APPROVED BY
SUPERVISING COMMITTEE:

Supervisor:

Todd A. Helwig

Michael D. Engelhardt

Assessment of Remaining Fatigue Performance of High Mast Illumination Poles

by

Konstantinos Victor Belivanis, D.C.E.

Thesis

Presented to the Faculty of the Graduate School of

The University of Texas at Austin

in Partial Fulfillment

of the Requirements

for the Degree of

Master of Science in Engineering

The University of Texas at Austin

May 2014

Dedication

To my family…

«Ο σωστός δρόμος είναι ο ανήφορος»

Νίκος Καζαντζάκης

(The right way is the uphill)

Nikos Kazantzakis

Acknowledgements

First and foremost, I would to express my gratitude to Dr. Helwig for giving me the chance to participate in this research program. His trust in me, a new student in the graduate program, helped me to familiarize with new aspects of structural engineering and to get involved in the great community of the Ferguson Structural Engineering Laboratory.

I also want to express my deep appreciation to Dr. Frank. Despite his retirement from The University of Texas, he was always willing to be at the lab for endless talks about cracking in steel and innovations in the art of construction. The efficiency with which he communicated concepts, previously unknown to me, makes him stand out of every professor I have met. Furthermore, I would like to thank Dr. Engelhardt for serving as a second reader and being always available for discussion.

Nothing written in the next pages could not have been done without the help of two exceptional technical assistants I was lucky to work with. This is why I want to thank Andrew Valentine and Blake Stasney for the invaluable help in building and repairing the test setup I used.

Last but not least, I would like to thank the many exceptional characters I met at Ferguson Lab. First, Vasilis Samaras for being a rock support, motivating me when needed, and helping adjusting so fast in the lab. Jeremiah Fasl for the help with instrumentation and for being the "old and wise" of the lab. Michalis Hadjioannou for borrowing me his desk during the first year. Jose Gallardo, Jaime Barredo, Eulalio Fernandez, Hemal Patel, Hossein Yousefpour, and Joel Blok for making my lab hours an unforgettable experience. I am sure I am forgetting someone, and I am really sorry about it.

Abstract

Assessment of Remaining Fatigue Performance of High Mast Illumination Poles

Konstantinos Victor Belivanis, M.S.E.
The University of Texas at Austin, 2014

Supervisor: Todd A. Helwig

Failures of high mast illumination poles (HMIP) around the US have raised the concerns of officials because of their location close to areas with important human activity. Previous research, conducted at the University of Texas proved that those failures were fatigue type failures and that cracking initiated at the shaft to baseplate connection, specifically at the bends of the shaft. However, no research has been conducted on the remaining fatigue life of poles after they have been in service. This thesis investigates the remaining fatigue life of a pole, removed from service after severe cracking has been observed on it, via laboratory testing. Moreover, nondestructive and destructive testing procedures were implemented to investigate the initiation and evolution of fatigue cracks. The results validated the procedures for the in-situ validation of the remaining fatigue life of those poles. Last, the destructive test results enhanced the arguments that initial cracking at the toe of the weld at the shaft to baseplate connection is a result of the galvanizing process.

Table of Contents

List of Tables

List of Figures

CHAPTER 1: INTRODUCTION

1.1 Introduction

High mast illumination poles (HMIPs) are frequently used in transportation applications to provide lighting around highway intersections in urban environments. A typical application is shown in Figure 1.1. The heights of the poles vary in height, but may reach as high as 180 ft. in some applications.

Figure 1.1: High Mast Illumination Pole in service at highway intersection

The poles are often multi-sided hollow steel sections that are tapered along the height of the poles. Because the poles can be relatively long, to accommodate shipping and erection the HMIP usually consists of multi-stage poles where lower stages nest inside

higher stages, which results in relatively efficient connections along the length of the pole. The lower section of the pole must connect to a foundation which is typically fabricated from concrete with threaded rods to anchor the HMIP to the ground. As a result, the lower section of the pole typically consists of the hollow shaft connected to a relatively thick base plate through which the anchor bolts pass through. A typical base plate connection is shown in Figure 1.2.

Figure 1.2: Typical base plate connection

While HMIPs have been frequently used throughout the transportation network, in recent years there have been a number of issues with the connections between the poles and the foundations. There have been instances where fatigue cracks have grown while the poles are in service that have resulted in the collapse of the pole, which obviously can pose a dangerous condition for the travelling public. In addition to failures of the HMIPs, there have also been a number of poles in which significant cracking has been identified between

the pole shaft and the base plate. These past studies have focused on the cause of the cracking as well as methods of predicting the long-term fatigue life. In many instances, the cracking often occurs during the fabrication process, which includes galvanizing the poles to improve the long-term corrosion resistance. However, while many of these studies have focused on the source of the cracking, there are not clear guidelines on the impact of the cracking on the long-term fatigue life of these poles.

The research outlined in this thesis is focused on measuring the remaining fatigue performance of the shaft-to-baseplate connection used in an in-service high mast illumination pole. A severely damaged HMIP pole was removed in service (Figure 1.3) and subjected to laboratory testing to assess the remaining fatigue life. The remaining fatigue life was evaluated using the results of full scale experimental testing as developed in previous phases of this study at The University of Texas at Austin.

Figure 1.3: HMIP taken out of service

Finite element modeling was used to investigate the impact of the geometry of the connection on the crack growth. Results were correlated with measurements obtained from strain gages in the locations of interest.

Apart from studying the previously-in-service HMIP, the behavior of a connection repaired and using ultrasonic impact treatment (UIT) was observed and conclusions on the repair method were drawn. A definition of the problem is provided in the next section, followed by an overview of the thesis.

1.2 Problem description and objective

During the previous Phases of this study details suitable for HMIP base plate connections for newly-fabricated poles were proposed. However, what remained unanswered was the impact on the fatigue performance of cracks that existed between the base plate and shaft of in-service HMIPs with older connection details. The objective of the current thesis is provide an overview of laboratory tests on an HMIP removed from service to investigate the long-term fatigue performance. The results from these tests can be compared with estimates on the fatigue life that have been made from field studies on the pole in previous studies.

1.3 Thesis scope and organization

The thesis is organized in 5 chapters including this introductory overview. Chapter 2 provides an extensive literature review of the research that has been conducted at The University of Texas for high mast illumination poles and shorter luminaire highway structures. Chapter 3 details the destructive and non-destructive experimental procedures followed in this testing program. Chapter 4 outlines results obtained by both the destructive

and non-destructive tests and tries to perform some correlation with finite element studies. Also, it provides some tools for HMIP service inspectors. Chapter 5 provides a summary of observation and results and concludes with recommendation for future work.

CHAPTER 2: BACKGROUND INFORMATION

2.1 Introduction

Failures of high mast illumination poles (HMIP) in the US have raised concerns that the current design provisions/fabrication practices have potentially led to problematic behavior that is not well understood with regards to performance. Many of the concerns were related in the lack of understanding of the fatigue performance of the poles. Due to concerns on the safety of the public as well as evaluating the lives of the HMIP inventory, the Texas Department of Transportation (TxDOT) sponsored a research at the University of Texas at Austin to address the design concerns and to better understand the in-service behavior of HMIP. Based upon previous work that was conducted as part of this research program it was concluded that the previous HMIP failures were associated with fatigue. Also, it was observed that cracking initiated at the shaft to base plate connection, and specifically at the bends of the shaft. Initial research phases included full scale laboratory testing and parametric finite element analytical (FEA) studies. The results of the first research phase were utilized to developed design recommendations for improving the fatigue performance of the HMIPs.

The second phase of the research focused on verifying the design recommendations by conducting laboratory tests on HMIP. Full scale tests showed substantial differences in the fatigue performance between the initial analytical models and tests. The main source of this inconsistency was found to be the cracking at the base of the poles that were initiated during the galvanizing process.

The later phases of the research focused on the evaluation of the performance of the poles during the galvanizing process and of the HMIP in-service field response to wind loads. The goals for the later phases of the research was to provide a better understanding of the condition of the pole before and while in service and to develop recommendations for mitigating the cracking during the galvanizing process.

This chapter summarizes the results from past studies on the fatigue performance of the base connections of HMIP systems. In addition, the theory of an ultrasonic impact treatment as a repair technique for cracked HMIP shaft to base plate connections is also discussed.

2.2 University of Texas Research (Phases I – V)

2.2.1 PHASE I –RESEARCH

The results from the first phase of the research conducted at the University of Texas at Austin are summarized by Rios (2007) who presented test results for sixteen HMIP specimens. The variables tested were the connection detail, the base plate thickness and the number of holes equally spaced in a circular pattern at the base plate. The variables kept constant were the pole diameter (24-inch pole diameter was used), the wall thickness (5/16-inch) and the pole taper angle (0.14-inches/foot). The taper angle is based upon reducing the likelihood of vortex shedding effects as outlined in AASHTO Section 11.7.2 (REFERENCE). The basic geometry of the specimen is depicted in Figure 2.1.

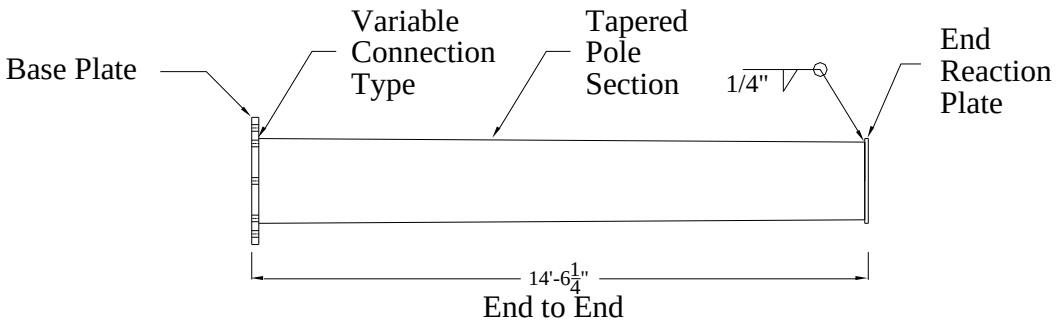

Figure 2.1: Test Specimen Fabrication Drawing (Rios, 2007)

Three different connection details were tested representing the wide range of the base plate to shaft connections that are used throughout the US. The following three subsections provide an overview of the connections that were tested.

2.2.1.1 Fillet Welded Socket Connection

The fillet welded socket connection detail consists of a connection in which the pole shaft is inserted into a hole in the base plate. The shaft is welded to the base plate with an unequal fillet weld around the outside of the shaft wall and a seal weld is made around the interior of the base plate hole. The fillet welded socket connection details are depicted in Figure 2.2 and Figure 2.3.

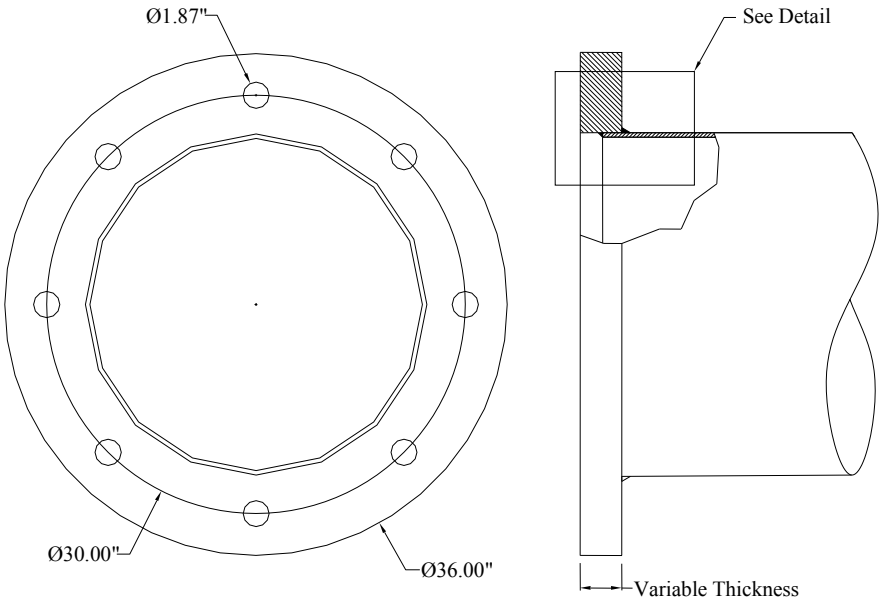

Figure 2.2: Fillet Welded Socket Connection Detail (Rios, 2007)

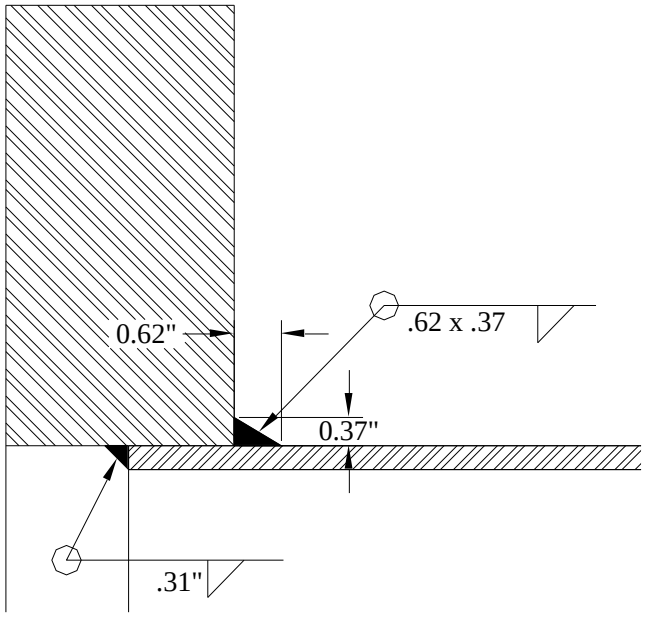

Figure 2.3: Socket Connection Weld Detail (Rios, 2007)

2.2.1.2 Full Penetration Welded Connections (Texas and Wyoming details)

Rios conducted tests with two variations of full penetration welded connections. One variation included a back-up ring similar to the design used by the Wyoming department of transportation. The Wyoming connection details are shown in Figure 2.4 and Figure 2.5.

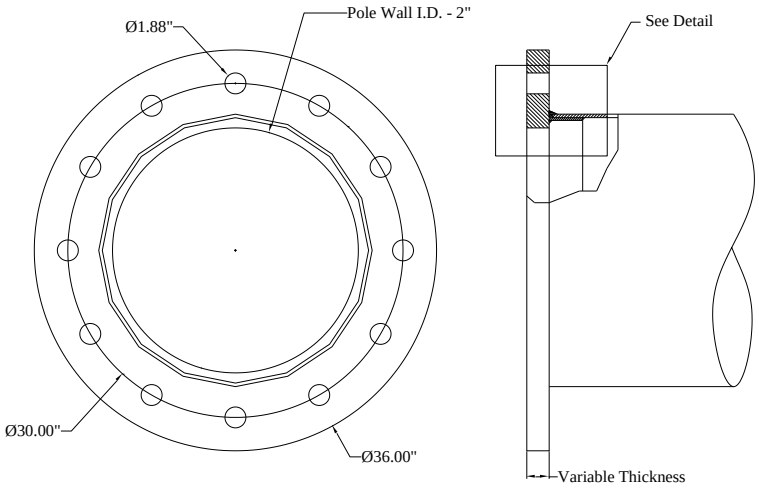

Figure 2.4: Wyoming Connection Detail (Rios, 2007)

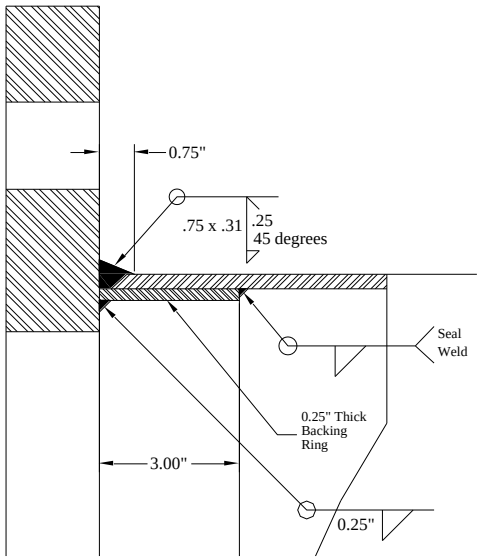

Figure 2.5: Wyoming Connection Weld Detail (Rios, 2007)

The other detail was based upon the connection details used by TxDOT and are shown in Figure 2.6 and Figure 2.7. Although there are some differences in the weld sizes for the base plate to shaft, the big difference between the Wyoming and Texas details are the backup ring that is used in the Wyoming detail.

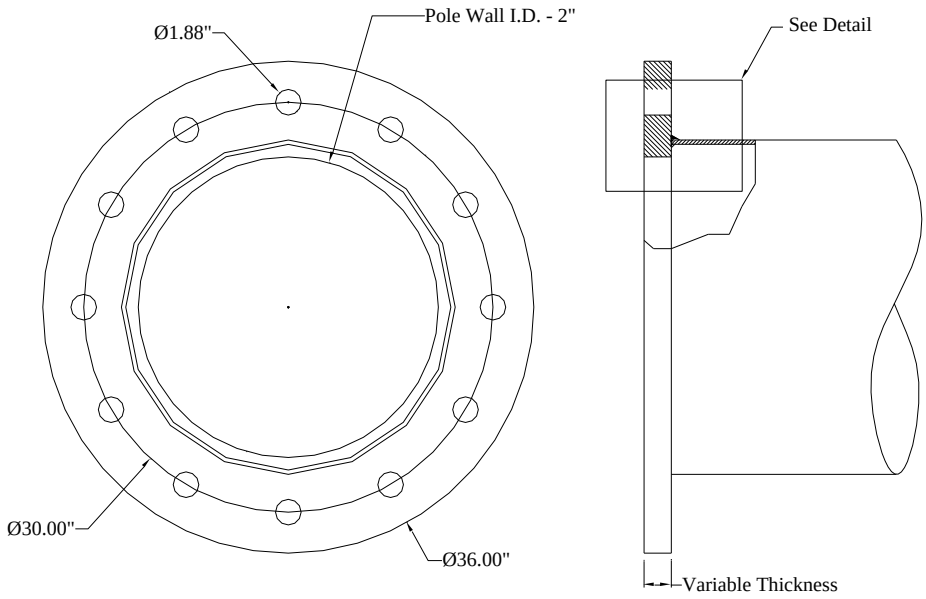

Figure 2.6: Texas Connection Detail (Rios, 2007)

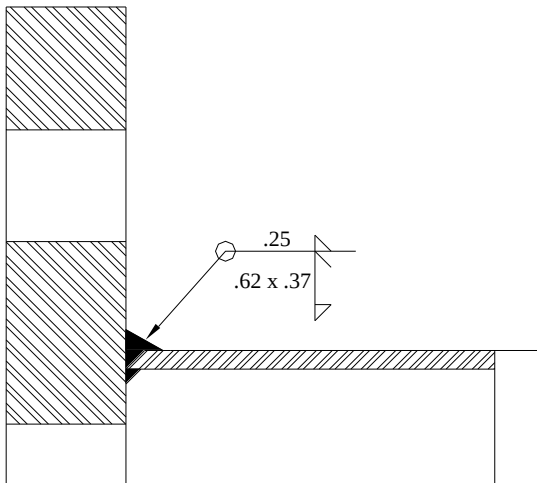

Figure 2.7: Texas Connection Weld Detail (Rios, 2007)

2.2.1.3 Stool Base Detail

The last detail that was tested by Rios is the stool base detail connection that used vertical stiffener plates in conjunction with a cap plate. The whole setup is welded to the shaft of the pole and the base plate providing a stiffened connection. The stool base details are shown in Figure 2.8 and Figure 2.9.

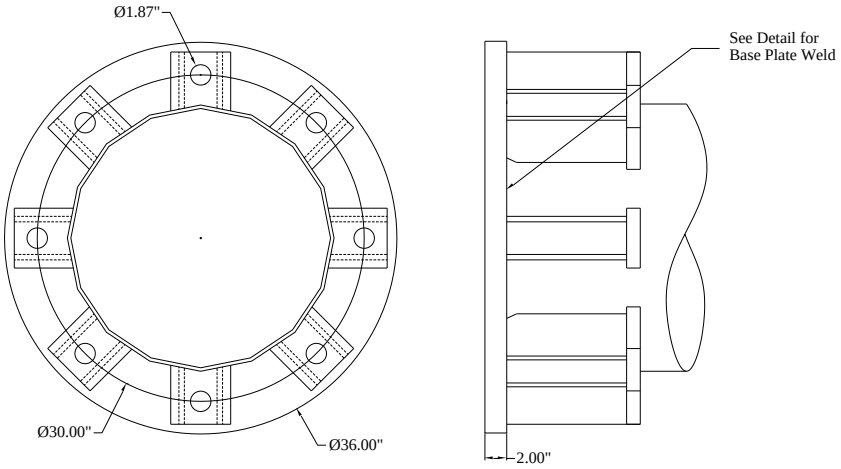

Figure 2.8: Stool Base Connection Detail (Rios, 2007)

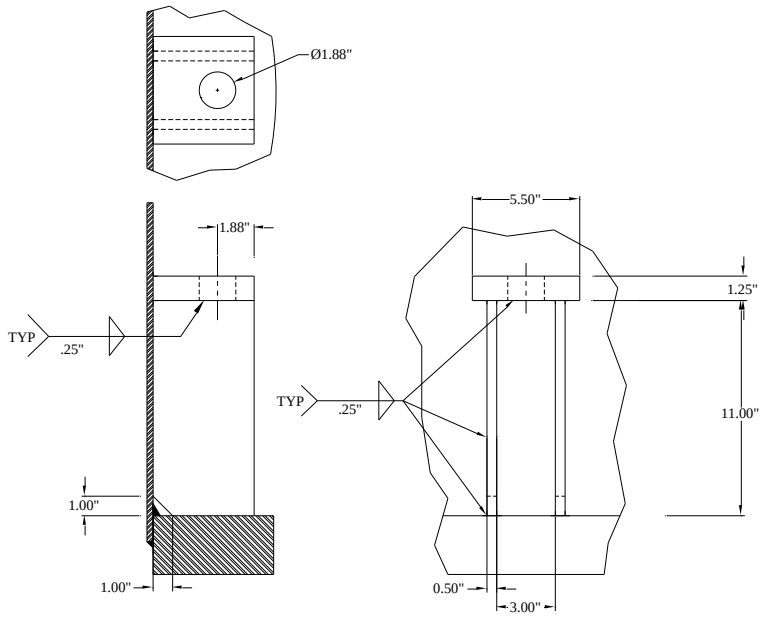

Figure 2.9: Stool Chair Detail (Rios, 2007)

2.2.1.4 Naming Scheme

In order to associate each pole with a unique label the naming scheme shown in Figure 2.10 was developed.

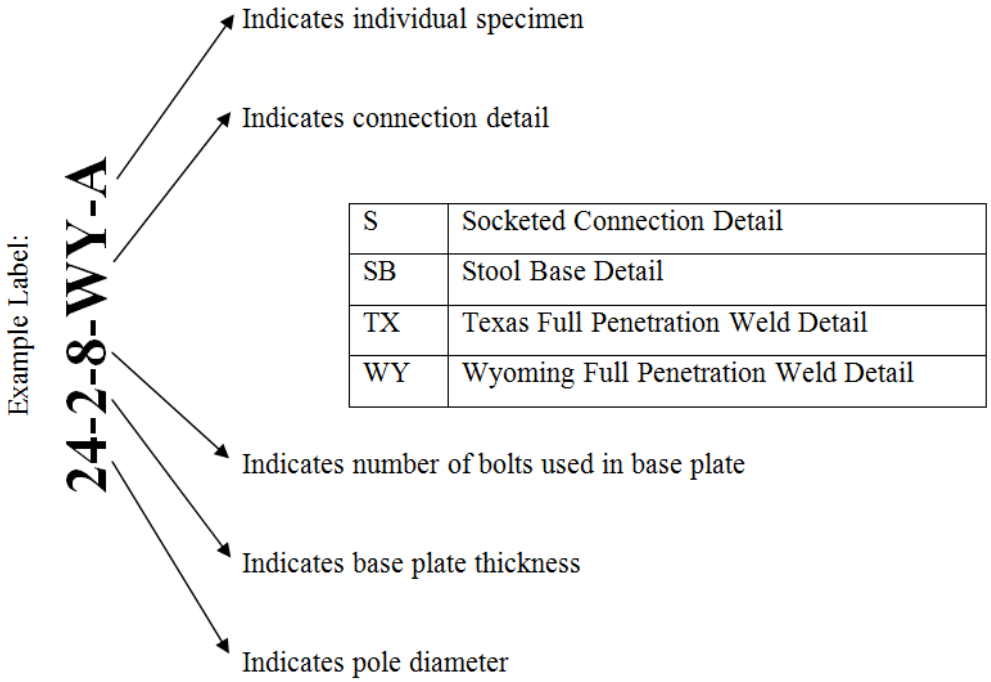

S	Socketed Connection Detail
SB	Stool Base Detail
TX	Texas Full Penetration Weld Detail
WY	Wyoming Full Penetration Weld Detail

Figure 2.10: Naming Scheme of HMIP test specimens (Rios, 2007)

2.2.1.5 Testing Procedure

The test setup that was used in the fatigue tests at the University f Texas consisted of two pole sections coupled at the base plate to a stiff loading box. Supports at the ends consisted of a pin connection and a roller connection. The system behaved as a beam with pinned ends. An upward load was applied to the load box with an MTS hydraulic actuator (55 kip capacity) placed in a loading frame as shown in Figure 2.11.

The main benefit of this test setup was the simultaneous testing of two specimens with the same nominal stress range. The main drawbacks were the lack of direct information on where the fatigue damage is concentrated and the inability of stress reversal (compression – tension cycles) since the actuator was supported on two pins at its ends and thus was unstable in compression.

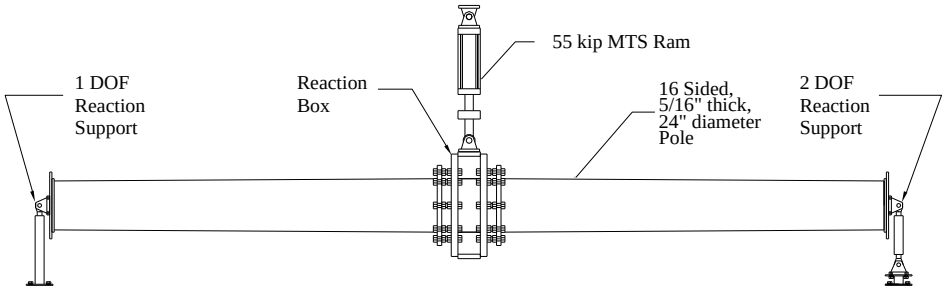

Figure 2.11: Test setup (Rios, 2007)

The stress range level with which the tests were conducted was selected to be 12 ksi, with respective minimum and maximum stresses of 10 ksi and 22 ksi. Due to the large mass of the system, resonance could cause instabilities to the closed-loop hydraulic system. The testing speed (cyclic load frequency) was chosen to be at 1.75 Hz to minimize dynamic effects.

Another factor that was defined is the failure criterion. The designation of failure was selected based upon the change in force range as a function of the maximum and minimum displacements in the pole. Failure of the pole was selected for a value of 10% change in force over the displacement range. This was a reasonable choice, considering the inherent exponential nature of fatigue damage under constant amplitude cyclic loads. A summary of all test parameters for this phase is presented in Table 2.1.

Stress range	Minimum yield stress	Maximum yield stress	Frequency	Failure definition
12 ksi	10 ksi	22 ksi	1.75 Hz	10% reduction of recorded forces

Table 2.1: Summary of Phase I test parameters

2.2.1.6 Test Results and Conclusions

The results for each connection type are presented separately, along with illustrations of the crack propagation pattern. A summary of the results is then presented and discussed.

2.2.1.6.1 Results for Fillet Weld Connections

As noted earlier, Rios (2006) presented results from 16 tests. A total of 10 of these results consisted of fillet weld socket connections. One method of improving the fatigue performance of the HMIP was identified by increasing the stiffness of the connection at the base of the pole. Two potential methods of increasing the base stiffness are by increasing the number of bolts or by increasing the thickness of the base plate. Both of these methods increased the fatigue life of the specimen as shown in the S-N curves in Figure 2.12. Recalling from the nomenclature, the second number in the name refers to the base plate thickness, while the third number corresponds to the number of bolts in the base plate connection. The worst fatigue performance was in the 1.5 inch base plate connection with only 8 bolts. The trends in the fatigue performance showed improvement with either an increase in the thickness of the base plate or the number of bolts in the base plate connection.

The locations of the cracks are shown in Figure 2.13 and Figure 2.14Figure 2.13: Typical failure of fillet welded socket connection (Rios, 2007). The cracks initiated at the toe of the weld of the extreme tension fiber and propagated through the wall thickness and the connection cross-section.

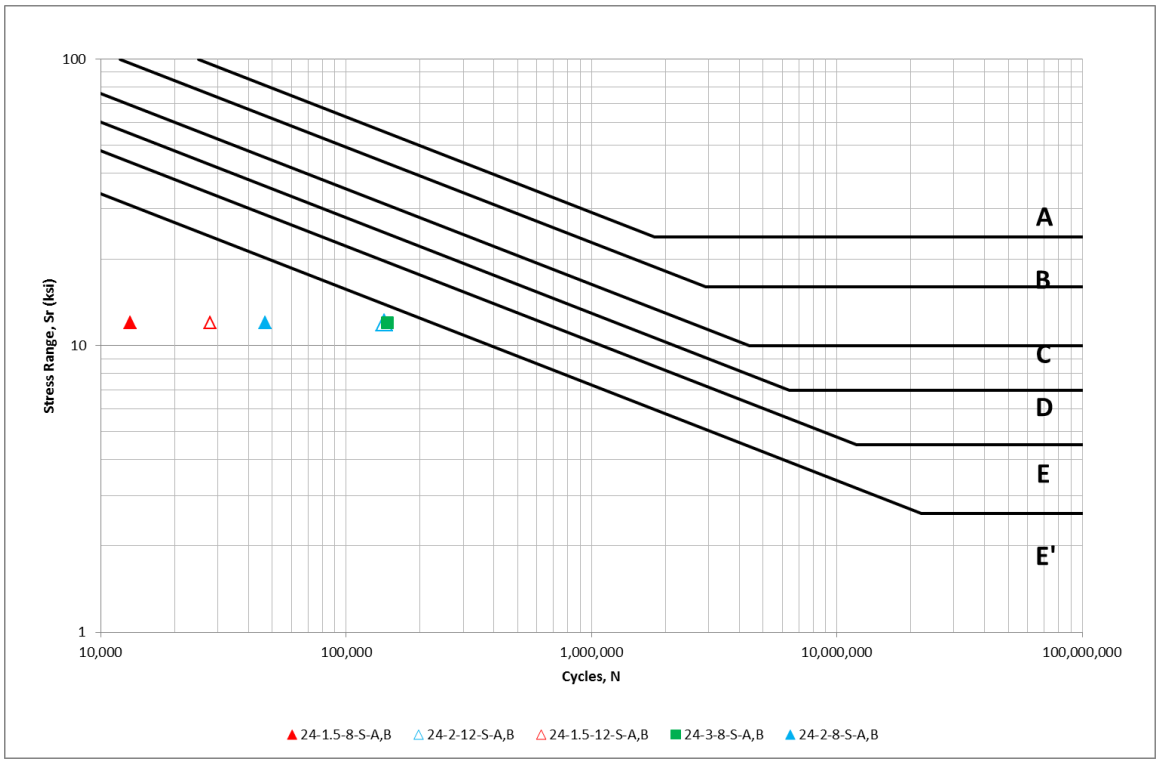

Figure 2.12: S-N plot of fatigue test results for fillet connection types

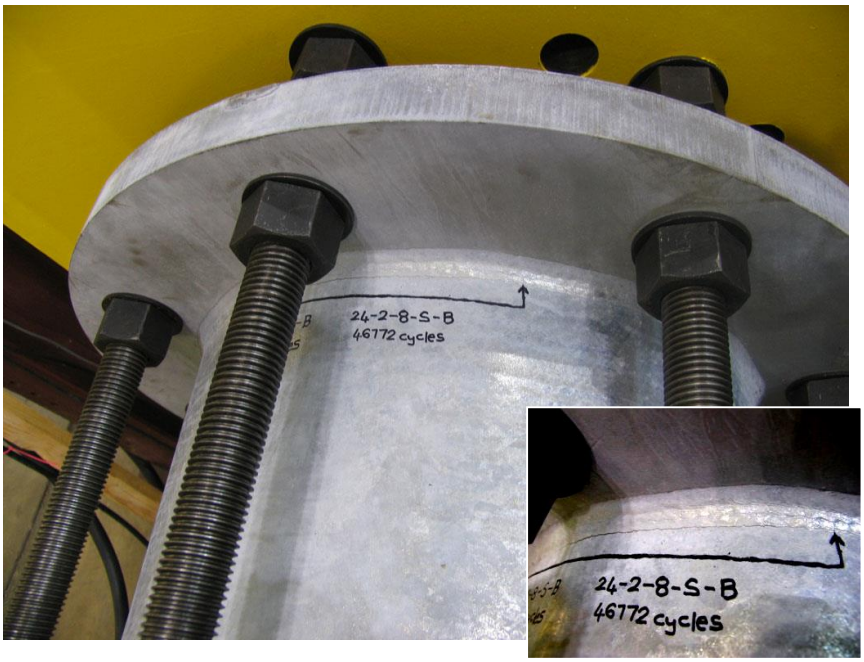

Figure 2.13: Typical failure of fillet welded socket connection (Rios, 2007)

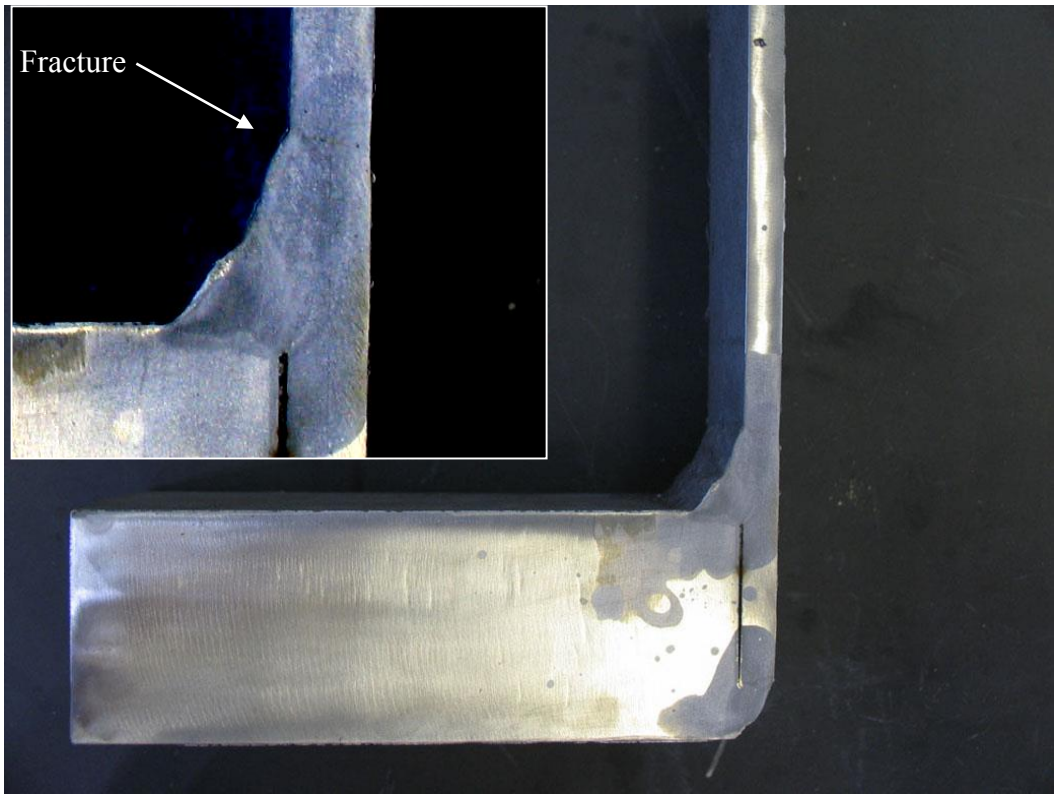

Figure 2.14: Etched cross section of fillet welded socket connection (Rios 2007)

2.2.1.6.2 Results for Full Penetration Weld Connections

Four of the sixteen tests carried out by Rios consisted of full penetration connections. A graph of S-N curve for the four tests are shown in Figure 2.15. The Texas detail with the 12-bolt configuration and 3-inch thick base plate performed better than the Wyoming detail with the 8-bolt configuration and 2-inch base plate. This fact again justified that stiffer base plates had better fatigue performance. Compared with the socketed connections, the full penetration base plate connections had better performance.

The location of the cracks is shown in Figure 2.16, Figure 2.17 and Figure 2.18. The cracks initiated at the toe of the weld of the extreme tension fiber and propagated through the wall thickness and the connection cross-section.

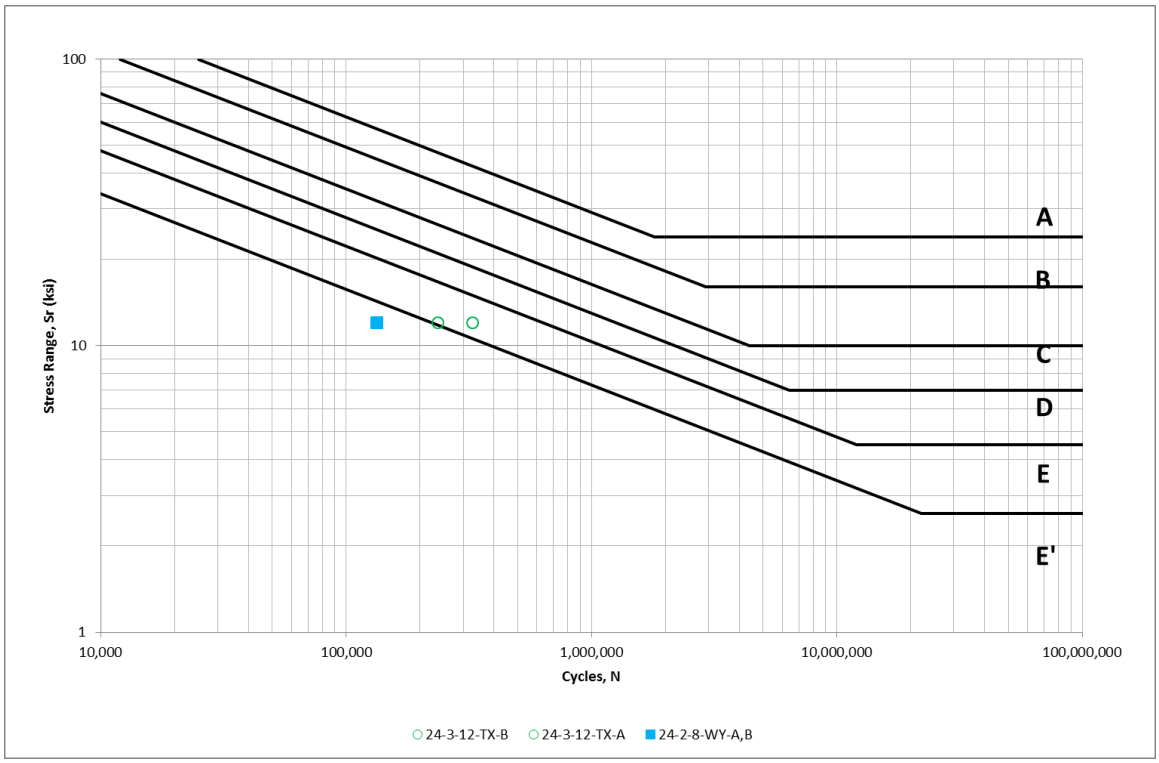

Figure 2.15: S-N plot of fatigue test results for full penetration connection types

Figure 2.16: Typical failure of Wyoming full penetration weld connection (Rios, 2007)

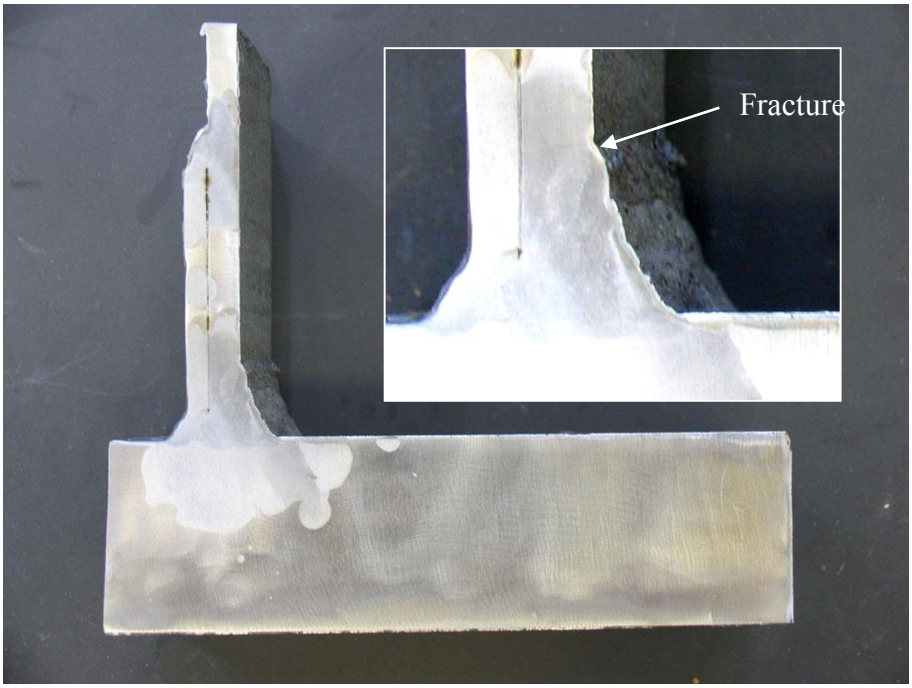

Figure 2.17: Etched cross section of Wyoming full penetration connection (Rios, 2007)

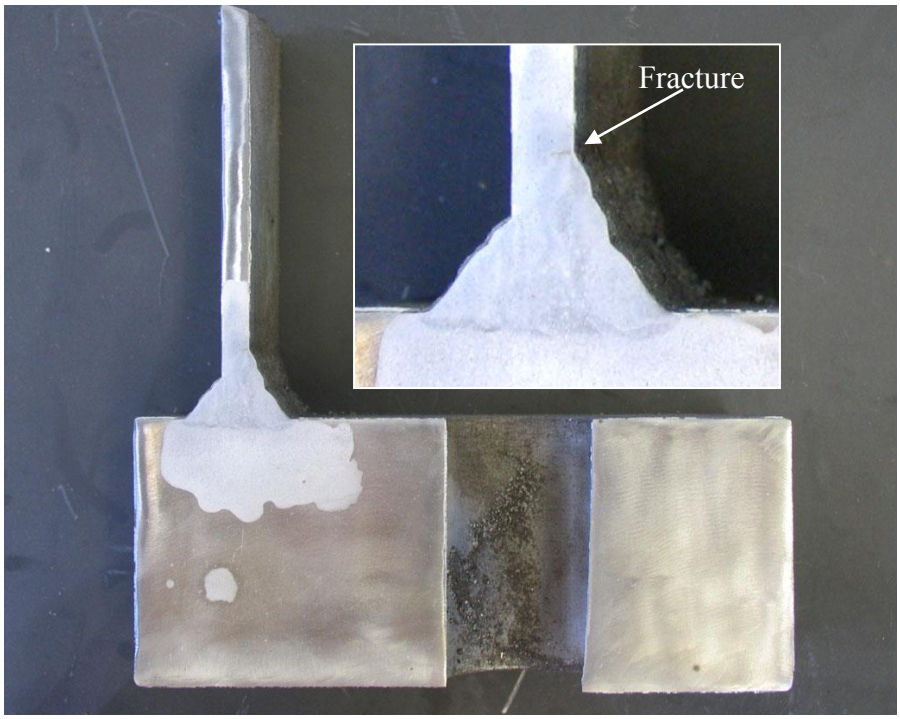

Figure 2.18: Etched cross section of Texas full penetration connection (Rios, 2007)

2.2.1.6.3 Results for Stool Base Weld Connections

The final two tests conducted by Rios consisted of stool base connections. A graph of the SN curve for the tests is given in Figure 2.19. As expected the stiffer base plate of this detail performed better than any other in the Phase I of the research on HMIP at the University of Texas at Austin.

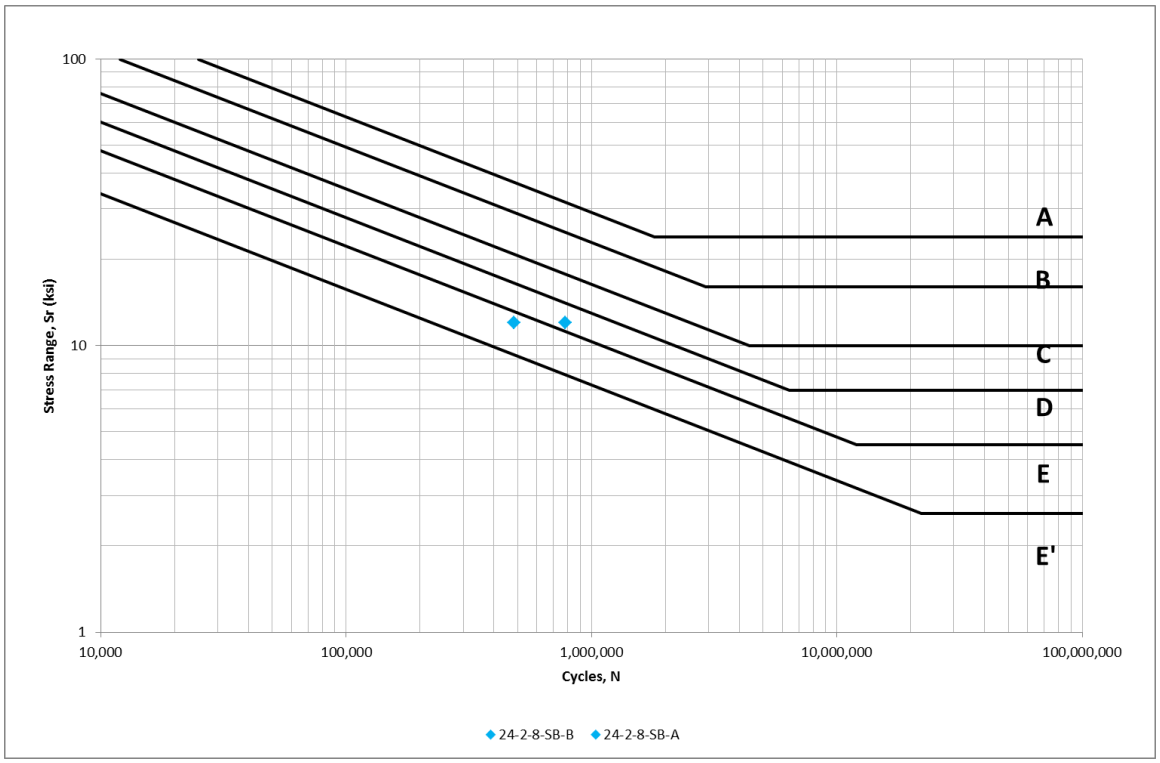

Figure 2.19: S-N plot of fatigue test results for stool base connection types

The location of the cracks can be shown in Figure 2.20. As opposed to the other crack locations, cracks in the stool base detail initiated at the toe of the cap plate weld and the propagated following the weld toe before continuing into the pole wall. This was a result of transferring the maximum stresses further away from the base plate.

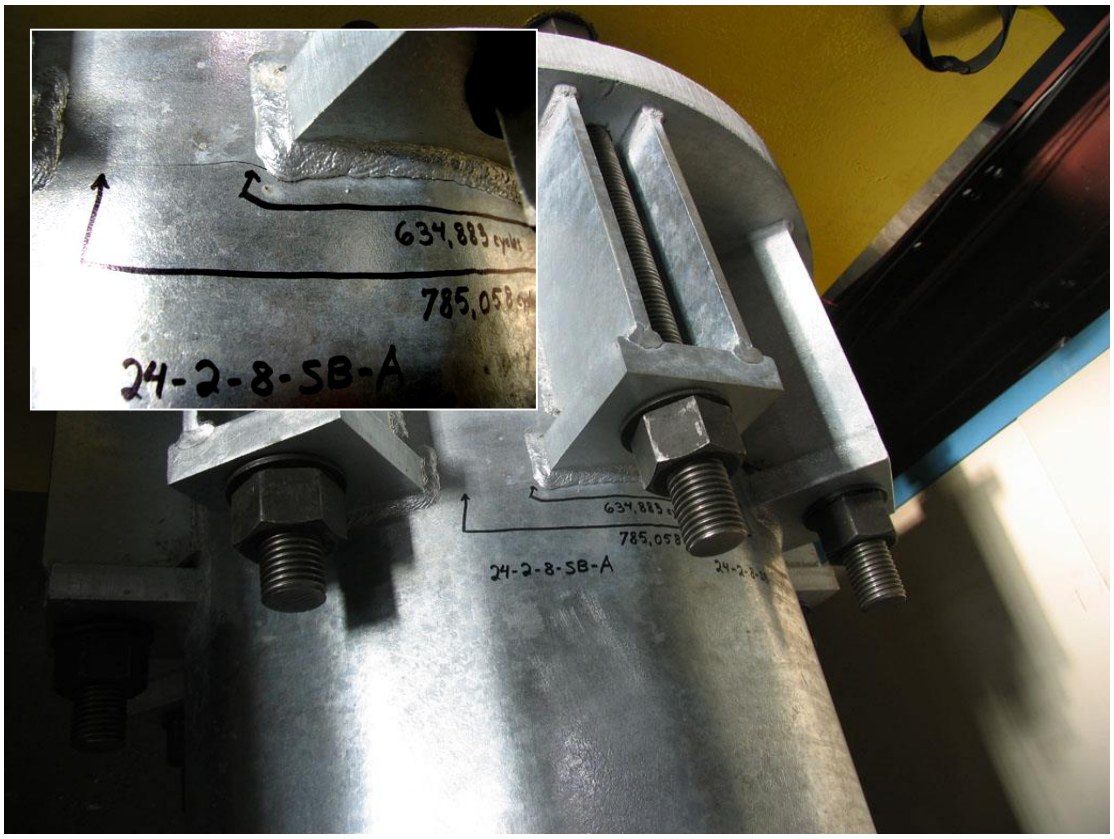

Figure 2.20: Typical failure of stool base detail connection (Rios, 2007)

2.2.1.7 Summary of Phase I research

The results of the Phase I tests showed that there is a clear distinction in the performance of each weld detail. Even though the details were designed in accordance with the AASHTO specification, they did not meet Category E for full penetration weld type connections and Category E' for fillet welded socket type connections as specified by the design provisions. The summary of all the tests conducted by Rios is shown in Figure 2.21.

The stool base detail and the Texas detail met the category E requirements. The fillet welded detail connections showed the poorest performance by not meeting the category E' requirements and the full penetration detail connections did not meet the category E requirements.

As noted earlier, the tests from Rios demonstrated that increasing the base plate thickness and the number of bolts in the base plates improved the fatigue performance of the detail. The conclusion that can be drawn from these tests was that increasing the stiffness of the pole base provided improvements in the fatigue performance of the base detail.

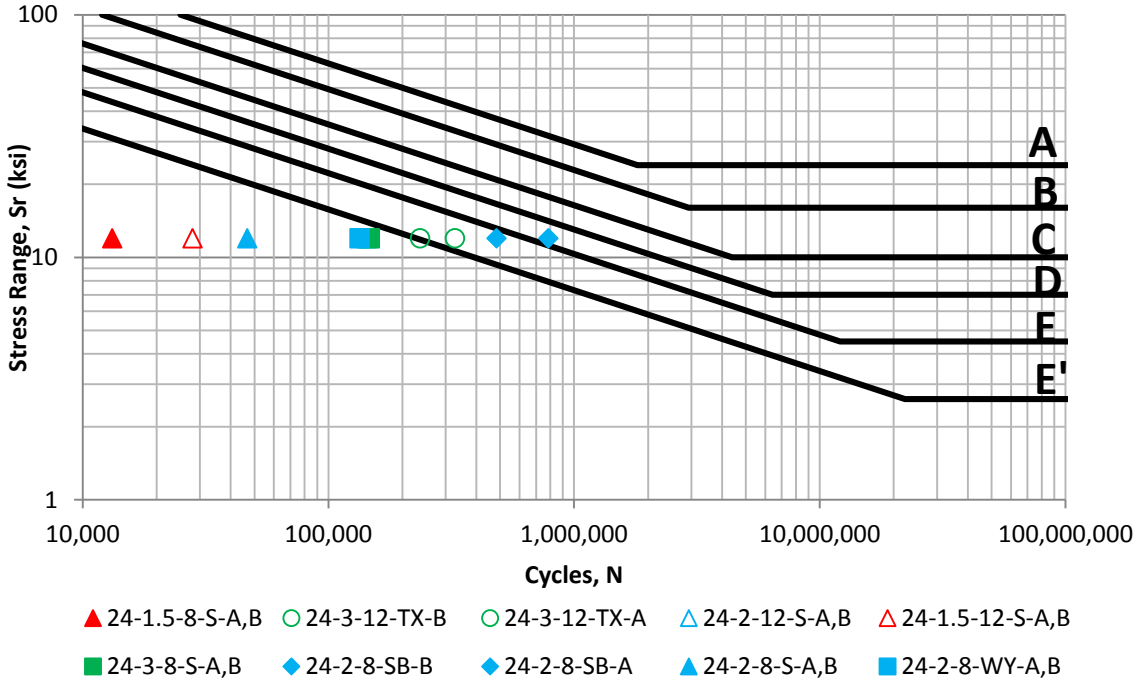

Figure 2.21: S-N plot of fatigue test results for all connection types

2.2.2 PHASE II

The work completed by Stam (2009) was to extend the Phase I research. Rios (2006), Anderson (2007), and Warpinski (2006), concluded that the fatigue performance was directly related to the rotational flexibility of the shaft to base plate connection. The rotational flexibility was related to the following parameters:

- The base plate thickness.

- The number of anchor rods.
- The connection and weld detail.
- The presence of external or internal stiffening device (collar, ground sleeve etc.).

A series of tests and FEA work were conducted in Phase II of the work to improve the fundamental understanding on the fatigue performance of the HMIP sections.

2.2.2.1 Test Specimens

Based on these results, the Phase II of the research concentrated on the performance of details with a thick base plate (2-inches for the stool base detail and 3-inches for the rest). Also, the use of stiffening devices was ongoing concurrently (Anderson, 2007) was shown a to have a significant contribution to the fatigue performance of the corresponding details. Stiffening details consist of either an additional collar or a stool base detail. The connection details and the summary of the specimens tested in Phase II are provided in Table 2.2. The talble identifies the baseplate to pole weld detail, the stiffening device as well as the thickness of the shaft wall and base plate.

Specimen Name	Connection Detail Name	Base Plate-to-Pole Weld Type	Stiffening Device	Wall Thick. (in)	Base Plate Thick. (in)
24-3-12-SEC-VG	Socket Ext. Collar	Fillet Weld	Collar	0.3125	3
24-3-12-TXEC-VG	Texas Ext. Collar	Full Pen. Weld	Collar	0.3125	3
24-3-12-WEC-VG	Wyoming Ext. Collar	Full Pen. Weld	Collar	0.3125	3
24-3-12-WTh-VG	Wyoming Thick Wall	Full Pen. Weld	None	0.5000	3
24-2-8-STL-VG	Continuous Stool	Fillet Weld	Stool	0.3125	2
24-2-12-STL-VG	Continuous Stool	Fillet Weld	Stool	0.3125	2
24-2-12-STL30-VG	Cont. Stool (30deg)	Fillet Weld	Stool	0.3125	2
24-3-16-SEC-PG	Socket Ext. Collar	Fillet Weld	Collar	0.3125	3
24-3-12-WY-PG	Wyoming	Full Pen. Weld	None	0.3125	3
24-3-12-TX-PG	Texas	Full Pen. Weld	None	0.3125	3

Table 2.2: Summary of specimens tested in Phase II (Stam, 2009)

2.2.2.2 Experimental Results

The location of the cracks for the unstiffened sections was the toe of the weld of the shaft to the base plate. For specimens with external collars, the crack locations varied as showed in Figure 2.22 and Figure 2.23. For specimens with the stool base connection, the location of the cracks was the toe of the weld of the shaft to the stool plate as shown in Figure 2.24.

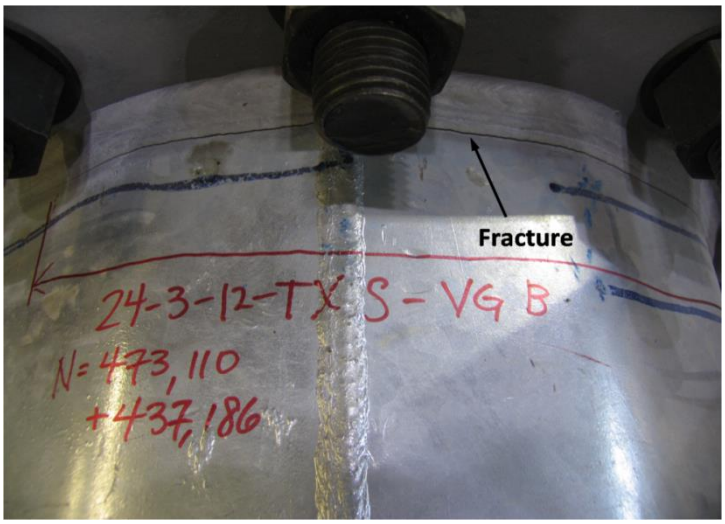

Figure 2.22: Shaft to base plate crack location (Stam, 2009)

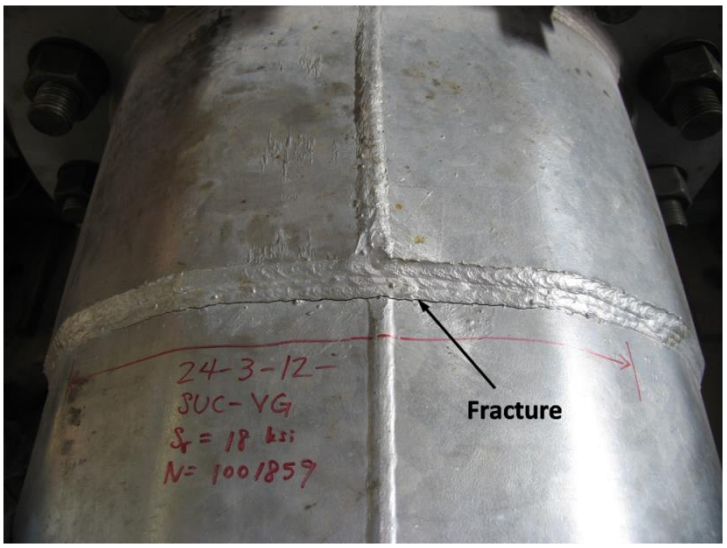

Figure 2.23: Shaft to external collar crack location (Stam, 2009)

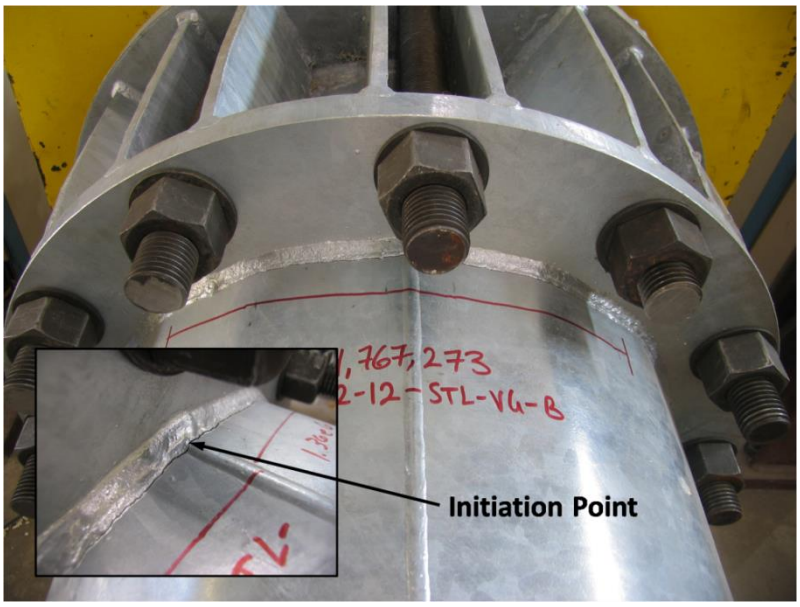

Figure 2.24: Stool base connection crack location (Stam, 2009)

The summary of the Phase II test results is shown in Table 2.3. In addition to the number of cycles leading to failure, the fatigue coefficient A is presented. The fatigue coefficient provides a useful reference variable that helps in comparing the fatigue test performance of details conducted with different stress levels. A is given as ():

$$A = N \cdot S_r^3$$

where, N=cycles to failure, and S_r^3 = nominal stress range.

Table 2.3 shows that test 24-3-12-TXEC-VG-A did not meet the requirements for failure and was designated as a run out specimen.

Specimen	Nominal S_r	Life, N	A (x 10^8)	AASHTO Category	Crack Location
24-3-12-SEC-VG-A	18	540,520	31.5	D	Base plate WT
24-3-12-SEC-VG-B	18	345,542	20.2	E	Base plate WT
24-3-16-SEC-PG-A	18	137,693	8.0	E'	Collar WT
24-3-16-SEC-PG-B	18	95,799	5.6	E'	Collar WT
24-3-12-TXEC-VG-A	12	4,034,441[1]	69.7	C	Base plate WT
24-3-12-TXEC-VG-B	12	4,034,441	69.7	C	Base plate WT
24-3-12-WEC-VG-A	18	1,330,470	77.6	C	Collar WT
24-3-12-WEC-VG-B	18	1,001,859	58.4	C	Collar WT
24-3-12-WYTh-VG-A	11.4	862,107	12.8	E	Base plate WT
24-3-12-WYTh-VG-B	11.4	680,613	10.1	E'	Base plate WT
24-3-16-TX-PG	18	238,372	13.9	E	Base plate WT
24-3-16-WY-PG	18	366,092	21.4	E	Base plate WT
24-2-12-STL-VG-A	12	2,160,059	37.3	D	Stool WT
24-2-12-STL-VG-B	12	1,680,547	29.0	D	Stool WT
24-2-12-STL30-VG-A	12	2,068,561	35.7	D	Stool WT
24-2-12-STL30-VG-B	12	1,389,066	24.0	D	Stool WT
24-2-8-STL-VG-A	12	1,240,413	21.4	E	Stool WT
24-2-8-STL-VG-B	12	1,357,965	23.5	D	Stool WT

1 - Runout Specimen

Table 2.3: Summary of Phase II results (Stam, 2009)

The research results in Both Phase I and Phase II showed that a stiffer shaft-to-base-plate connection improved the fatigue performance of the details. A stiffer connection was achieved by increasing the number of anchor rods and/or increasing the base plate thickness. However, there were a number of factors that varied in the design of each of the specimens tested. This led to specimens with multiple variables, which made the direct comparison more complex. For this reason, in the following figures the variables are isolated so as to evaluate the impact of the variable on the fatigue performance.

The first comparison that was made was the evaluation of performance of socketed over non-socketed connections.

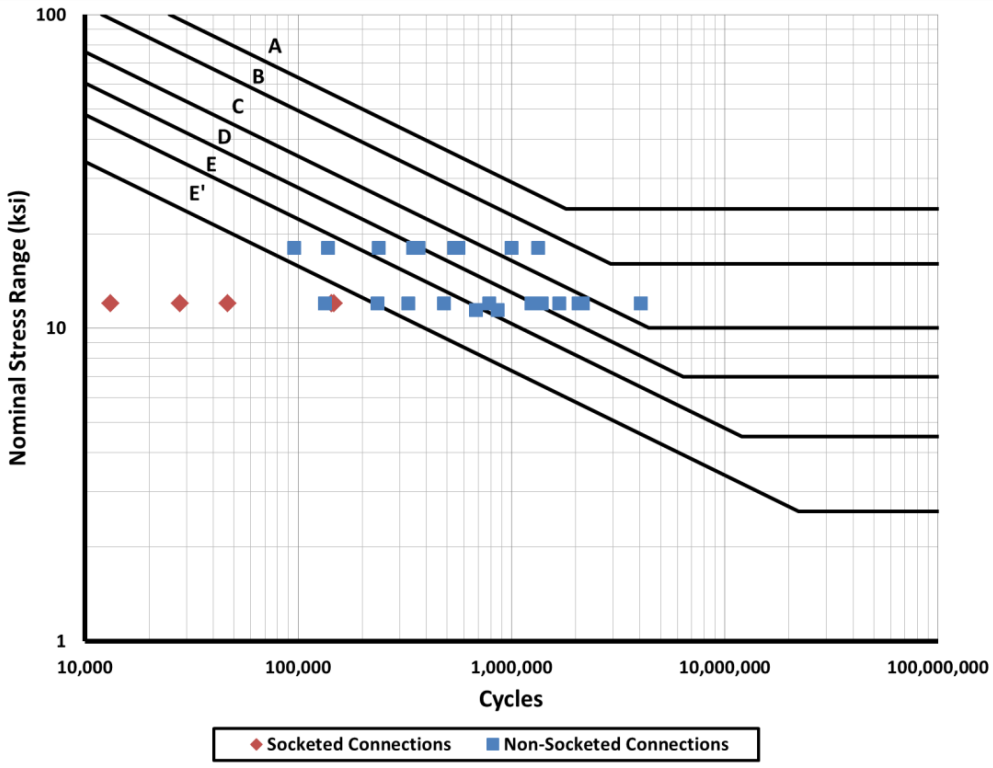

Figure 2.25: S-N plot showing the performance of socketed vs. non-socketed connections

The term "socketed" denotes connections with the detail shown in Figure 2.3. Figure 2.25 shows the substantial difference in the performance of the socketed versus the non-socketed connections. This is a result of the relatively small rotational stiffness provided at the base plate from the socketed connections. One of the reasons for the smaller rotational capacity can be identified as the unleveled location of the welds inside and outside, creating a "force couple" and thus, reducing the rotational stiffness that the connection provides.

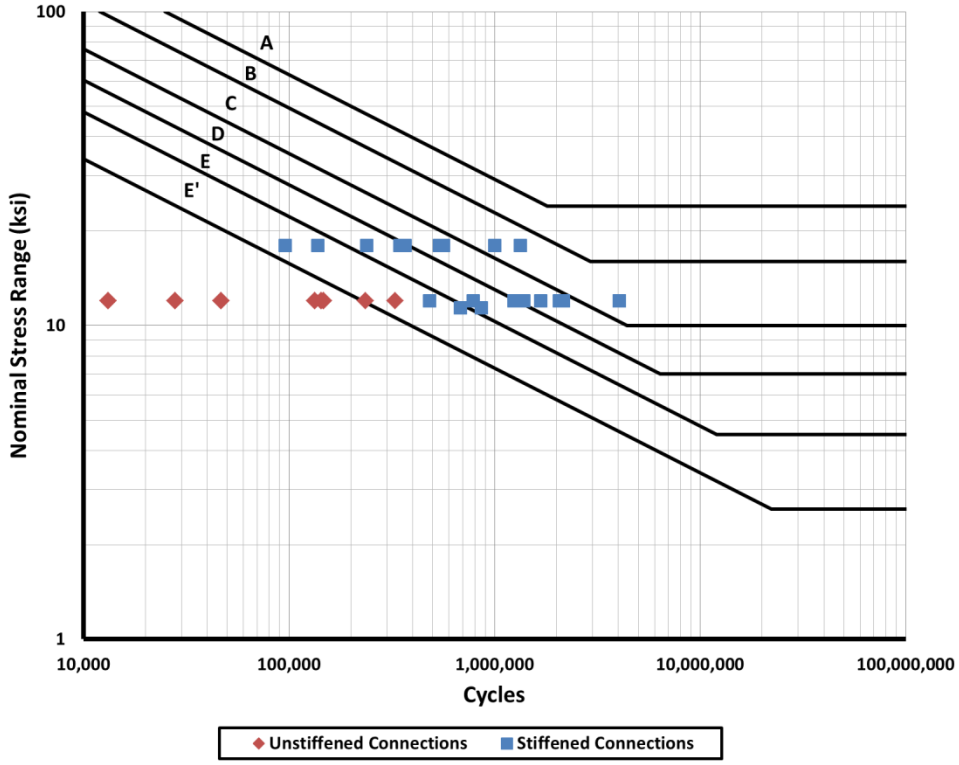

Figure 2.26: S-N plot showing the performance of stiffened vs. unstiffened connections

The effect of stiffening devices on the fatigue performance is shown in Figure 2.26. The term "stiffened" denotes connections using any sort of stiffening device (collar, stool etc.). This is also a result of the improved rotational stiffness that is added to the base connection with the stiffened detail. The disadvantage of those connections, is the higher manufacturing costs associated with them.

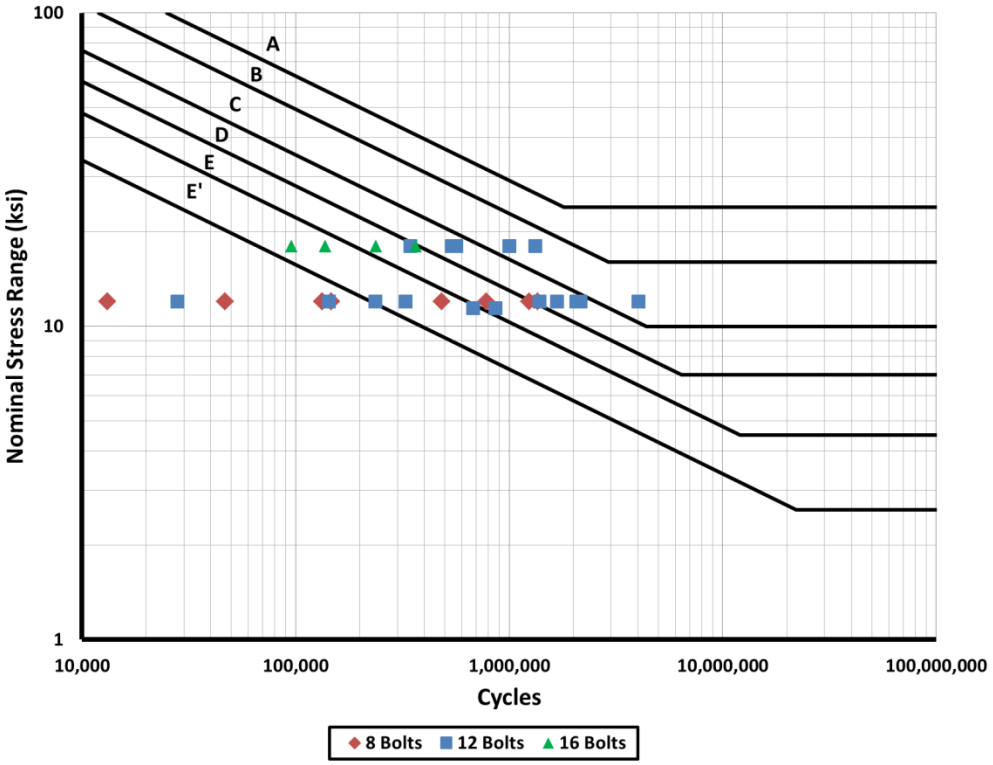

Figure 2.27: S-N plot showing the fatigue performance of the connection with respect to the bolt number

Figure 2.27 shows the effect of the number of bolts on the fatigue performance. There is not a general trend with regards to the impact of the number of anchor bolts on the fatigue performance of the connection. This led researchers to the conclusion that the number of bolts does not have a significant effect on the fatigue performance of the structure. However, the fatigue resistance of the bolts themselves should be considered.

The last comparison of the test results is shown in Figure 2.28. The conclusion that can be drawn is that the increase in the base plate stiffness (thickness) results in better fatigue performance. In addition, out of the 2 inch base plate specimens, a better performance was achieved by specimens which had a stool (stiffer) detail.

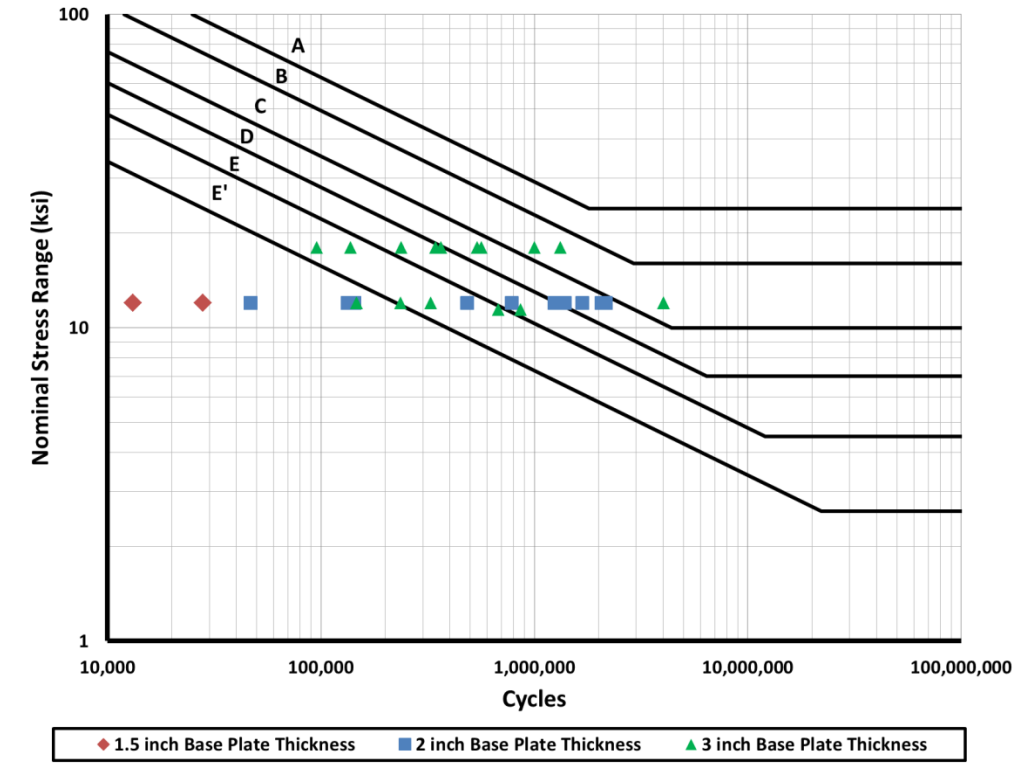

Figure 2.28: S-N plot showing the fatigue performance of the connection with respect to the base plate thickness

2.2.2.3 Analytical Study and Results

To confirm the effect of each parameter in the fatigue performance of the shaft to base plate connection, an analytical parametric study was conducted. The analytical results showed a significant stress gradient close to the toe of the weld due to the change of the geometry of the cross-section at that region, resulting in an increased stress (hotspot stress). The stress concentration factor (SCF) was defined as the ratio of the hotspot stress to the nominal stress as calculated by the bending formula, $\frac{M \cdot c}{I}$, which was determined for each of the cases of the parametric study.

The variables examined in the analytical parametric study were the shaft diameter, shaft thickness and base plate thickness for the non-socketed connection type. In addition,

the shaft diameter and thickness were examined for the socketed detail. As mentioned in 2.2.2.2 the number of anchor rods was proven to have no impact on the fatigue performance of the connection. This was evaluated in the analytical studies and is shown in Figure 2.29. Socket describes a socketed connection and the Texas describes a Texas detail connection with varying the base plate thickness.

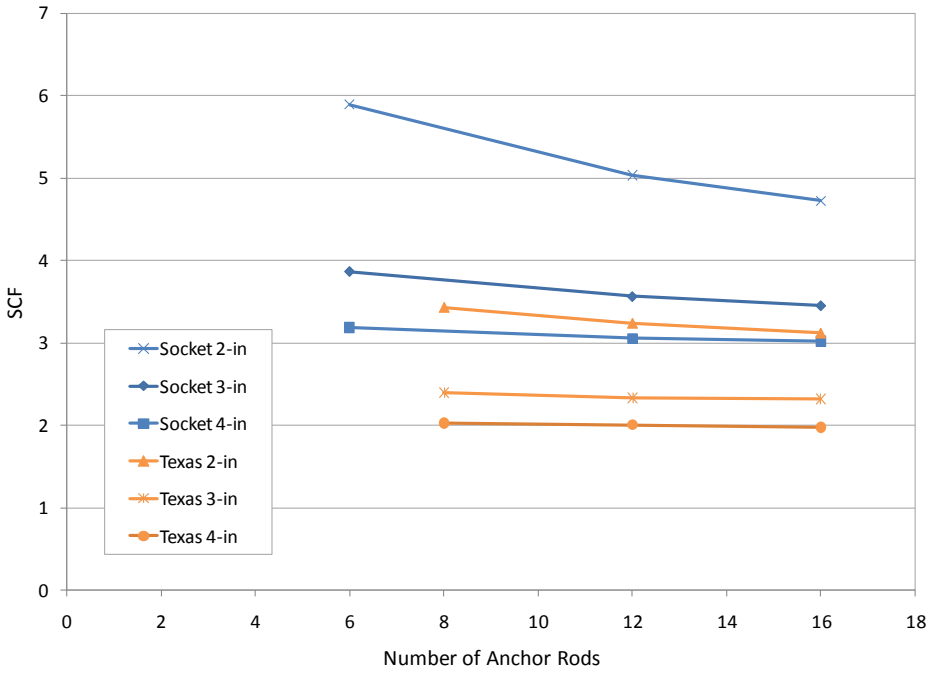

Figure 2.29: Results of anchor rods parametric study (Stam, 2009)

Two shaft diameters (24 inches and 36 inches) were considered with two shaft thicknesses (5/16 inch and ½ inch) for each. For a given bending moment, an HMIP with a larger diameter (and as a result section modulus) provides increased bending resistance and a larger cross-sectional area. The increased section modulus and area lead to an increase in the SCF as illustrated in Figure 2.30. While the increase in the SCF for the

larger section is at first counter-intuitive, the problem is related to the relative stiffness compared to the base plate. The reduction in the relative stiffness of the base plate to the shaft makes the system softer at resisting the double curvature imposed in the base plate by bending.

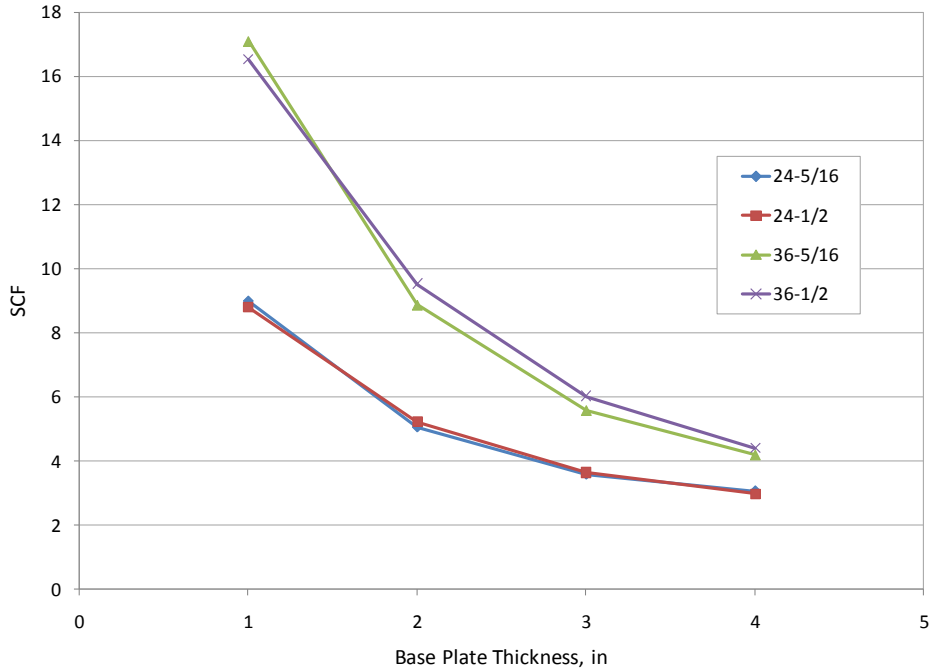

Figure 2.30: SCFs for Socket Details in Wall Thickness and Shaft Diameter Parametric Study

However, as seen in Figure 2.29 the SCFs reach even lower values when the detail under consideration is the Texas detail, which is a result of the inherent stiffness of the detail. Furthermore, increases in the base plate thickness have a beneficial effect in the SCF reduction.

2.2.3 PHASE III – POOL'S RESEARCH

The Phase III study was essentially an extension of the variables studied in Phase II. In Phase II, the effects of galvanization on the fatigue behavior of larger HMIPs were

studied. Initial cracking due to galvanization at the toe of the weld of the shaft to base plate connection was validated, which led researchers to thoroughly investigate the effects of the initial cracking on the fatigue performance of the connection. In addition, the variables that lead to the initial cracking were studied. This investigation was conducted through destructive and non-destructive testing.

2.2.3.1 Test Specimens

The first pair of specimens that was tested in this phase had larger values of the shaft diameter (33 inches) and the base plate thickness (3 inches). However, the major difference from the previous tests was the testing of a non-galvanized specimens, which are referred to as "black" specimens and companion galvanized specimens. In this way a direct comparison of the effects of the galvanization was made.

The next pair of specimens was made by a different manufacturer and galvanizer to test the effect of the exterior factors in the initial cracking. The effects of the manufacturer and galvanizer were evaluated through testing to measure the fatigue performance of the connections.

The previous specimens were repaired after failure with the exception of the "black" specimen. The "black" specimen had no signs of cracks after being used as a companion (pair) specimen for the previous galvanized specimens but was used for the simulation of a shop repair procedure. After being repaired, the specimens were tested again, testing in this way the efficiency of the weld repairs as a way of mitigating the cracking at shop but also potentially in-service poles.

The last two specimens had the external collar incorporated in the detail. As previous research has shown (Stam, 2009), the use of external stiffening devices significantly improved the fatigue performance of the connections.

Summarizing, a total of 8 tests were conducted. All specimens had a base plate thickness of 3 inches, a shaft diameter of 33 inches, a shaft thickness of 0.3125 inches and 12 holes to the anchor rods. The primary difference among the specimens was galvanized versus black specimens as well as the manufacturers of the HMIPs. A summary of the specimens used in Phase III is presented in Table 2.4.

Specimen Code	Connection Detail	Galvanized	Manufacturer
33-3-12-TX-SG-A	Texas	Yes	Structural Metals
33-3-12-TX-SB-B	Texas	No	Structural Metals
33-3-12-TX-VG-A	Texas	Yes	Valmont
33-3-12-TX-VG-B	Texas	Yes	Valmont
33-3-12-TX-VG-A (FLIP)	Texas	Yes	Valmont
33-3-12-TX-VG-B (FLIP)	Texas	Yes	Valmont
FIELD REPAIR	Texas FCAW Repaired	Yes	Valmont
SHOP REPAIR	Texas SMAW Repaired	No	Structural Metals
33-3-12-TXEC-SG-A	Texas w/ External Collar	Yes	Structural Metals
33-3-12-TXEC-SG-B	Texas w/ External Collar	Yes	Structural Metals

Table 2.4: Summary and names of specimens tested during Phase III of the Study (Pool, 2010)

2.2.3.2 Non-Destructive Testing Results

The non-destructive testing method that was used in Phase III consisted of ultrasonic testing. The ultrasonic testing was conducted prior to destructive testing in order to determine the existence of cracks in previously unloaded specimens as well as an attempt to improve the understanding of the variables that affect the initial cracking. Table 2.5 summarizes that cracks that were found in the specimens with the one black specimen identified under the Detail category. As it can be seen in Table 2.5, initial cracks were found only in the galvanized specimens, resulting in the hypothesis that the galvanizing process is responsible for the creation of the initial cracks.

Specimen Code	Detail	Volume Ratio	Bends Cracked (%)
33-3-12-TX-SG-A	Full Penetration	10.16	100.00
33-3-12-TX-SB-B	Full Penetration (black)	10.16	0.00
33-3-12-TX-SG-B	Full Penetration	10.16	75.00
33-3-12-TX-VG-A	Full Penetration	10.16	30.00
33-3-12-TX-VG-B	Full Penetration	10.16	40.00
33-3-12-TXEC-SG-A	External Collar	4.57	16.7
33-3-12-TXEC-SG-B	External Collar	4.57	25.00

Table 2.5: Summary of Non-Destructive Testing Results (Pool, 2010)

2.2.3.3 Destructive Testing Results

The testing procedure followed in this phase of the Study was identical to the procedure followed in the first two phases. Comparing the test results obtained from galvanized and black specimens, the conclusion that can be drawn is that initial cracking during galvanizing plays a significant and detrimental role in the fatigue performance of the HMIP connection. Another conclusion, made obvious after Phase III testing, is that the presence of an external stiffening device improves the fatigue performance of the connection. The results supporting the conclusions are presented above is shown in Figure 2.31.

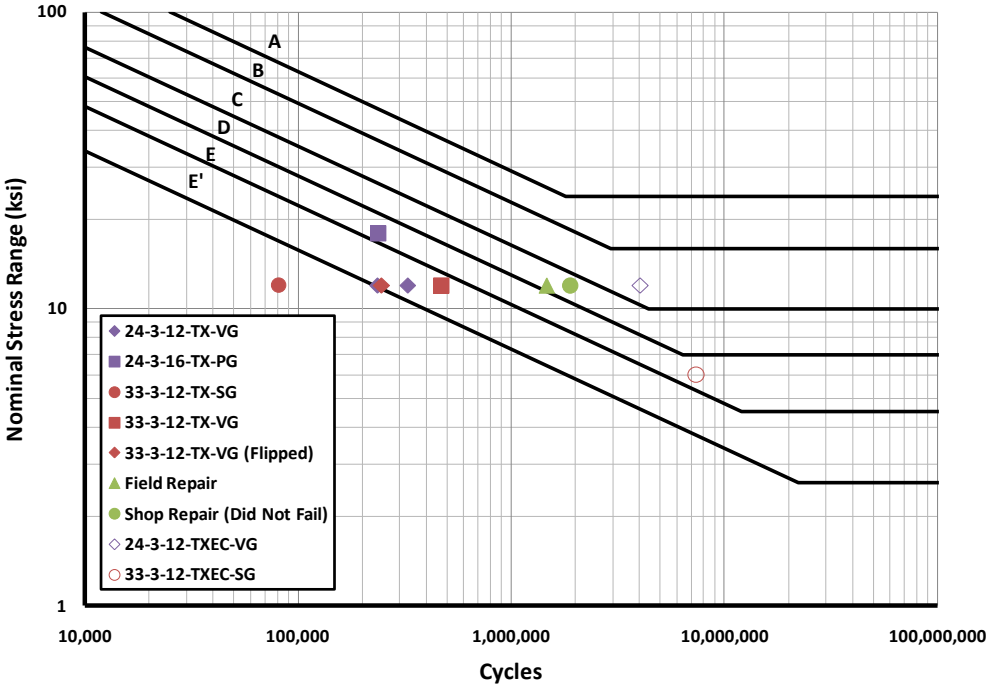

Figure 2.31: S-N plot showing Phase III results (Pool, 2010)

2.2.4 PHASE IV – KLEINECK'S RESEARCH

Conclusions extracted from Phase III of the Study led researchers to investigate the cause of the cracking in the shaft to base plate weld that occurs during the galvanizing process. Therefore, in Phase IV, thermal studies during the galvanizing process and its results were conducted.

2.2.4.1 Initial Testing Results

Parameters such as bend radius, weld design geometry as well as chemical composition of the galvanized coating were examined. However, no direct relation between these parameters and initial cracking occurrence was observed. In addition, the orientation

of the cracks and the non-reactivity of the galvanizing bath with steel led researchers to investigate the thermally induced stresses in the HMIP due to the galvanizing process.

2.2.4.2 Field Instrumentation Results

As part of the research conducted in this phase of the research, HMIP speciemns were instrumented prior to galvalizing in an attempt to gain a measure of the thermal gradients and resulting strains that develop as the sections are immersed in the zinc bath. The resulting data included the variation of strains and temperatures, throughout the cross-section, during the galvanizing. Temperature gradients were established by embedding thermocouples into the shaft and base plate at various locations around the section. The thermocouples therefore allowed the measure of the changes in HMIP temperature as the section was slowly dipped in the zinc bath. The strain gages that were used were not intended to capture the strain through the entire galvanizing process but instead to capture the changes in the strain near the top of the pole as the section began to be lowered into the bath. The data gained during these tests provided a valuable means for calibrating finite element models that were used to further study the behavior. During the visits to galvanizing plants it was discovered that no codified galvanizing procedure is currently implemented concerning the galvanizing of HMIPs. Moreover, the formation of galvanizing cracks is not related to the existence or not of external stiffening devices. The thermal gradient that the HMIPs experiences during the galvanizing process was successfully captured by the instrumentation as illustrated in Figure 2.32 and Figure 2.33, which show the changes in temperature at various locations in the shaft and base plate as a function of time after immersion in the zinc bath. The instrumentation in the shafts showed much faster temperature gains compared to the much thickner base plate. As a result, the shaft tends to expand relative to the base plate section due to the relative thermal gradient.

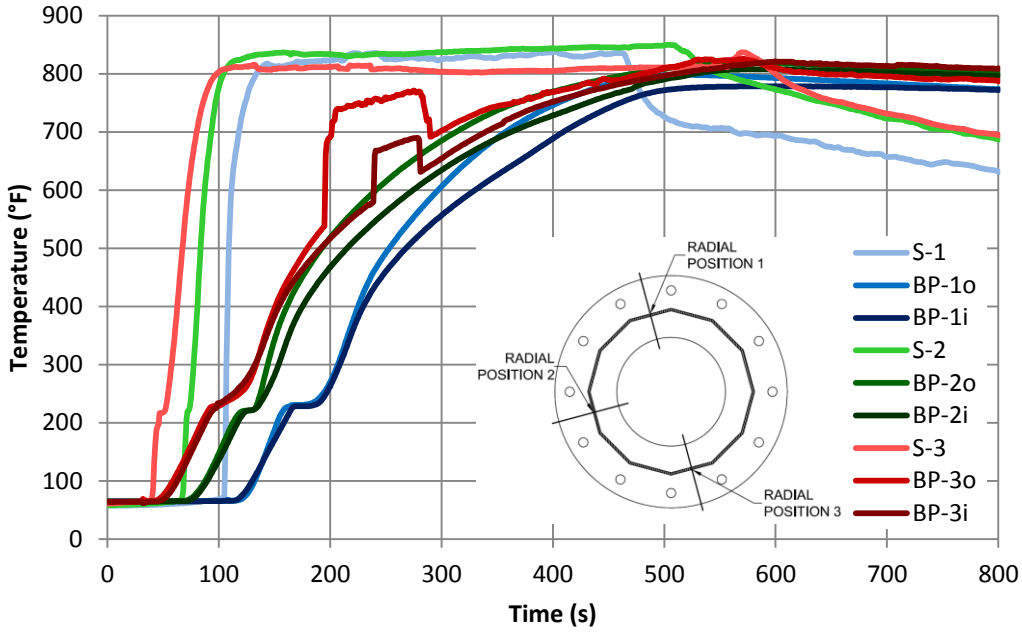

Figure 2.32: Typical thermal results from galvanizing process (Kleineck, 2011)

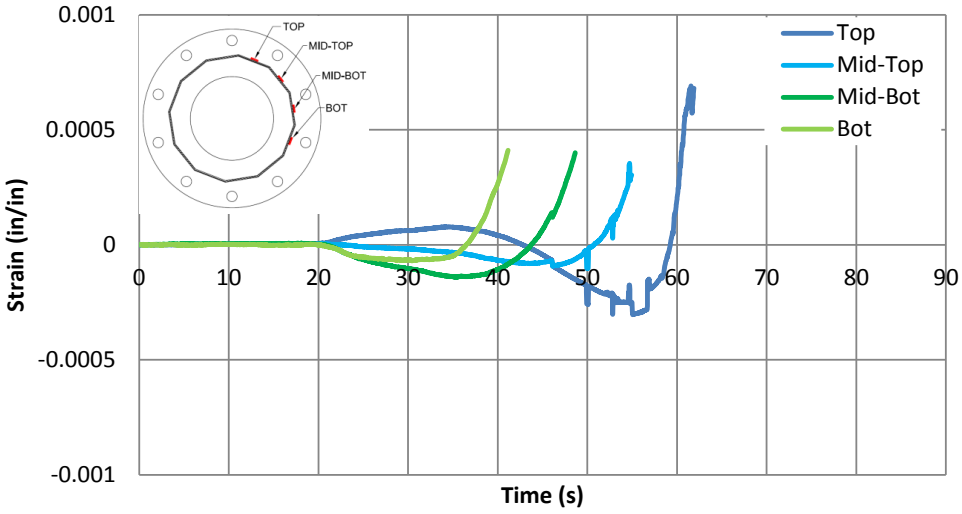

Figure 2.33: Typical thermal strain results from galvanizing process (Kleineck, 2011)

2.2.4.3 Analytical Studies Results

The valuable experimental field data that was obtained from the instrumentation during the galvanizing was used to develop analytical models for predicting the thermal and strain state of HMIPs during the galvanizing process. Parametric tests were carried out considering various pole geometries. A major result that was observed was that the strain gradient that develops during galvanizing varies throughout the cross-section. Specifically, at the weld toe of the shaft to base plate connection the strain that the HMIP experiences is higher than the strain that occurs at the flat regions. This phenomenon is illustrated in Figure 2.34 and is more apparent as the shaft diameter to shaft thickness ratio increases.

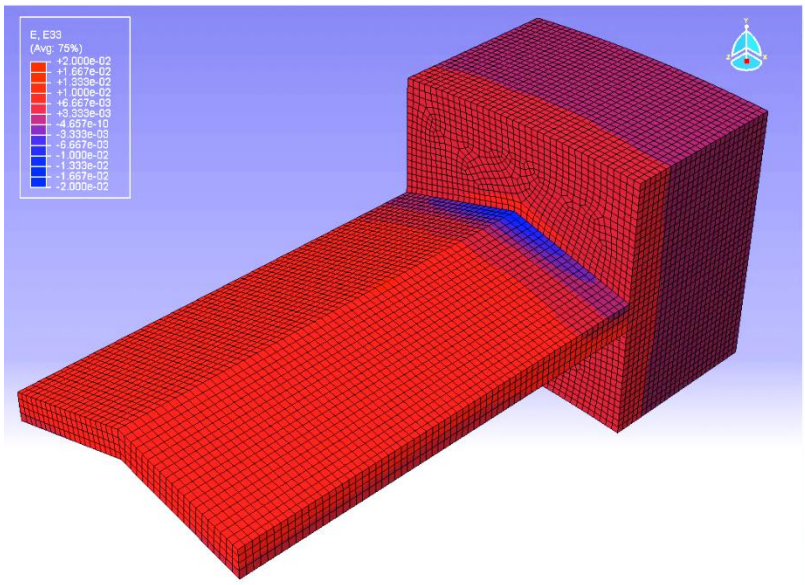

Figure 2.34: Typical submodel showing the concentration of stresses at the shaft to base plate connection after the galvanizing process (Kleineck, 2011)

The above information obtained from the parametric study matched with field and previous study results that the initial cracks from the galvanizing are formed due at the toe of the weld at the bend locations. Table 2.6 shows the parameters of the three models that were used in the parametric study and Figure 2.35 shows the results obtained. The results show clearly that one method of mitigating and possibly eliminating crack formation is to increase of the shaft thickness.

Model Designation	Corresponding Field Test	Shaft Thickness (in)	d/t ratio	v (in/s)	θ_{dip} (degrees)	θ_{long} (degrees)
SG-C	33-3-12-TX-SG-C	0.313	104	0.525	8	0
SG-SA	33-3-12-TX-SG-SA	0.438	75	0.609	4	6
SG-SC	33-3-12-TX-SG-SC	0.500	65	0.719	4	6

Table 2.6: Parameters of the three finite element models used (Kleineck, 2011)

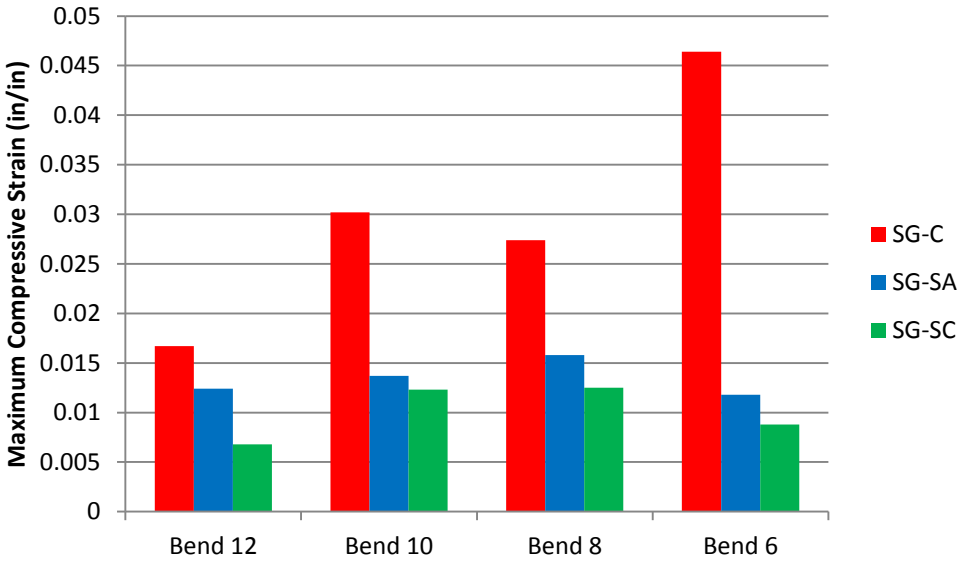

Figure 2.35: Results for maximum compressive strain at each bend for each of the models used (Kleineck, 2011)

2.2.5 PHASE V – MAGENES' RESEARCH

Pool's research outcomes were that galvanizing may be the reason of initial cracking in some poles and that poles with initial cracking show decreased fatigue performance. As a result, in parallel of the research on the effects of galvanizing in initial cracking, a field monitoring study was conducted on five in-service HMIPs located at four locations throughout Texas with different wind characteristics. The reasoning behind this decision was to acquire better insight on the level of stresses the HMIPs experience while in-service. The poles were monitored for an extended time so that an average behavior could be observed as well as the performance during extreme events such as storms. The obtained stress history was used to estimate equivalent average stresses that the HMIP are subjected to. Finally, using cumulative damage theories, the remaining service life of the structures were estimated.

2.2.5.1 Field Instrumentation

A total of 5 HMIPs were instrumented in 4 different locations in Texas to capture the in-service stress history experienced by HMIPs at various locations throughout the state.

The locations of the instrumented poles were as follows:

- Austin, Mo-Pac @ Parmer Ln.
- El Paso, IH-10 @ Brown St.
- El Paso, US-54 @ Hercules St.
- Corpus Christi, IH-37 @ SH-286
- Lubbock, US-62 @ SH-289

The instrumentation included strain gages and anemometers to capture the stress at particular locations of the pole in relation with the wind speed and direction. It also

included a solar recharged battery operated Data Acquisition System (DAQ) and wireless modems connected to a cellular network for remote access to data. A representative scheme of the field instrumentation setup is illustrated in Figure 2.36.

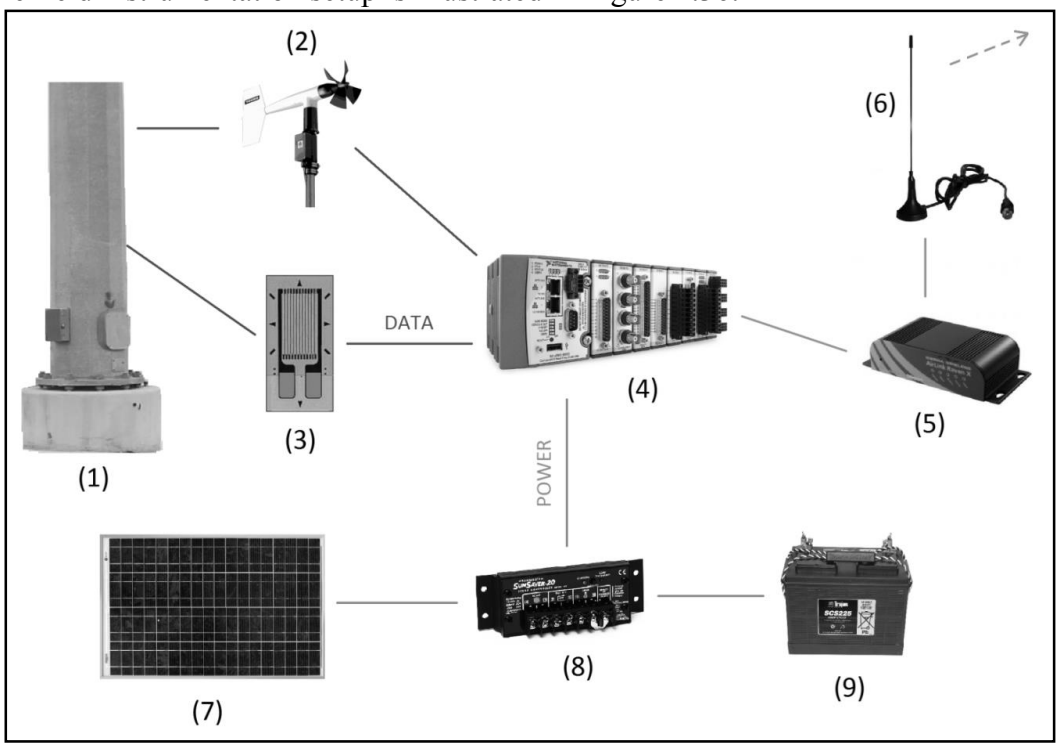

Figure 2.36: Scheme of the Instrumentation: (1) High Mast Pole, (2) Anemometer, (3) Strain Gages, (4) DAQ, (5) Wireless Modem, (6) Antenna, (7) Solar Panel, (8) Charge Controller, (9) Battery (Magenes, 2011)

This instrumentation was capable of conducting a rainflow analysis, which is a method using an algorithm to discretize the wind loading cycles from continuous to discrete bins of increasing amplitude with its correspondent number of equivalent cycles. Moreover, apart from the continuous rainflow analysis that was running on the DAQ system, an event capture program was running as well. This program was able to capture wind velocity and strain values for a short period of time, when a user-specified threshold was exceeded. This allowed researchers to capture continuous raw strain and wind data for

a prescribed amount of time when the wind speeds exceeded specific values. The data from the event captures allowed the researchers to study the dynamic behavior of the structure without overloading the system with data.

2.2.5.2 Field Instrumentation Results and Data Analysis

The event capture program resulted in valuable data that provided an indication of the dynamic behavior of the poles was with respect to wind loading. A typical graph showing the record of such an event is shown in Figure 2.37.

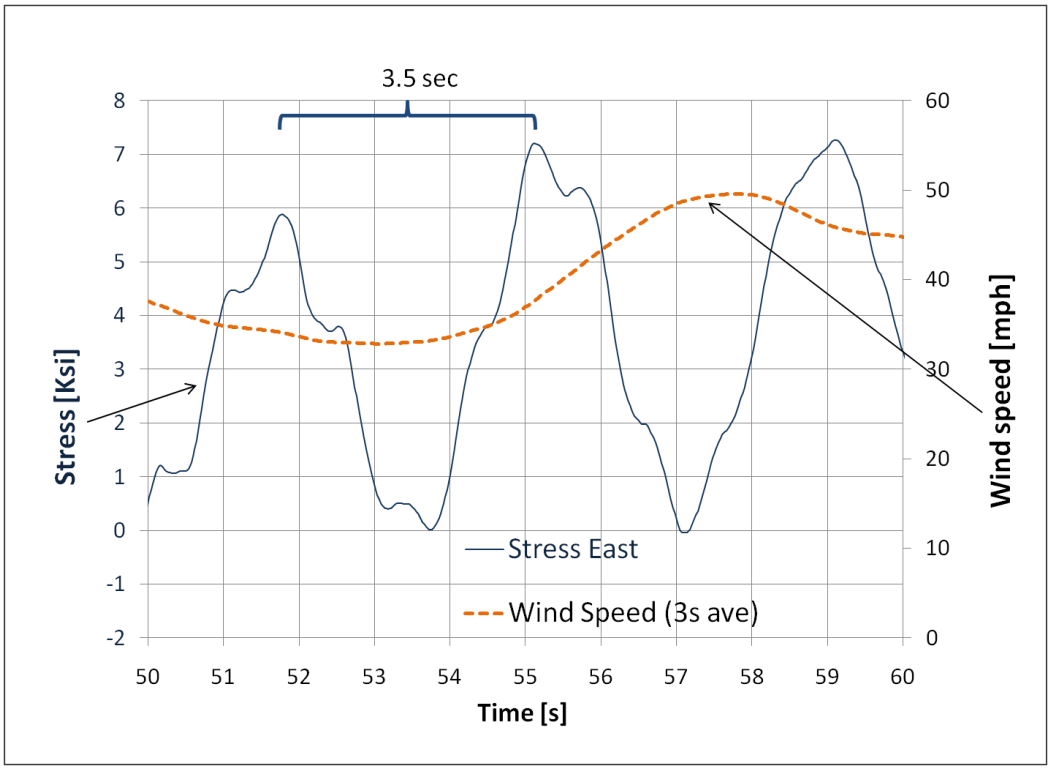

Figure 2.37: Event recorded on the El Paso US-54 pole at a 50mph wind speed (Magenes, 2011)

In order to understand more about the dynamic behavior of the HMIPs, the data was analyzed in the Frequency Domain after performing Fast Fourier Transformation (FFT). In addition to the FFT, the cumulative Root Mean Square (RMS) was utilized to analyze the data produced in the Frequency Domain. This resulted in graphs showing the contribution of each mode in the total stress that the HMIP experiences at each case of triggering wind speed, as shown in Figure 2.38.

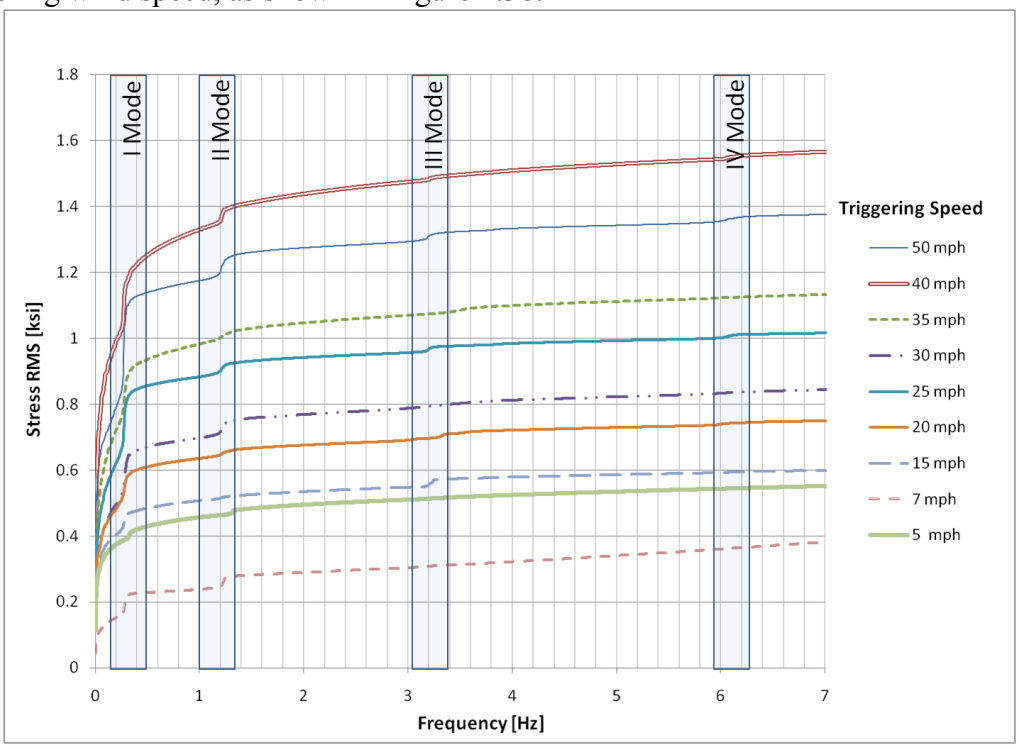

Figure 2.38: Cumulative RMS of stress records at different triggering wind speeds (Magenes, 2011)

As it can be shown from Figure 2.38 the main contributor to the stress generated in the HMIP is the static wind push. Among the natural vibratory modes, the first one contributes the most to the stress generation. It can also be observed that that the second mode generates stresses comparable in intensity with the first mode when wind speeds are

close to the critical vortex shedding speed (≅ 7 mph). Finally, it is shown that the third and the fourth vibratory modes have almost zero contribution in the stress state of the HMIP.

The previous results were demonstrated the behavior of the HMIP independently of their location. However, as the main target of the research was to estimate the remaining fatigue life of the HMIPs the rainflow counting for each location is of vital importance. The DAQ rainflow program resulted in the rainflow counting per day shown in Figure 2.39.

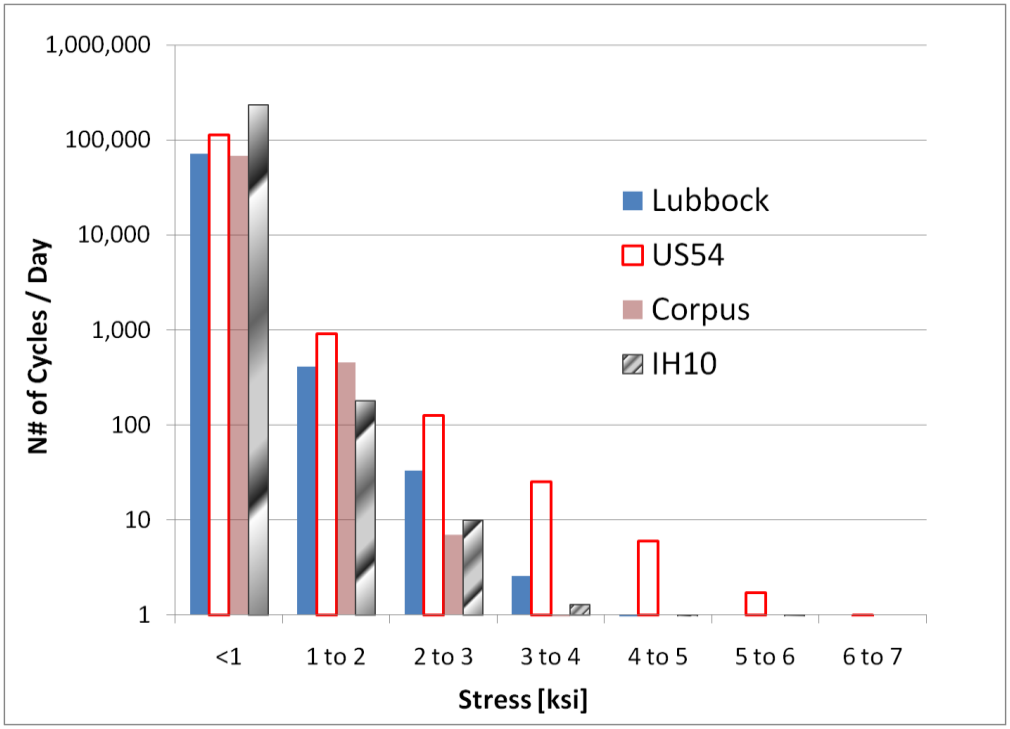

Figure 2.39: Rainflow Counting per day of record (Magenes, 2011)

As it can be seen from Figure 2.39 the tendency was the same in every location, however, the values can vary significantly. Following, the value of A/day is calculated as the sum of the products $N \cdot S_r^3$. The ratio of the value of A as calculated from Phase III in poles with initial cracking to the aforementioned value is the estimated fatigue life of the

HMIP at a specific location with the specific wind characteristics assuming the linear damage theory (Miner, 1945). Selecting a constant amplitude fatigue limit and adjusting this result for a short term monitoring period the results of the fatigue life of the instrumented poles are presented in Table 2.7. Some of the results raised concerns about the decisions to be made on in-service HMIPs since the fatigue lives of the damaged poles were quite high.

Location	Fatigue Life (E') [years]	Fatigue Life (Cracked) [years]
EL PASO - US54	73	26
EL PASO - IH10	515	184
LUBBOCK	358	128
CORPUS CHRISTI	207	74

Table 2.7: Fatigue life estimate of the instrumented HMIPs

Summarizing, Phase V of the Study developed useful tools for estimating the fatigue life of an HMIP. However, to validate the results and engage decision making, test results that can be directly linked to the field study are needed, which is the primary purpose of the study outlined in this thesis (Phase VI). In this phase, the El Paso IH10 from the field studies was taken out of service and was fatigue tested in the Ferguson Structural Engineering Laboratory. The results of the tests can help to demonstrate the likelihood of crack propagation at service load levels. Such tests can provide an indication of the rate of this propagation and how this affects the long-term performance of the HMIP.

CHAPTER 3: EXPERIMENTAL PROGRAM

3.1 Introduction

This outlines the details of test setup and procedures that were used in the laboratory tests in the study. The primary purpose of the laboratory tests was to obtain a measure of the remaining fatigue life of an HMIP section that was removed from service in the field. The primary components of setup that was used in the investigation was identical to the setup from the fatigue tests conducted at Ferguson Laboratory on the HMIP sections that were outlined in Chapter 2. An overview of the components of the setup is provided as well as the instrumentation used for data collection is explained. In addition, the testing protocol that was used is described. Finally, procedures and methods developed and used for more accurate results through nondestructive testing is presented.

3.2 Testing Program

As the primary goal of this phase of this study was to determine the remaining fatigue life of the HMIP that was in service, the test setup used in the previous investigations on HMIPs at Ferguson Laboratory was utilized. As the specimens were slightly different from the previous phases some pieces of the previous test setups were modified.

3.2.1 SPECIMEN SPECIFICATIONS

In order to maintain meaningful comparisons from the previous tests that were conducted, , the overall dimensions of the test setup remained the same with previous phases. A factor that contributed to some of the decisions on the geometry of the setup are

the dimensions of the actuator, as well as the spacing of the lab floor holes that provide the support conditions that were envisioned. The dimensions of the specimens used during this phase of the study are shown in Figure 3.1. In addition to the section removed from the field, a new pole was fabricated and galvanized to facilitate the testing. The pole section that was removed from service was cut to the proper length and a reaction plate was welded to the specimen so that the specimen could be anchored to the floor at the ends (labeled points A and C in Figure 3.1. The components of the setup at the two ends of each pole segment consisted of the pin fixtures and load box that were fabricated in the previous phases of the study. These components are discussed in more detail later in the chapter.

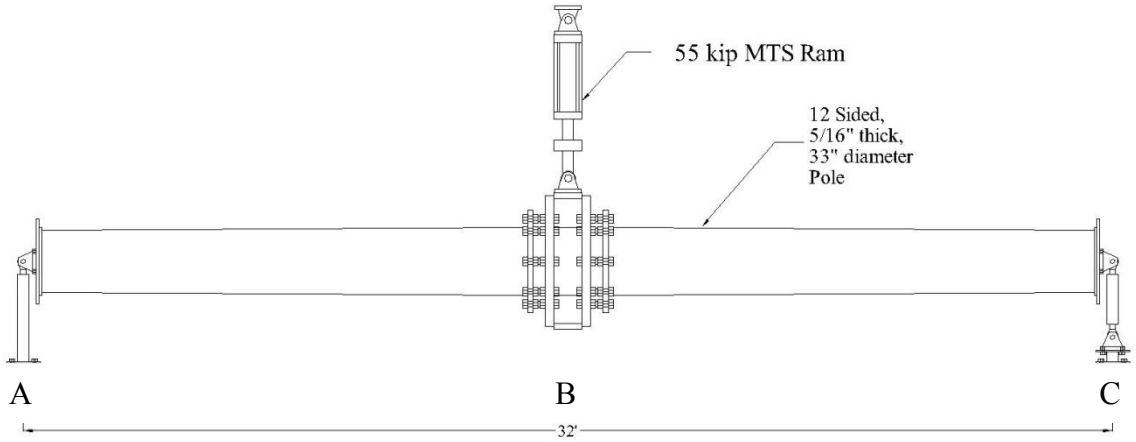

Figure 3.1: Test setup

3.2.2 NOTABLE PARAMETERS

The maximum stress range observed from the field studies conducted by Magenes (2011) was approximately 9 ksi. However, this was a single measurement that occurred during a storm and therefore represents a relatively rare event with respect to the fatigue performance of the pole. Figure 3.2 shows results from the rain flow counting based upon the number of cycles per day for 4 different sites from around the state of Texas from the

Magenes studies (2011). Although a stress range in the 1-3 ksi is likely more representative of predominate stress ranges that occur on the poles, a value of 5ksi ws selected to reduce the necessary time for the tests.

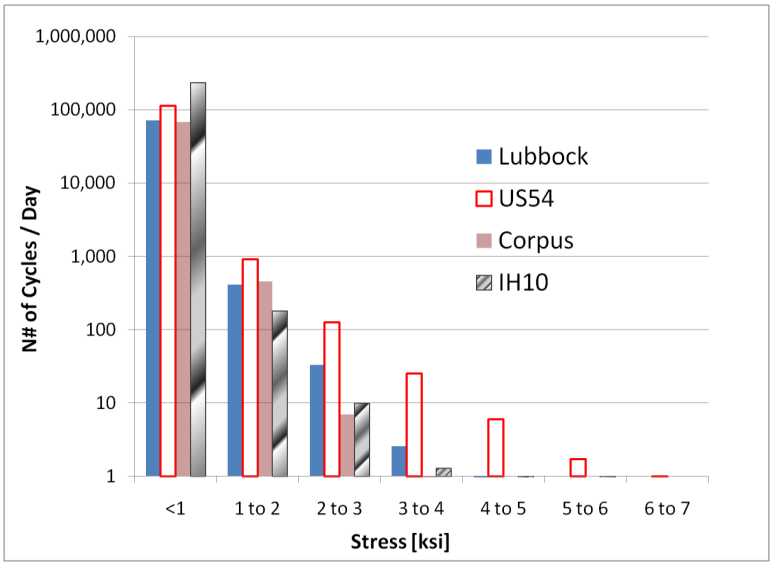

Figure 3.2: Rainflow counting per day of record (Magenes, 2011)

In Figure 3.2 it can be shown that the nominal stress range of 5ksi is an approximately upper bound of what an HMIP would experience during its service life in the absence of extreme events and thus, a reasonable value for the testing nominal stress range. In order to determine the necessary applied load to create this stress range the two pole segment shown previously in Figure 3.1 was idealized as a 32 ft. long beam with simple supports. The minimum nominal yield stress was chosen to be 4 ksi and the maximum nominal yield stress was chosen to be 9 ksi. The loads needed to produce the stress range of 5 ksi with the respective minimum and maximum yield stresses are presented in Table 3.1. The applied loads from the actuator caused the top of the HMIP assembly to experience tension in the top of the section and compression in the bottom of

the assembly. Therefore, the 5 ksi critical stress range occurred in the top of the section at the weld to the base plate.

Force (kips)	Nominal Stress (ksi)
41.78	9
27.68	4

Table 3.1: Forces required to produce 9 and 4 ksi nominal stress at the base of the HMIP

In order to verify that the above nominal stresses were applied to the connection, the stresses at a section away from the base plate (quarter points) were monitored with strain gages. In this way, the influence of local effects in the stress measurement was mitigated providing an accurate verification method of the nominal applied stresses. In addition, strain gages were also installed to the HMIP section in the vicinity of the welds to obtain a measure of the variation in the stresses near the welds.

3.3 Destructive Testing Setup

As noted earlier, many of the components of the setup were fabricated from previous tests on HMIP sections. A brief description of the primary components of the setup are provided in this section.

3.3.1 SUPPORTS

The simply supports at the end of the paired HMIPs were achieved using elevated rod-eyes as shown in Figure 3.3. The apparatus that was used at the north end of the section provided a single rotational degree of freedom and thus was a pin. In order to simulate a roller on the opposing south end, two rod-eyes were connected through a steel pipe providing rotational and translational degrees of freedom.

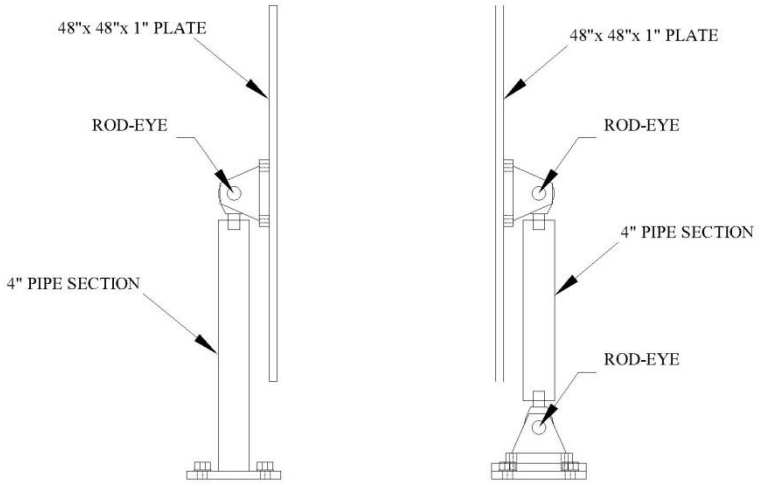

Figure 3.3: Test setup end supports

3.3.2 LOAD BOX

The apparatus that joined the two HMIP sections and provided continuity of the system is referred to as a load box. In addition to the continuity between the two HMIP sections, the load box also provides the connection point in the setup to the actuator that displaces the specimens and induces the desired stress range. A schematic of the load box is shown in Figure 3.4. The connections between the load box and the HMIP sections were made with threaded rods that are similar to the anchor rods used to connect the poles to the foundation in the field. The anchor bolt connections to the load box provide a good simulation of the stress flow that occurs in the base plates of poles in the field. The load box that was used was originally fabricated with an anchor rod pattern based upon the HMIP geometry had a 12 bolt pattern; however the pole that was removed from the field only had 10 bolts around the circumference. The load box had to therefore be modified to

fit the anchor bolt pattern from the specimen in the field. The shifted holes can be observed in Figure 3.4.

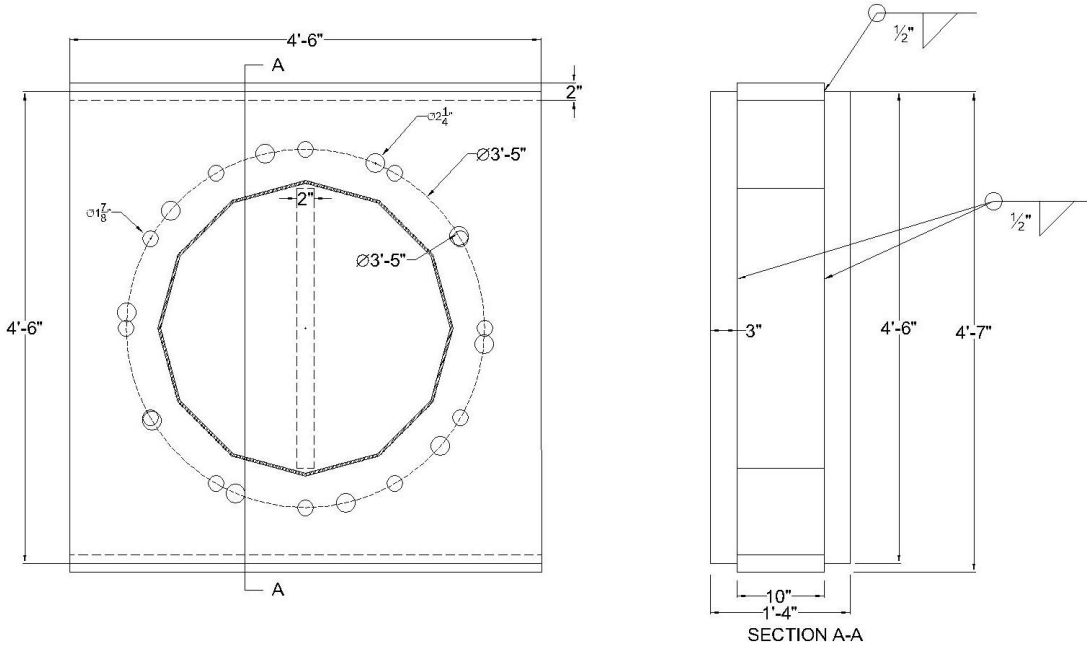

Figure 3.4: Design of Load Box

3.3.3 HYDRAULIC ACTUATOR, CONTROL SYSTEMS, AND TESTING PROCEDURES

Consistent installation procedures were followed for the tests to ensure that the support conditions simulating a simply supported beam were maintained. As this testing procedure was developed at the University of Texas at Austin during previous phases, the methods proposed and documented in Phase II (Stam, 2009) were followed in the tests. The purpose of this procedure is to ensure uniform boundary conditions along the perimeter of the baseplate supports.

A 55 kip MTS hydraulic actuator was used to cycle the specimens through the desired range of tensile stresses. The actuator was controlled using an MTS Flexcontrol hydraulic control unit. The force and displacement of the actuator was monitored using

the integrated load cell and linear voltage displacement transducer (LVDT) in the MTS actuator. The test was run in displacement control mode with the maximum and minimum displacements determined by manually measuring the displacement for a given force level in the actuator. In order to be consistent with the all the previous phases of this study, the test was terminated when 10% loss of stiffness was measured.

3.4 Instrumentation

3.4.1 Strain Gages

Bondable, 350-ohm, foil strain gages were used for the stress measurement at the desired locations. Before the application of the gages, the galvanizing layer was removed for better adhesion and accuracy of results. In addition to removing the galvanizing layer, gage installation methods were followed to ensure a good bond was achieved between the gages and the base metal. To protect the adhesive from humidity, a micro-crystalline wax coating was applied shortly after the gages were installed. The locations of the gages are outlined in the following sections.

3.4.2 Gage Locations

The gages were placed throughout the cross-section. Specifically, they were placed in pairs (in line with no gap between them) as shown in Figure 3.5 at the bends and at flats. The pair of gages was used to try to capture the stress gradient that is observed to occur at the shaft to base plate connection as observed in the analytical approach of these study (Stam, 2009).

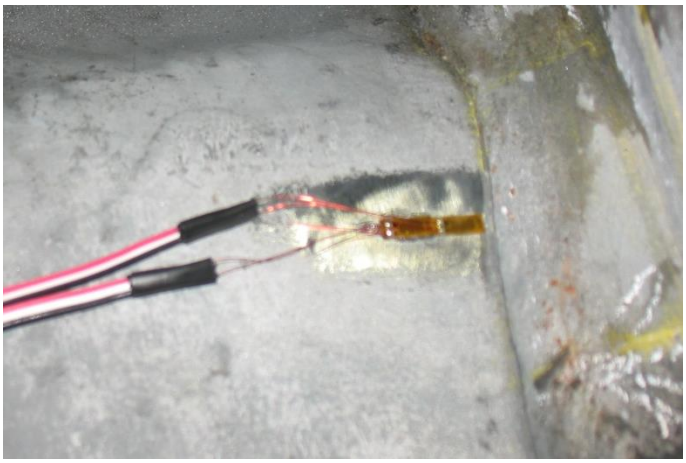

Figure 3.5: Typical strain gage installation

Each pair of strain gages was placed at the place where maximum tensile stress range was expected to occur during each phase of the tests that were conducted on the HMIP sections. As is discussed later in this thesis, the specimens were rotated so that multiple tests could be conducted on the HMIP. For example, when a crack formed and began to approach the critical stage, the specimen could be rotated so that the crack location is either at or below the neutral axis of the section. At the neutral axis of bending, the imposed bending stress is zero, while if the crack is below the neutral axis, the section is subjected to net compression during the tests. Because the specimen was rotated, multiple sets of strain gages were necessary around the HMIP sections.

Based upon the results the stress concentration factor (SCF) was calculated and also the progression of the crack growth, if any, was monitored. This was observable as, with crack formation and propagation, stresses are released leading to potentially zero stresses (free end stress) when the crack was fully open.

Moreover, pairs of strain gages were placed throughout the portion of the cross-section that was in tension during the fatigue test. Figure 3.6, Figure 3.7, Figure 3.8, and

Figure 3.9 show the position of the strain gage pairs along the cross-sections of both test specimens for each test. The figures of the pole removed form service show a structural member that passes across the diagonal of the pole. The structural member consisted of steel channel that was welded between the channel and the wall of the high mast pole. The channel serves has an anchor for a winch system that is used to raise and lower the lighting ring when bulb replacement or other maintenance is necessary.

In the "new" pole that was fabricated as a companion for the pole removed for service, a large crack occurred that approached a critical size. The researchers worked with the sponsor to contract with a company that specializes in repairing high mast pole sections that have large cracks. Although the repair procedures and performance are discussed in more detail later in this thesis, no additional cracking was found in the pole after the repair. Since the gages were installed in the system after the cracking was observed and repaired in the "new" pole as shown in Figure 3.9, the position of the gages in the "new" pole remained unchanged as the pole didn't experience any failure of any kind after it was repaired.

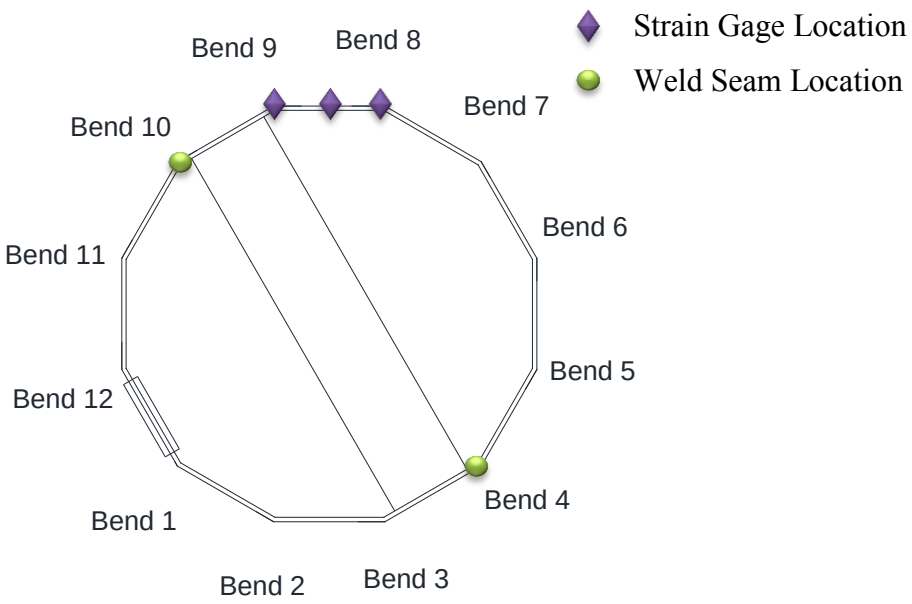

Figure 3.6: Orientation of in-service pole and location of strain gages during test #1

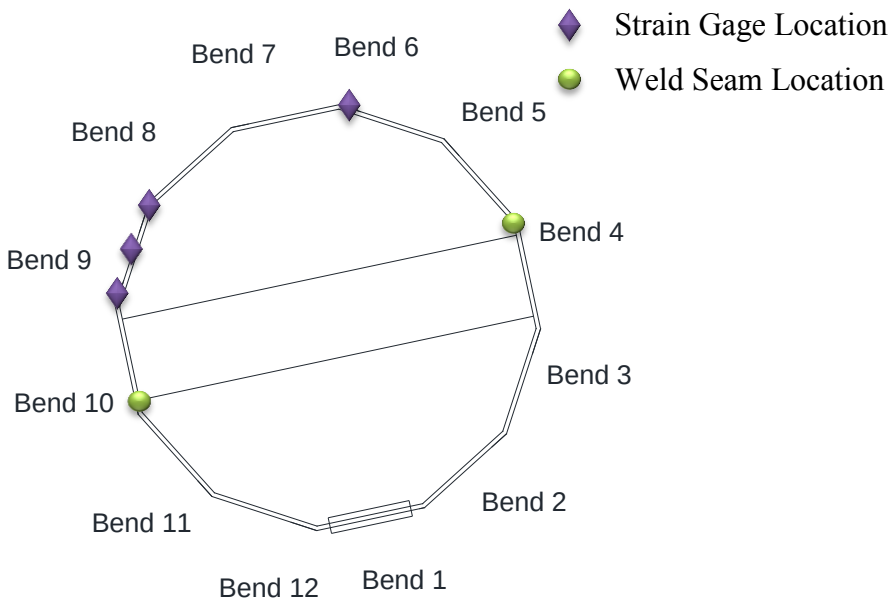

Figure 3.7: Orientation of in-service pole and location of strain gages during test #2

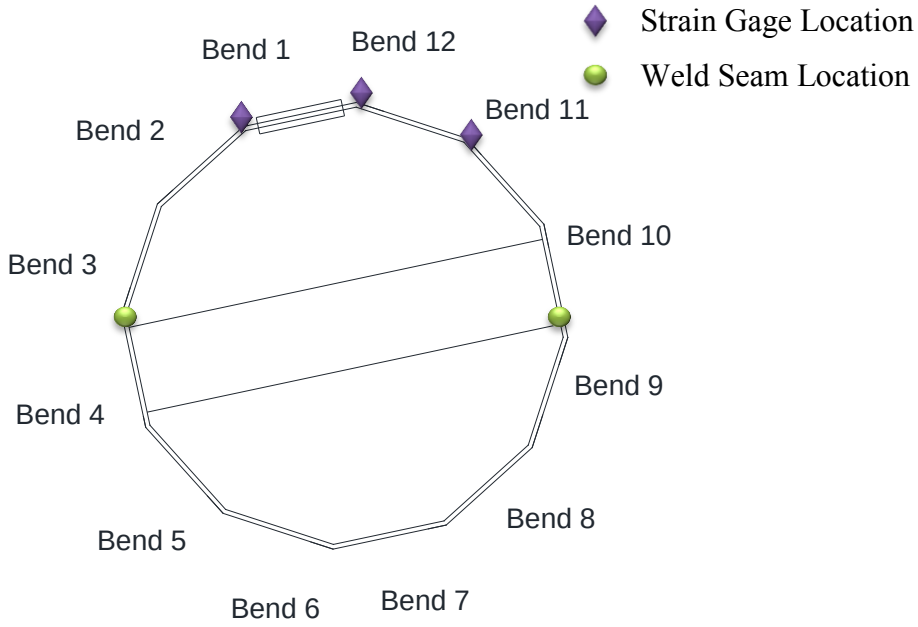

Figure 3.8: Orientation of in-service pole and location of strain gages during test #3

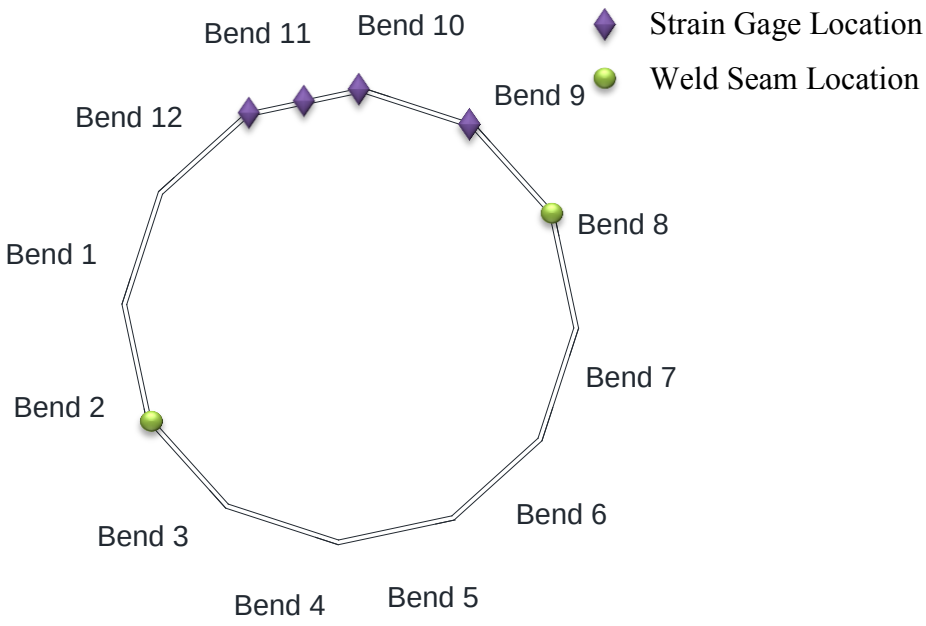

Figure 3.9: Orientation of "new" pole and location of strain gages during all tests

3.4.3 DATA ACQUISITION SYSTEM

The data from each pair of strain gages was acquired using a National Instruments (NI) CompactRIO 9024 system equipped with NI9237 modules to accommodate each channel. A program was developed in NI LabVIEW 2012 (Fasl, 2013) to store and process the data. The process involved automated counting of the number of cycles, calculating the force range experienced by the two-pole system, and evaluating the stress range experienced by the poles at each strain gage location.

3.5 Nondestructive Testing

In recent years, the field of Nondestructive Testing (NDT) of structures has experienced significant interdisciplinary developments in order to evaluate the condition, the remaining useful life, and the risk of failure of the structure. As its name implies, NDT

techniques generally have no (or a negligible) affect the serviceability of the structure. As a result, such techniques offer cost-effective tools in the decision-making procedure of repairing or replacing the HMIPs. During this phase of the testing, the applicability of Magnetic Particle Testing (MT) was tested, using the well-established techniques of Ultrasonic Testing (UT) that are often used in the aviation industry. Furthermore, as both testing methods under consideration were proved to be operator-dependent, charts facilitating the UT signal interpretation were developed.

3.5.1 ULTRASONIC TESTING

Ultrasonic Testing is a Nondestructive Testing method which uses high frequency sound waves emitted into a material to detect flaws and discontinuities. Ultrasonic Testing is based on the principle that in solid materials, sound waves are propagated through the material without reflection. These waves are created by a pulser/receiver and penetrate into the specimen through coupling with a piezoelectric transducer. When a discontinuity (e.g. crack or change of material properties) is located in the sound path, sound waves will be partially or entirely reflected as shown in Figure 3.10. The reflected sound signal is transformed to an electrical signal and the signal received by the transducer is shown at a display device in the time domain. Finally, based upon the velocity and orientation of the sound wave in the material, the specimen dimensions and the travel time in it the horizontal location (skip distance) and vertical location of the discontinuity (reflector) with respect to the transducer can be calculated as shown in Figure 3.11.

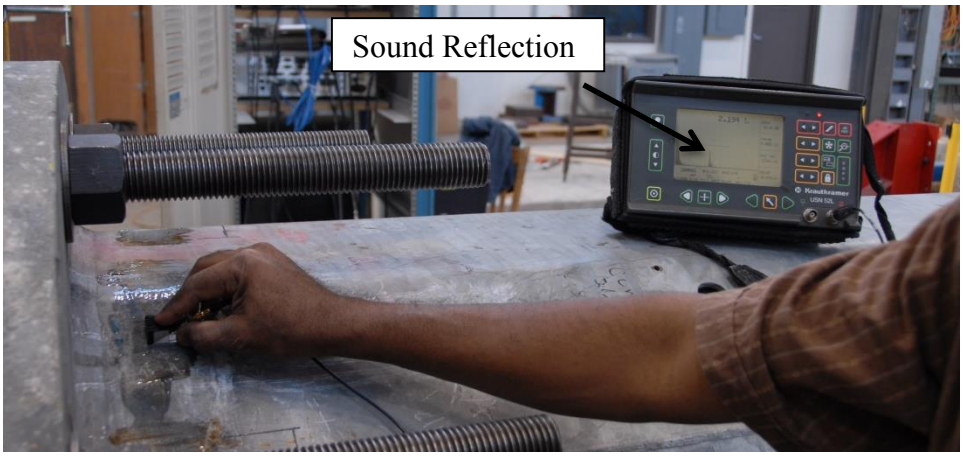

Figure 3.10: Technician performing UT on a HMIP while being tested at FSEL

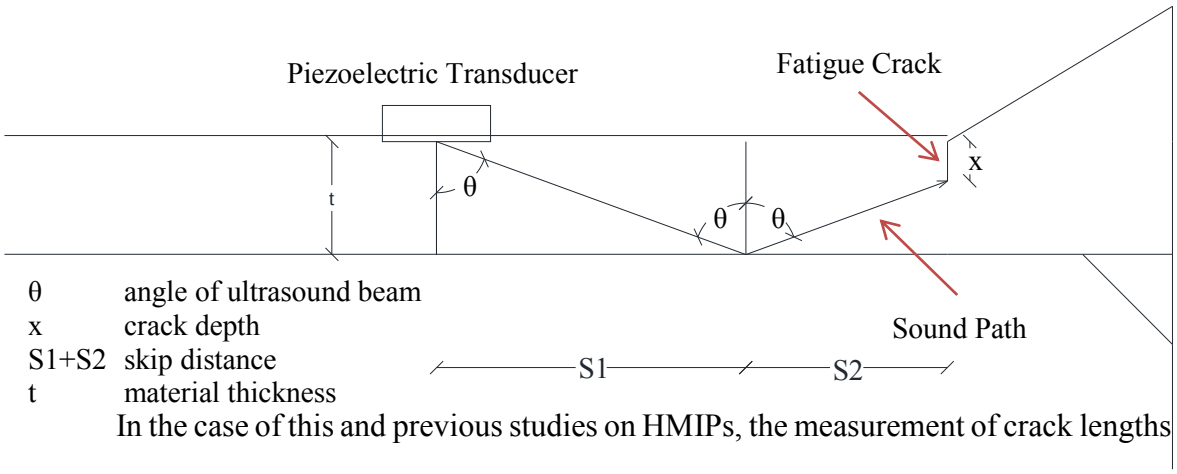

Figure 3.11: Typical Ultrasonic Test and test measurables

and depths initiated at the toe of the shaft to baseplate weld is of particular importance. However, it has been observed in the previous studies (Pool, 2010) that in some cases the fatigue cracks propagate in a direction different than normal to the shaft wall. This is inherent to the weld design as action and reaction forces are not concentric as depicted in the free body diagram in the figure below.

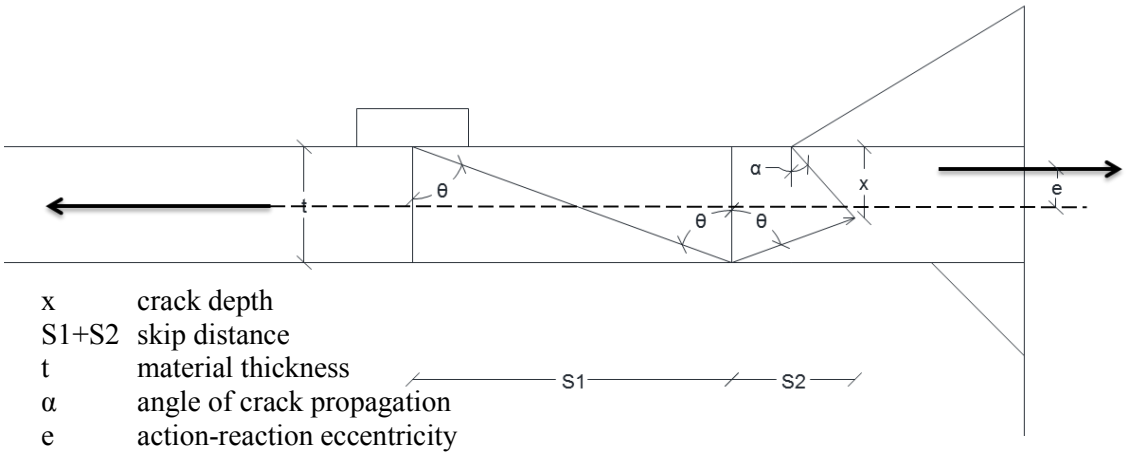

Figure 3.12: Eccentricity of action and reaction forces at the shaft-to-baseplate connection

Although the UT technique is a well-established method of testing in other industries such as aviation, there is no standard procedure for interpreting results in the field of structural engineering. Within the scope of this thesis, charts for UT operators on HMIPs were developed for the procedure to be standardized and thus results to be as objective as possible.

3.5.2 MAGNETIC PARTICLE TESTING

Magnetic Particle Testing is a nondestructive method which uses magnetic fields and their properties in ferromagnetic metals along with small magnetic particles to detect flaws in structural components. The basic principle of this testing method is that if iron particles are sprinkled at an area close to a defect in a material subjected to a magnetic flux (applied through an electromagnetic yoke), a cluster of those particles (easier to detect) will tend to bridge the gap of the defect providing the magnetic flux a shorter path as illustrated in Figure 3.13 and Figure 3.14.

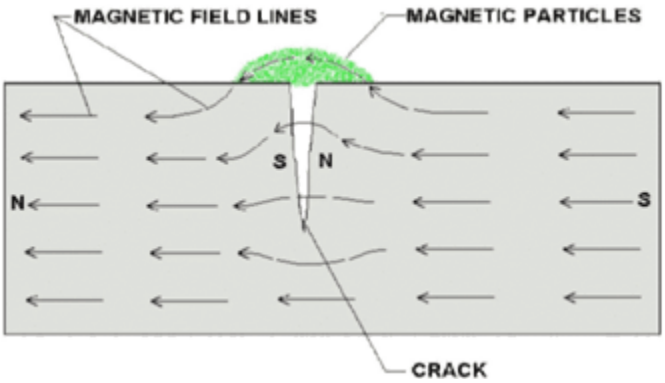

Figure 3.13: Magnetic flux in a ferromagnetic metal and magnetic particle accumulation at the defect location (image courtesy of www.ndt-ed.org)

Although MT is a user-friendly method that has a success rate with relatively low frequency of operator-dependent differences in defect detection, there are several drawbacks listed as follows:

- The method can only detect surface flaws;
- The method cannot estimate the depth of the defect;
- The method can be applied only to ferromagnetic metals (aluminum is a non-ferromagnetic metal)

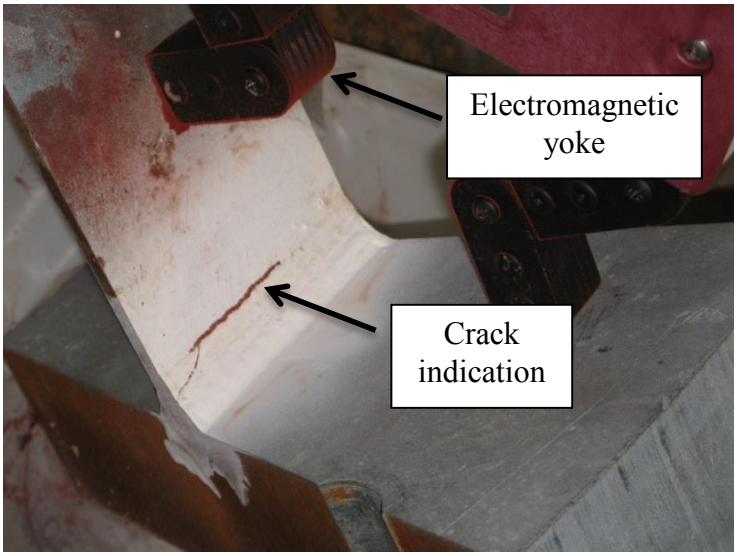

Figure 3.14: UT performed on a section cut of a HMIP (white powder is paint for making the iron particle more detectable)

The procedure that was utilized is listed as follows:

- Removal of galvanizing (optional)
- Cleaning the area prior to applying UT
- Applying UT (Figure 3.14)
- Measuring the defect length
- Demagnetizing the tested component
- Cleaning and applying galvanizing paint

Within the scope of this study, was the research of the applicability of MT on HMIPs in field conditions with in-service poles, as debris and galvanizing could affect the results.

3.6 Summary

This chapter presents the experimental program followed to acquire the results that are presented in Chapter 4. Researchers tried to validate destructive and nondestructive techniques in the field of structural engineering for the components under consideration. This led to the development of tools (charts, procedures) for facilitating the procedure of testing and improving the credibility of the acquired results.

CHAPTER 4: RESULTS

4.1 Introduction

Results are presented in this chapter from both the analytical and experimental phases of the study on HMIPs. A detailed overview of the data collected is provided as well as a discussion of the experimental and FEA results. Finally, results from the non-destructive tests are presented.

4.2 Strain Gage Results – Stress Monitoring

Strain gages that were installed on the HMIPs provided key data during all of the tests. A key role of the strain gages was to provide a measure of the Stress Concentration Factors (SCF) in the experiments. Results from the experimentally measured SCF were compared with results from the FEA studies and provided a basis for fatigue evaluation. Another purpose of the strain gages were to provide a measurement of the stresses for the purpose of monitoring the stress variation at locations close to the toe of the weld along the perimeter of the cross-section. In the following subsections, the SCFs that were calculated according to the Det Norske Veritas (DNV) method are presented and compared with the SCFs obtained through FEA studies. Multiple orientations of the HMIP removed from service in El Paso were used in the experiments. Each of the orientations is referred to as a test in the following subsections.

4.2.1 STRESS CONCENTRATION FACTORS (TEST 1 – EL PASO)

The orientation of the El Paso pole during Test 1 is shown in Figure 4.1. Bends 8 and 9 and the corresponding flat portion of the pole were positioned at the top of the test specimen. With this orientation, one end of the wench channel was also positioned near the top of the section. The location of the wench channel was 6 in. above the base plate.

Strain gages were placed at the bend locations and in the middle of the flat. Prior to Test 1, significant crack growth that had occurred in the field was observed at bend 8, while no crack growth could be recorded at bend 9. Initially, researchers hypothesized that the winch channel was acting as a stress reliever for bend 9. After conducting FEA studies for an undamaged connection researchers concluded that the stress profile at the bend is independent of the proximity to the winch channel (assuming it is located 6 in. away from the toe of the weld). Results obtained from the FEA studies regarding the stress profile for bends close and away from the winch channel are illustrated in Figure 4.2.

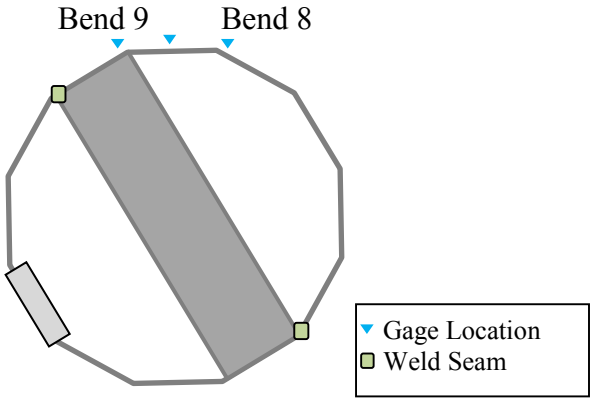

Figure 4.1: Orientation of El Paso pole and strain gage locations during test 1

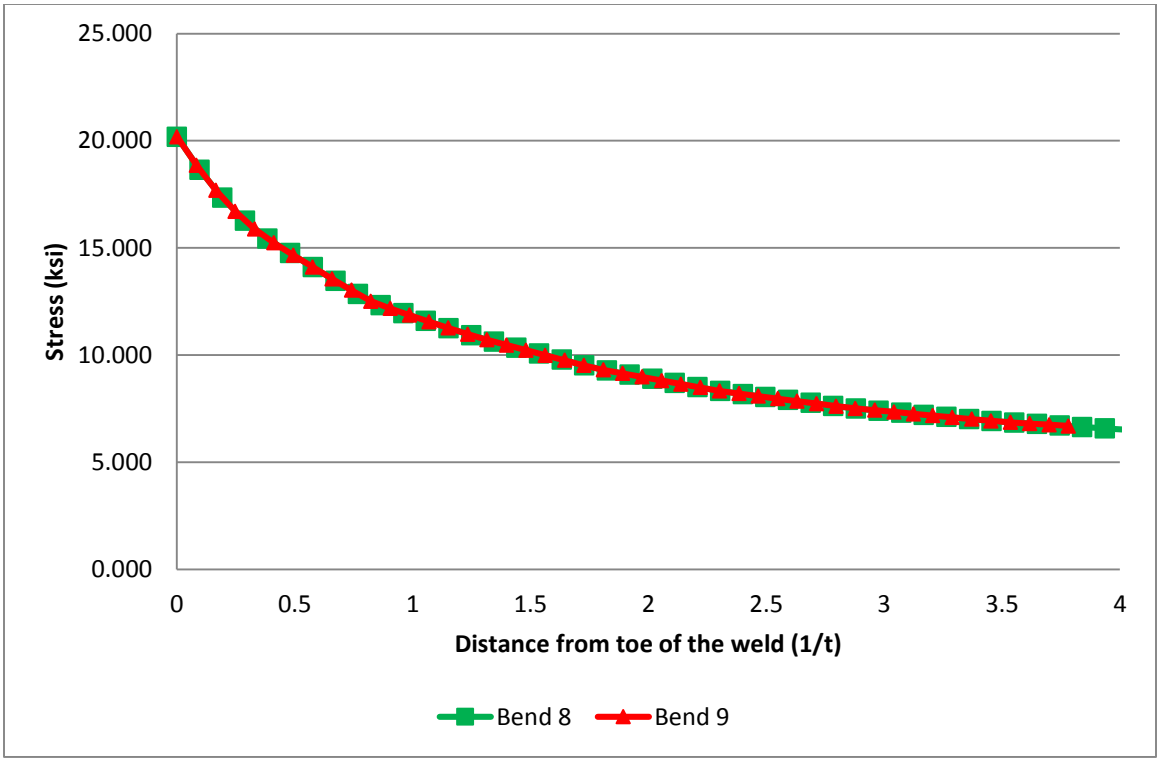

Figure 4.2: Stress profile close to the toe of the weld (FEA)

After studying the location of the pole and the geometry of the connection researchers concluded that the reasons leading to this behavior were the following:

- Bend 8 was unfavorably located in the field, as it was facing the direction of the stronger winds to which the HMIP was exposed.
- Bend 8 might have had a larger initial crack that may have occurred during fabrication and galvanizing, leading to more severe damage accumulation.

In order to achieve better bonding to the steel surface the strain gages were placed 0.16 in. away from the end of the bend. Figure 4.3 illustrates the FEA results for different locations along the perimeter of the cross-section of the pole. Note that the stress is raised significantly close to bends, justifying the initiation of the cracks at those locations. The

curves show FEA solutions at the bend locations and the flat locations on the pole. Two locations are shown for the bend locations, one at the weld location and one at the location where the strain gage was placed. Both bend locations have significantly higher stresses compared to the stresses predicted on the flats of the poles.

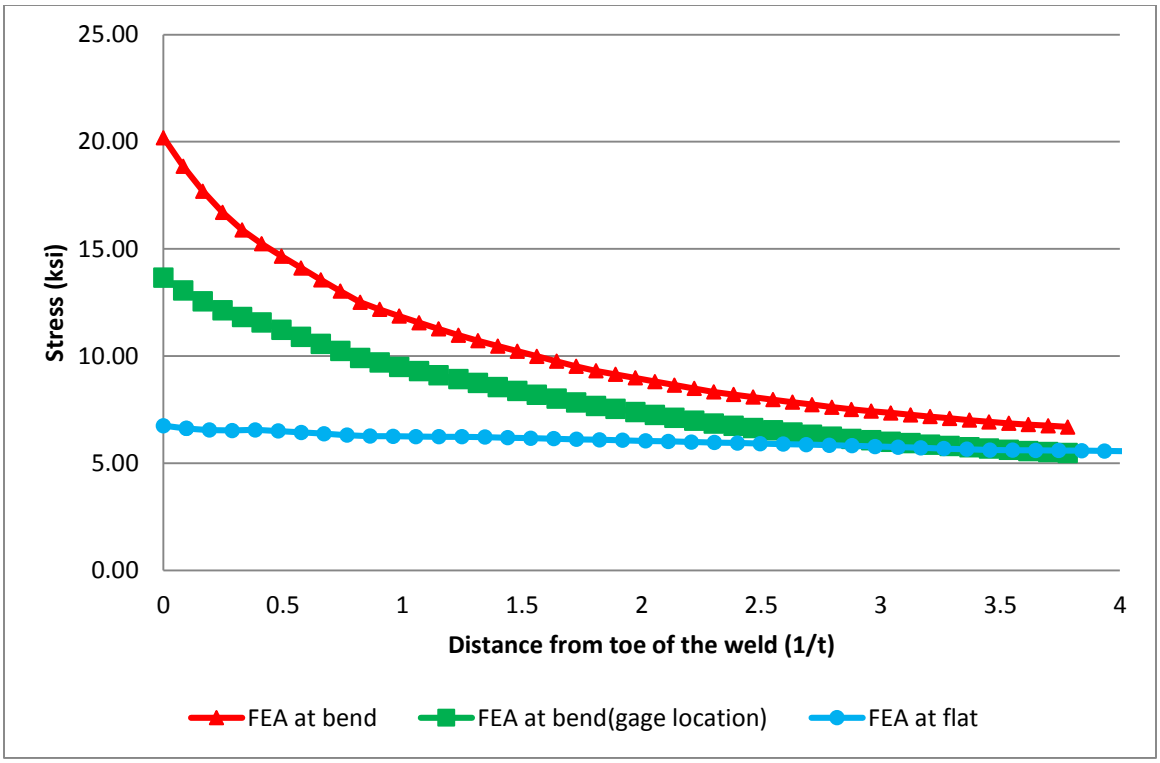

Figure 4.3: Stress profile for each location along the cross-section (σn= 5ksi)

Figure 4.4 and Figure 4.5 illustrate the stress rise close to the toe of the weld (distances up to 4t) as estimated by the FEA and as experimentally captured by the strain gages at the respective locations. The stress at the toe of the weld was extrapolated as per the Det Norske Veritas (DNV) method, from the stress values at distances of 0.5t and 1.5t. Due to the strain gage dimensions and in some cases the weld geometry the closest values

to those suggested by the DNV method were in the case of this study 0.6t and 1.8t respectively.

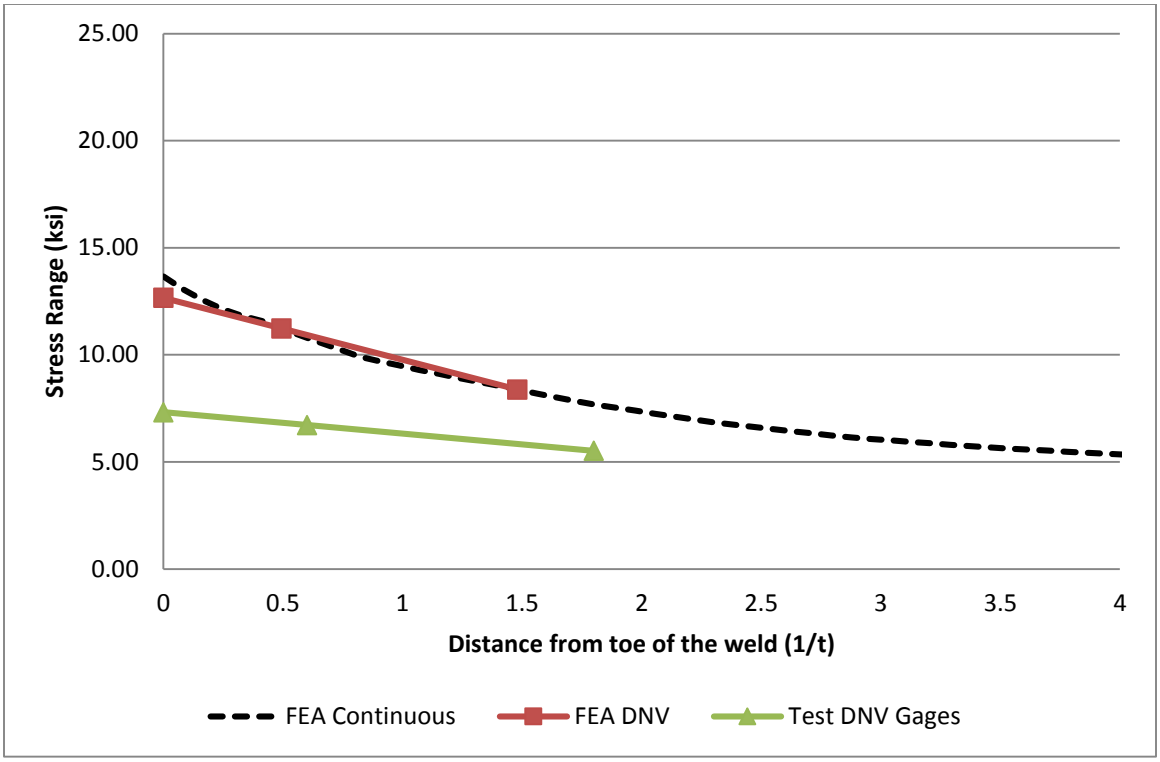

Figure 4.4: SCF - Test 1 - Bend 9

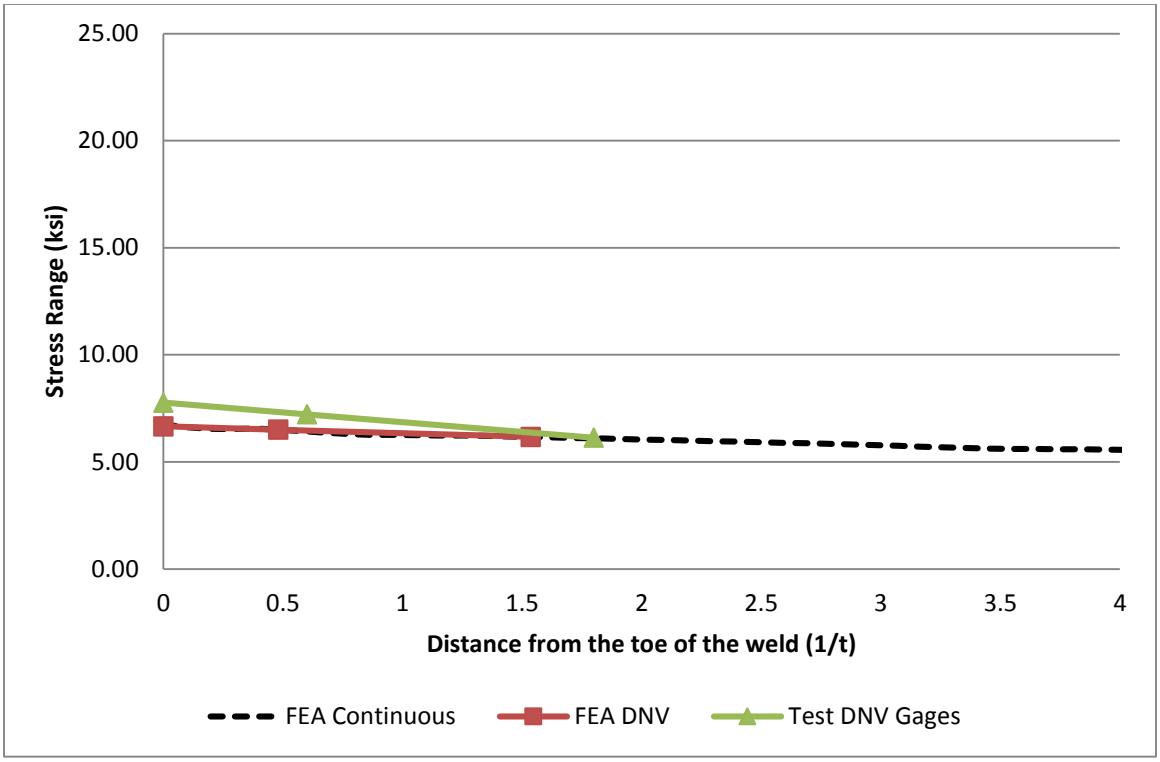

Figure 4.5: SCF - Test 1 - Flat (9-8)

The fact that the pole was previously in-service and was experiencing crack growth at the bend locations justifies that results presented in Figure 4.4 and Figure 4.5 show a closer agreement of experimental results with FEA results at flats than at bends. This is due to the fact that when a crack initiates from a surface and propagates through the thickness of the material, the stress flow changes towards the portion of the material that is continuous. As a result, the stress drop at the strain gage location is observed which should not be misinterpreted with a lower stress range acting in the connection. On the contrary, when a crack is initiated or propagating the stress range is increasing in the remaining cross-section, accelerating the damage accumulation procedure.

4.2.2 STRESS CONCENTRATION FACTORS (TEST 2 & 3 – EL PASO)

During Tests 2 & 3 the El Paso pole was placed with a bend being placed at the 12 o'clock position as shown in Figure 4.6 as opposed to the flat being placed at the 12 o'clock position in Test 1. In order to avoid the potential effects of the proximity to the winch channel Bend 12 and Bend 6 were selected to be placed at the 12 o'clock position. In addition to the winch channel effect, this configuration allowed for conducting 2 tests from the same pole. As the tests were "tension-only" tests, the lower part was always in compression which has minor impact to the fatigue life of the connection.

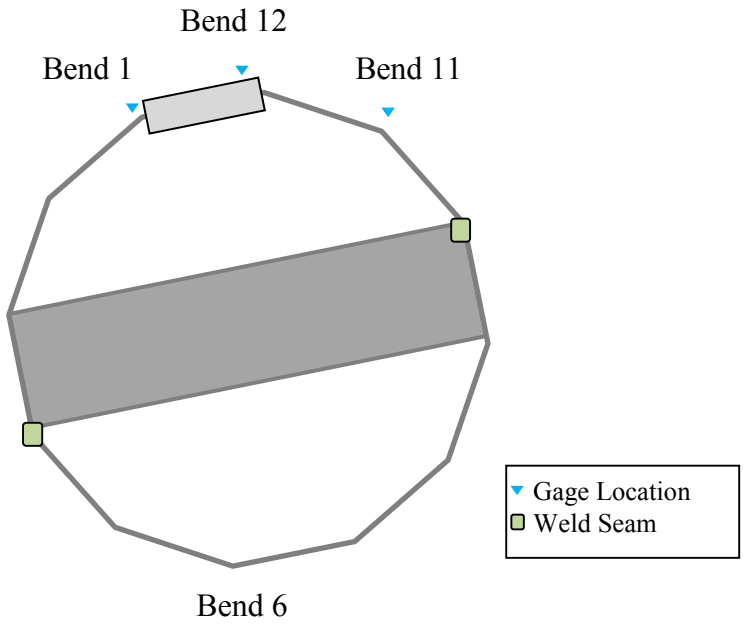

Figure 4.6: Orientation of El Paso pole and strain gage locations during tests 2 & 3

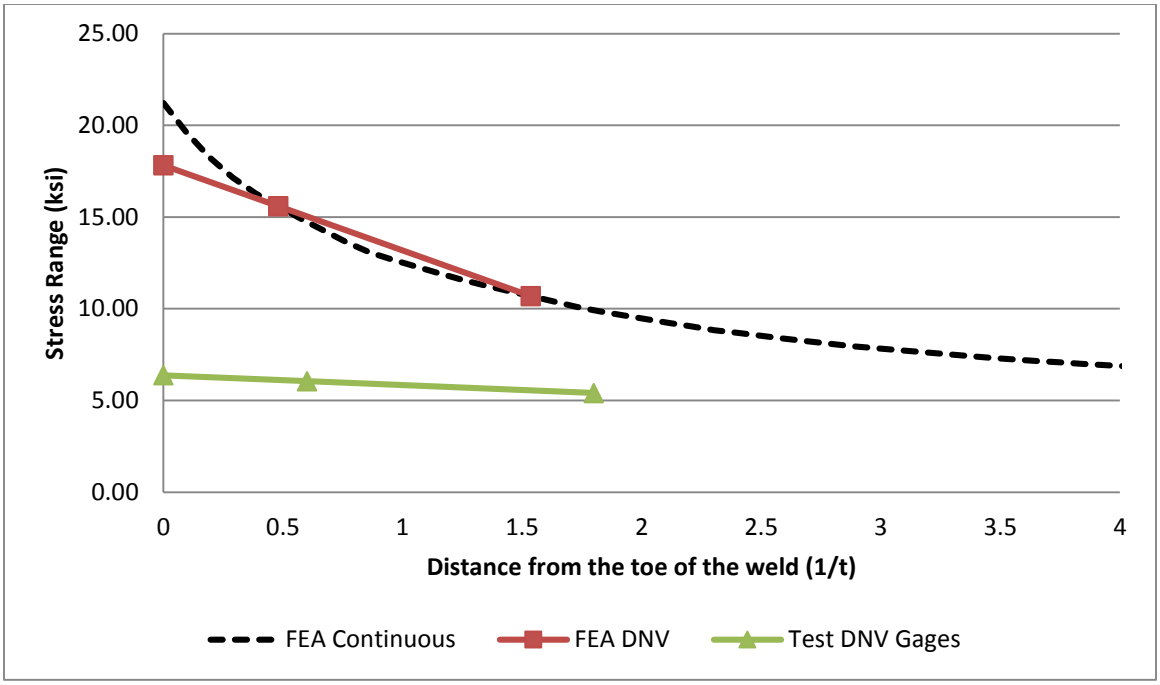

Figure 4.7: Stress profile close to the toe of the weld - Test 3 - Bend 12

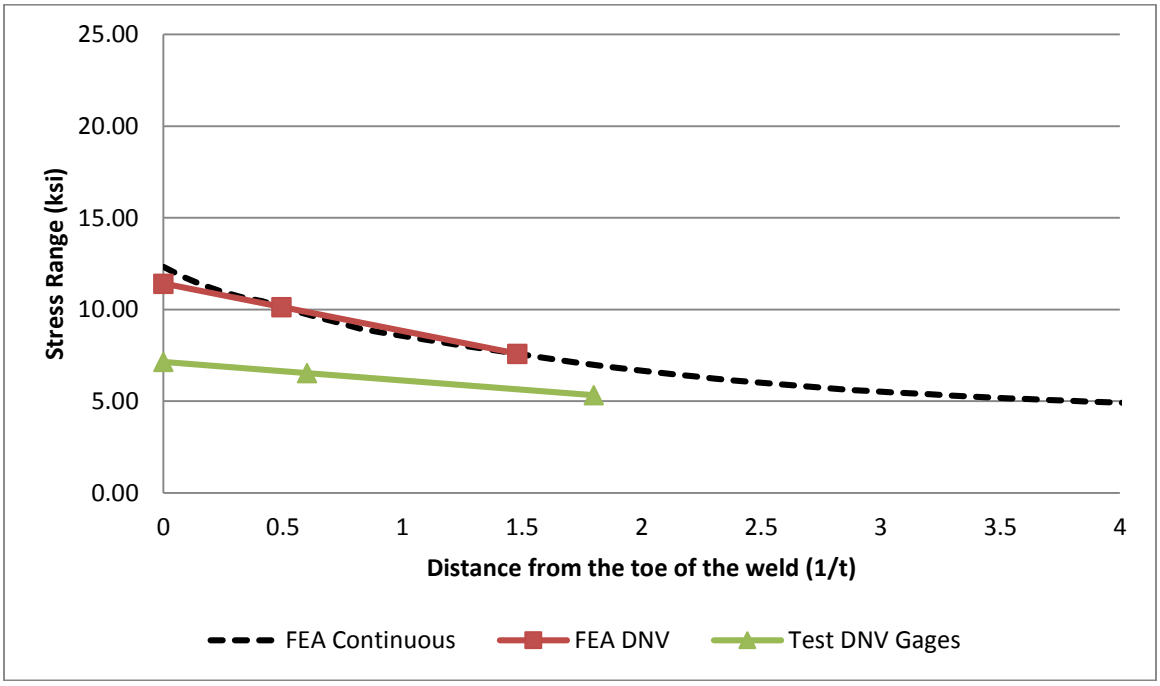

Figure 4.8: Stress profile close to the toe of the weld - Test 3 - Bend 11

Figure 4.7 and Figure 4.8 illustrate the experimental and analytical results for tests 2 & 3. The accuracy of the gage readings was again poorer at the location where the majority of the damage was occurring. This validates the hypothesis that the FEA can be a useful tool for analyzing undamaged poles, however non-destructive testing has to be conducted on a regular basis or field monitoring should be implemented in order to be able to evaluate the in-service condition of HMIPs.

4.2.3 STRESS CONCENTRATION FACTORS (TEST 1, 2 & 3 – S&S POLE)

Figure 4.9 depicts the orientation of the S&S pole during all the tests. Initially the pole was used as part of the test setup; however the pole failed before the El Paso pole. After its failure prior to the El Paso pole during Test 1, the pole was repaired and instrumented with strain gages at locations that are shown in Figure 4.9. As a part or the repair procedure the pole was subjected to ultrasonic impact treatment to improve the fatigue performance of the weld. A detailed description of the ultrasonic impact treatment procedure is described in Appendix A.

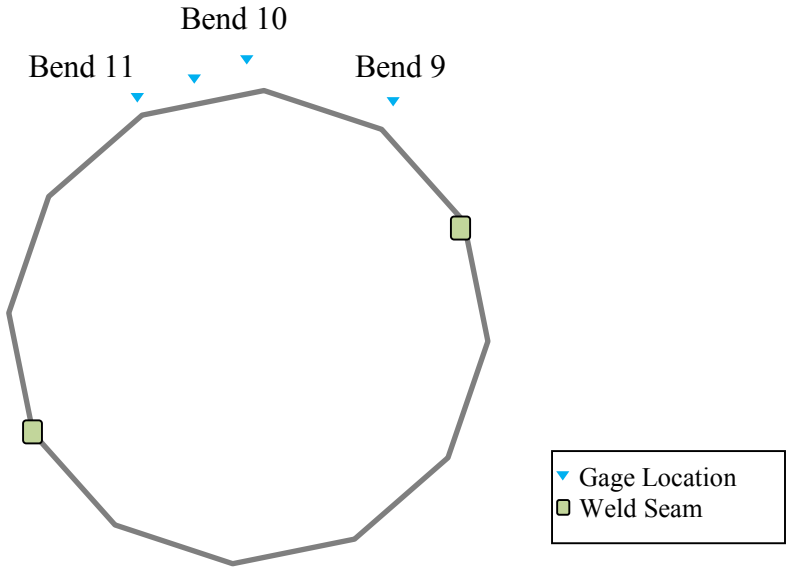

Figure 4.9: Orientation of S&S pole and strain gage locations during tests 1, 2 & 3

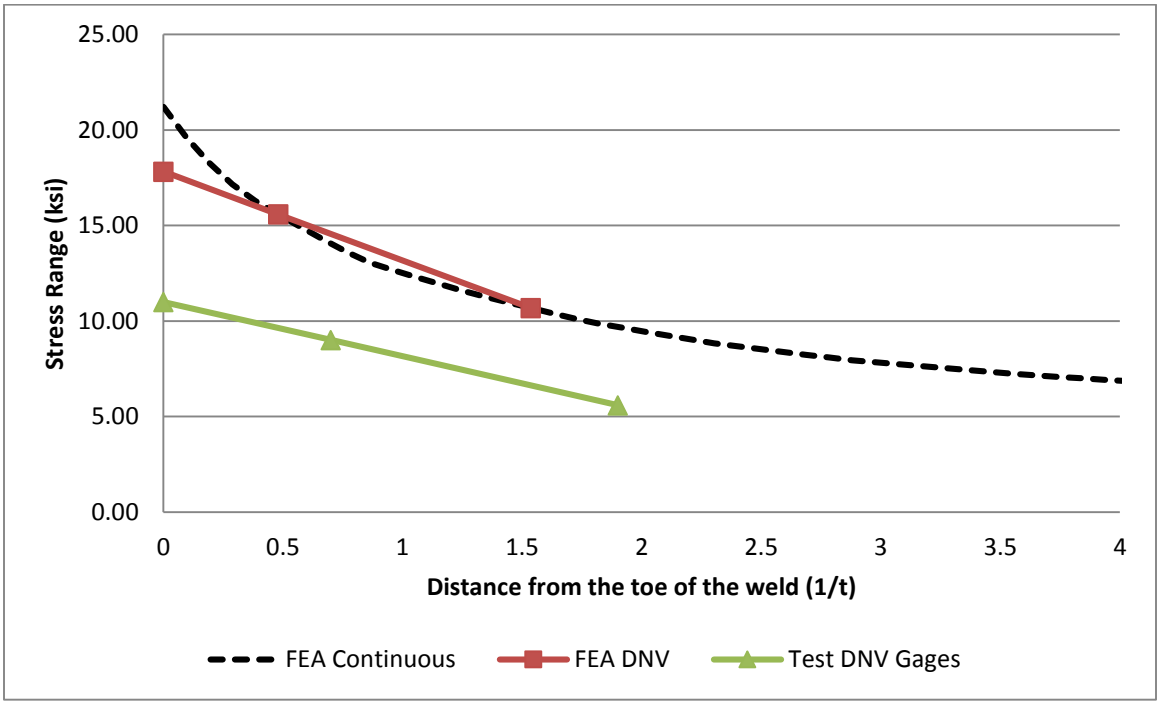

Figure 4.10: Stress profile close to the toe of the weld - All tests (S&S pole) - Bend 10

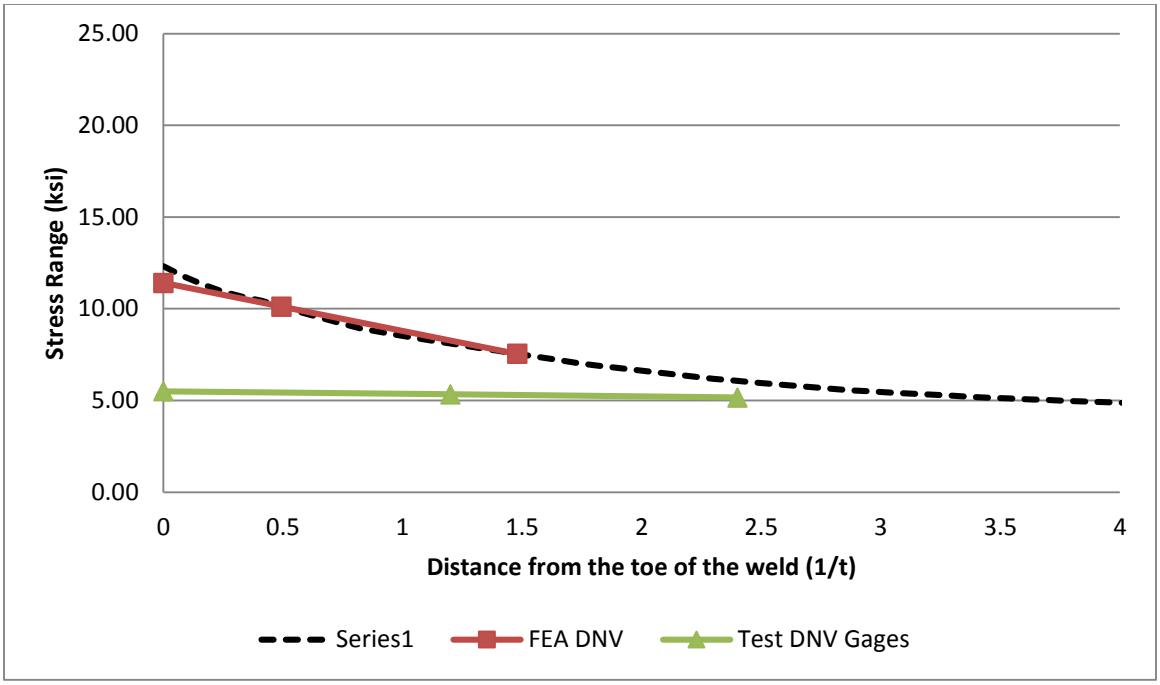

Figure 4.11: Stress profile close to the toe of the weld - All tests (S&S pole) - Bend 9 & 11

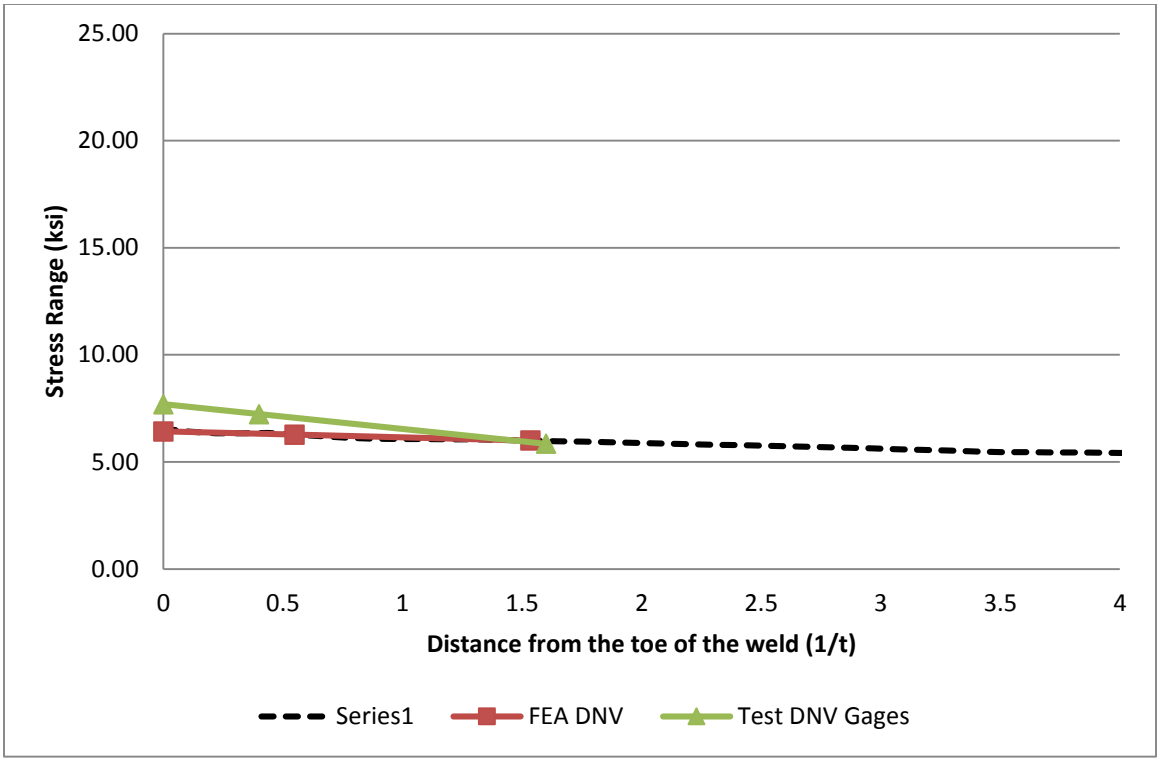

Figure 4.12: Stress profile close to the toe of the weld - All tests (S&S pole) - Flat 11-10

As can be seen from Figure 4.10, Figure 4.11, and Figure 4.12 while there is still a significant difference between the FEA and Test DNV results, the readings from strain gages in the case of the repaired pole are more closely related to the stresses predicted by the FEA than observed in the El Paso pole. A source that causes stress distortion close to the toe of the weld is the groove created by the UIT at the toe location, as can be seen in Figure 4.13. Another source of the inconsistencies can be the weld shape irregularity that was not modeled in the FEA studies.

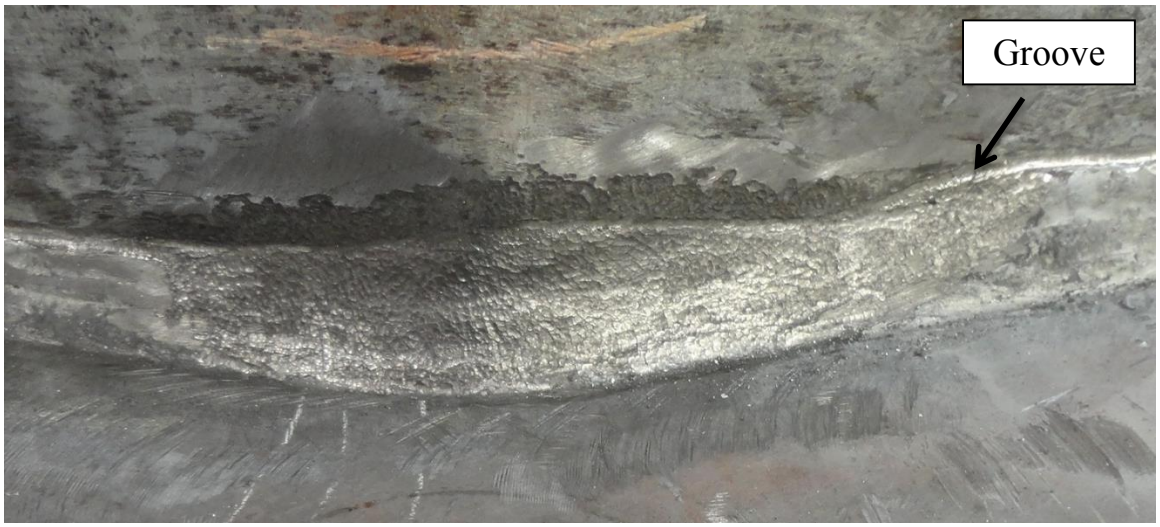

Figure 4.13: Weld after ultrasonic impact treatment

4.3 Fatigue results

In this sub-chapter, the results concerning the fatigue performance of the specimens is described. First the global test results are presented and then a representative recording of strain gages throughout the fatigue testing is introduced.

4.3.1 GLOBAL FATIGUE FAILURE

Figure 4.14 presents the summary of all fatigue tests conducted throughout this phase of the HMIP study. In the figure, solid markers indicate terminated tests whereas the hollow marker indicates a non-failure test. Specifically, S&S 1 represents the first test which was terminated due to the failure of the companion specimen and S&S 2 the cycles which the repaired specimen experienced until the project was ended.

Considering the scatter of the fatigue tests, the results suggest that the pole experienced a relatively uniform damage in the field. Upon this assumption, valid predictions can be made with field instrumentation data.

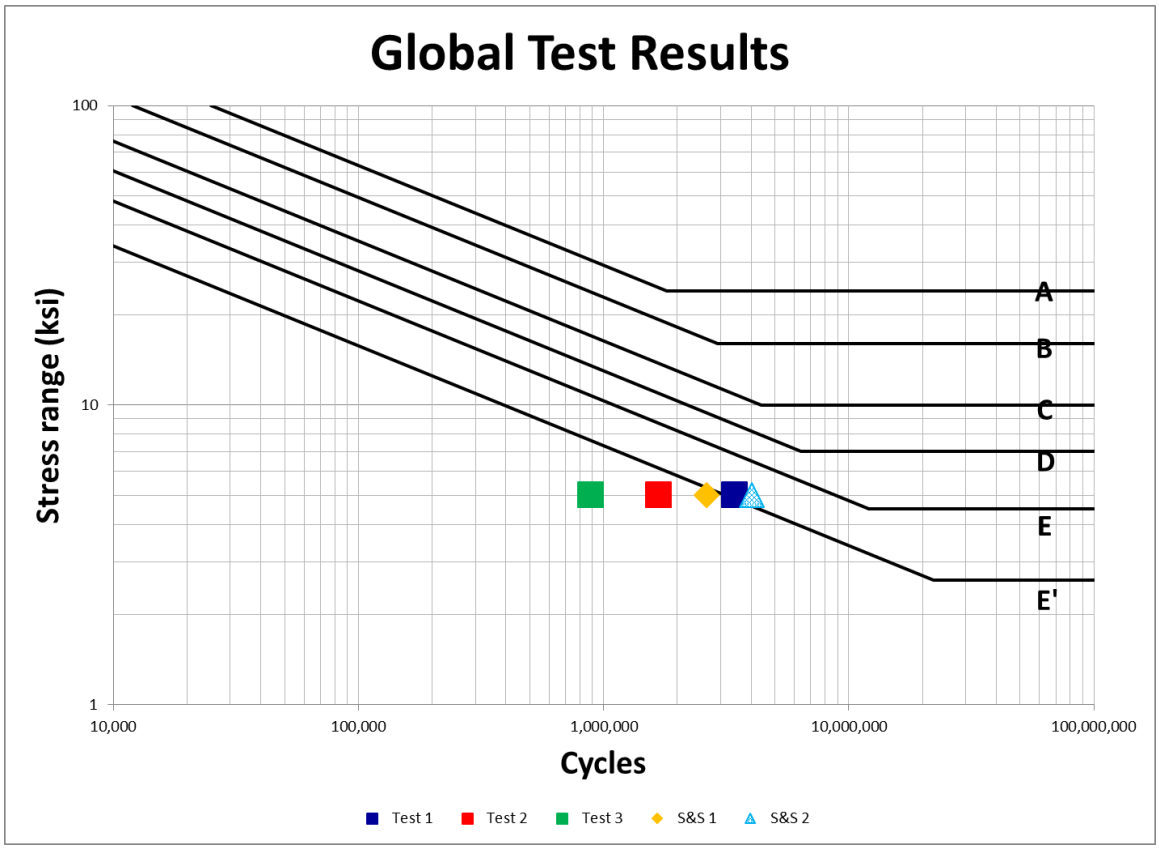

Figure 4.14: Global Test Results

Another outcome from this phase of the study is that the repaired and impact treated pole did not fail and that there were no evidence of cracks after the last test termination. This is encouraging repair as opposed to the replacement solution, especially when damage is observed.

4.3.2 CORRELATION WITH FIELD INSTRUMENTATION DATA

The main purpose of this research phase was the validation of estimating the remaining fatigue life of an in-service pole with field instrumentation data. To do so, the three tested details were kept either at the neutral axis or in compression prion to their testing. At the end of each test the fatigue coefficient A was calculated and compared with

the coefficient A proposed by Magenes. The results for all tests are presented and compared with the prediction in **Error! Reference source not found.**. As can be seen, all tests results are in reasonably close agreement with the estimates from the field instrumentation estimates. The divergence can be attributed to the inherent scatter of fatigue tests as well as the initial condition of the tested detail.

	Calculated Coefficient A	Calculated Remaining Fatigue Life [Years]	Estimated Remaining Fatigue Life (Magenes) [Years]	Difference (%)
Test 1	$1.5x10^8$	196	184	6.5
Test 2	$1.6x10^8$	209	184	13.6
Test 3	$1.1x10^8$	144	184	-21.7

Table 4.1: Remaining fatigue life based on laboratory testing

4.3.3 LOCALIZED STRESS RANGE DEGRADATION

Along with the monitoring of the number of cycles at which the HMIPs had lost 10% of their stiffness, the stress range at the gage locations was monitored as a result of the sinusoidal displacement that was imposed at the base of the pole. Figure 4.15 illustrates the rapid degradation of the stress range that was typically observed at locations were cracks were propagating once damage was accumulated. The “in” and “out” notation indicates the gage placed closer or further to the weld toe respectively.

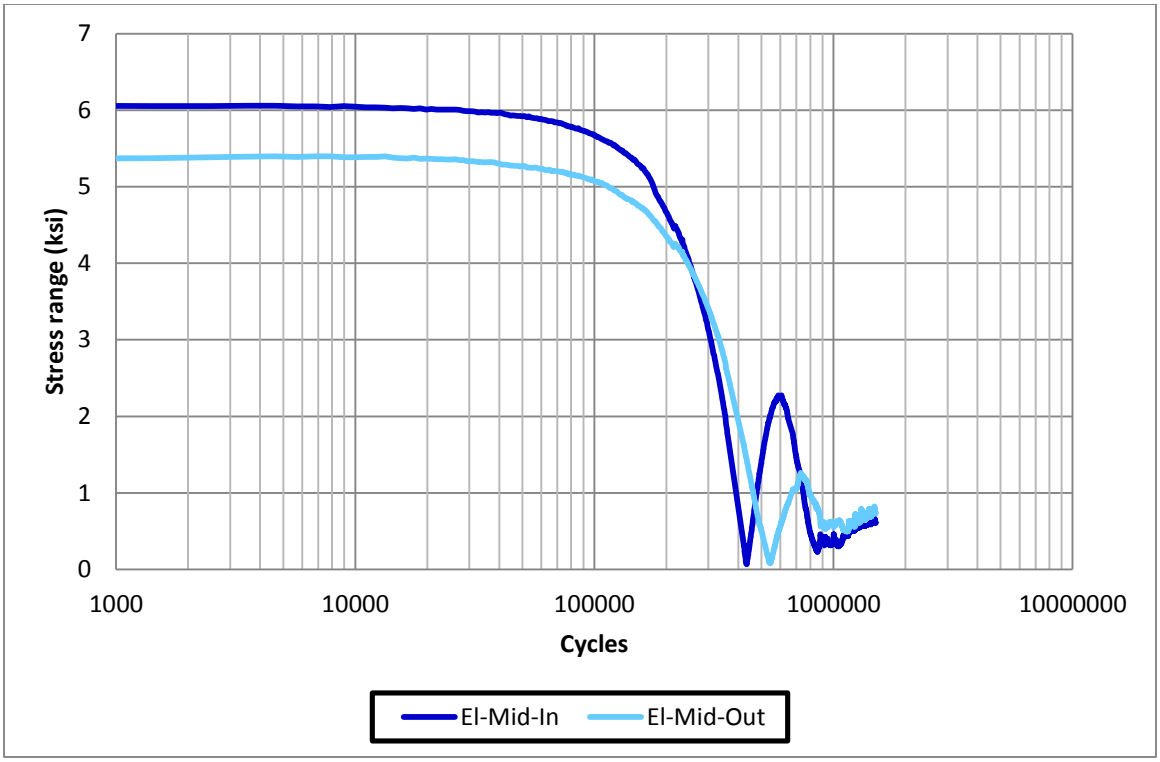

Figure 4.15: S-N curve (El Paso pole top shaft bend)- Test #3

As can be seen in the graph, after the stresses reached zero they increased and finally decreased to a level close to zero. This behavior can either be attributed to the crack interlock (destructive test pictures showed a non-plane crack surface) or to the potential redistribution of stresses while the crack was growing until the formation of a complete free edge.

Figure 4.16 illustrates the same data as Figure 4.15. The difference is that the data is acquired from gages close to the toe of the weld of a bend that had no initial cracking. As can be seen the stresses remained stable over the period of the testing and the minor fluctuations observed were due to the temperature change (affecting the oil pressure in the

hydraulics and the test setup) and required stops/restarts of the tests due to equipment maintenance.

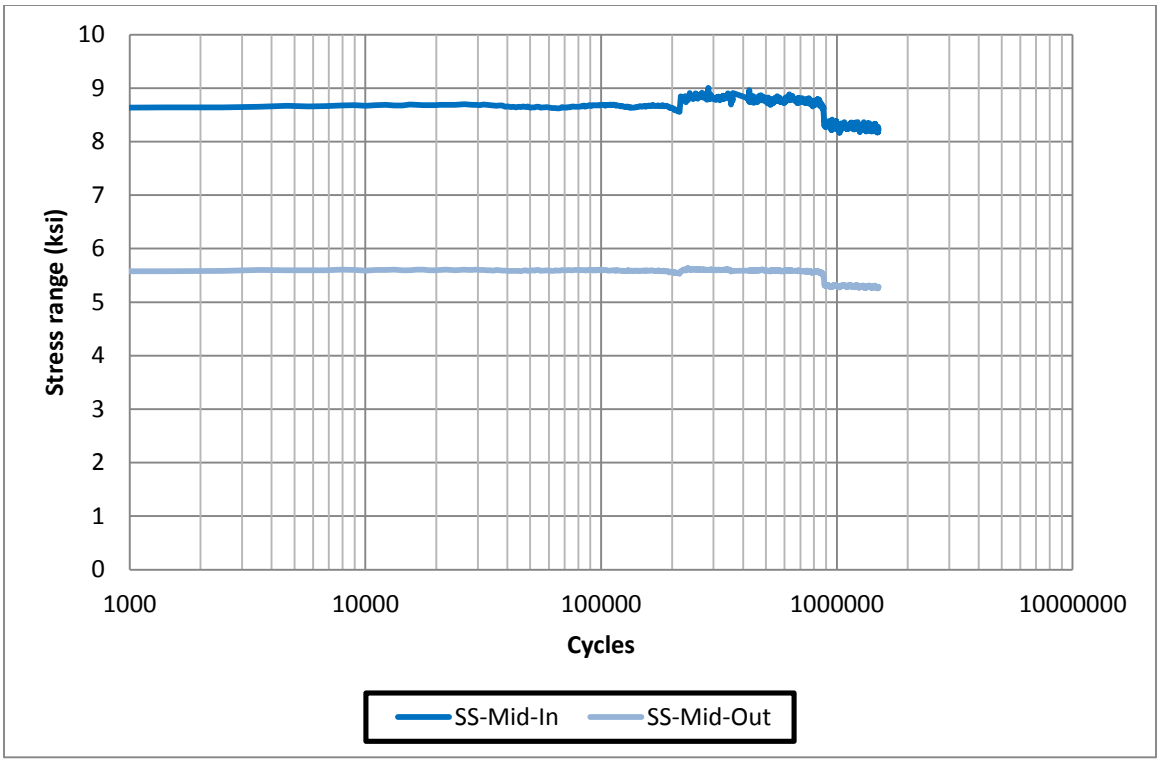

Figure 4.16: S-N curve (S&S Pole top shaft bend) - Test #3

4.4 Non-Destructive Testing

Non-Destructive Testing (NDT) is playing a major role in determining the reliability of in-service structures. One of the driving forces for NDT techniques are the comparisons between the increased cost of replacement as opposed to a potential repair if the damage can detected early and kept localized. In this study the Magnetic Particle Testing (MT) and the Ultrasonic Testing (UT) were used to determine the crack width and depth.

4.4.1 MAGNETIC PARTICLE TESTING

As its name imposes, MT uses particles that can be attracted by a magnetic field in order to locate cracks at the surface of a magnetically conductive material. Its limitation is mainly the ability to detect only cracks that have reached the surface of the metal. A major advantage of the technique is the ease of use, even by non-specially trained personnel.

For galvanized steel, the procedure for detecting cracks with MT involves the removal of the galvanizing as shown in Figure 4.17 and cleaning of the surface with pressurized air. The magnetic particles in the form of iron particles/filings are then applied, which may require the removal of excess particles. Once the magnetic field is applied, the iron particles interact with the magnetic field and provide an indication of the crack location which can be located and marked as shown in Figure 4.18. After the test, the specimen is demagnetized.

Figure 4.17: Galvanizing removal

Figure 4.18: Crack location and width using MT and UT

As can be seen from Figure 4.18, MT can be a reliable method for crack detection. However, in many cases MT did not detect any crack at locations where cracks were existent. Specifically, at locations where there was lack of fusion, MT could not differentiate the nature of the discontinuity (fatigue crack or lack of fusion).

In conclusion, MT can be proven a useful tool to detect the location or existence of cracks, however, is cannot be used to quantify the damage. The removal of the galvanizing

coating does not seem to have any major impact on the results obtained through MT. Finally, as questions were raised considering crack opening and closing over the year, MT was conducted under 5ksi nominal tension with no major effects in the MT results.

4.4.2 ULTRASONIC TESTING

Ultrasonic Testing (UT) is a Non-Destructive Testing method which uses high frequency sound waves emitted into a material to detect flaws and discontinuities.

4.4.2.1 Principles

Ultrasonic Testing is based on the principle that in solid materials, sound waves are propagated through the material without reflection. These waves are created by a pulser/receiver and penetrate the specimen through a piezoelectric transducer that is coupled with it. When a discontinuity (e.g. crack or change of material properties) is located in the sound path, sound waves will be partially or entirely reflected as depicted in Figure 4.19. The reflected sound signal is transformed to an electrical signal and the signal received by the transducer is shown at a display device in the time domain. The horizontal location and vertical location of the defect within the material are a function of a number of aspects related to the geometry of the specimen. These aspects include the velocity and orientation of the sound wave in the material as well as the specimen dimensions and the travel time in the material. Considering the geometry and sound wave velocity, the horizontal location (skip distance) and vertical location of the discontinuity (reflector) with respect to the transducer can be calculated.

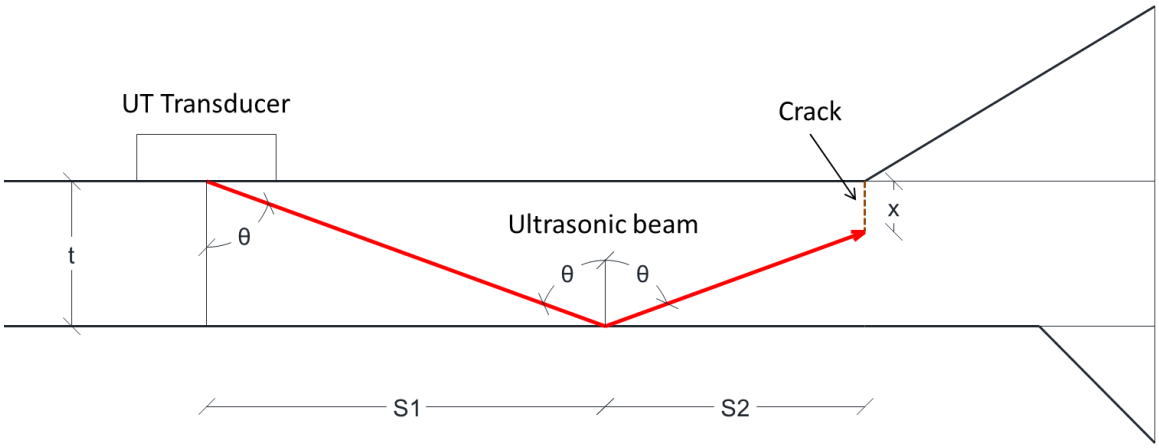

Figure 4.19: UT beam path

In the case of this study, the measurement of crack lengths and depths, initiated at the toe of the shaft to baseplate weld is of particular importance. However, it has been observed (Stam, 2009) that in some pole cases the fatigue cracks can propagate in a direction different than normal to the shaft wall. This is inherent to the weld design as action and reaction forces are not concentric.

In order to facilitate the operator of the UT equipment, graphs were developed for more accurate damage estimation. The first graph was developed to quantify the error in the readings if there was an inclined crack, based on the following equation:

$$e = \frac{x \cdot tan\varphi}{(2 \cdot t - x) \cdot tan\theta_p} \cdot 100, \qquad \text{Eq. 4-1}$$

Where e is the error (%) in the measured skip distance, x the crack depth, φ the crack inclination and θ_p the probe angle.

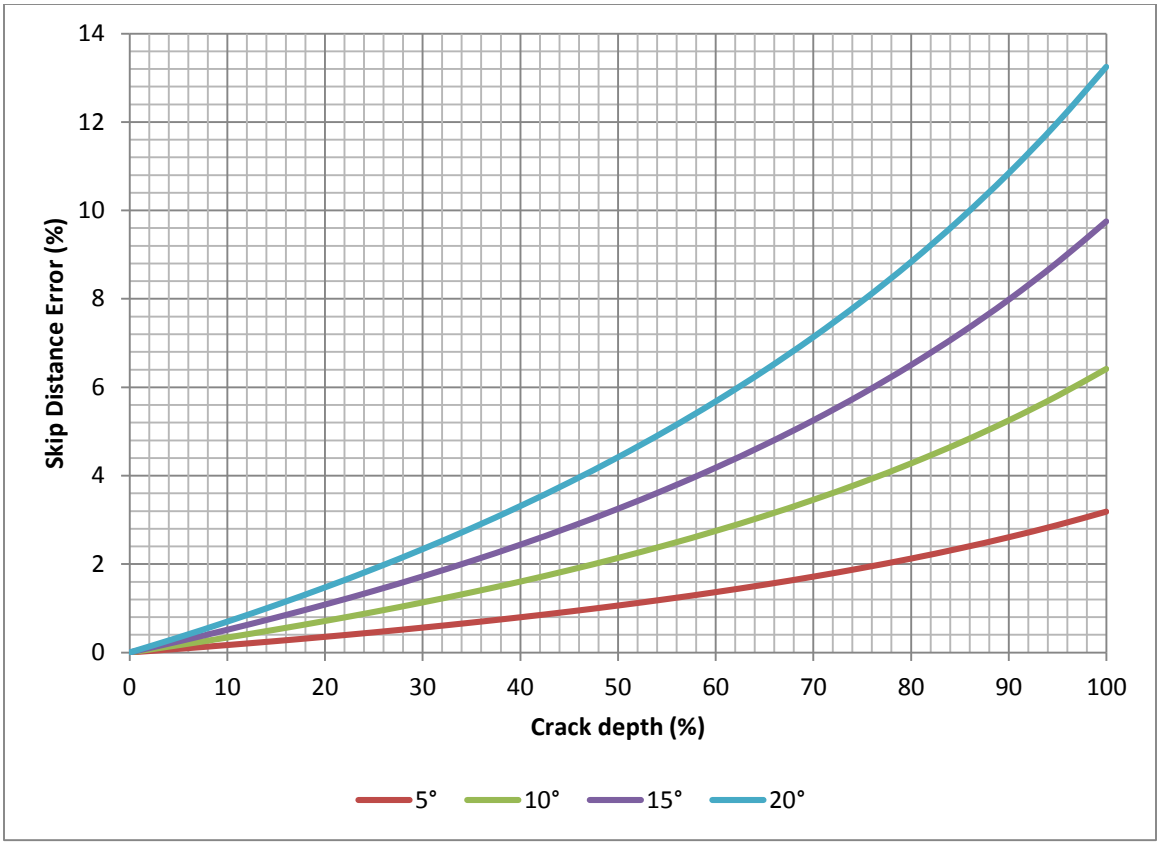

Figure 4.20: Crack depth (%) vs. Error (%) for different crack inclinations (γ)

As can be seen from Figure 4.20, as the angle of inclination of the crack increases, so does the eccentricity of the action and reaction forces. This second order effect accelerates the crack growth as the bending of the crack location becomes important. However, this chart assumes that the angle of inclination of the crack is normal to the wall. The graph in Figure 4.21 illustrates the error induced in the skip distance by different crack inclinations.

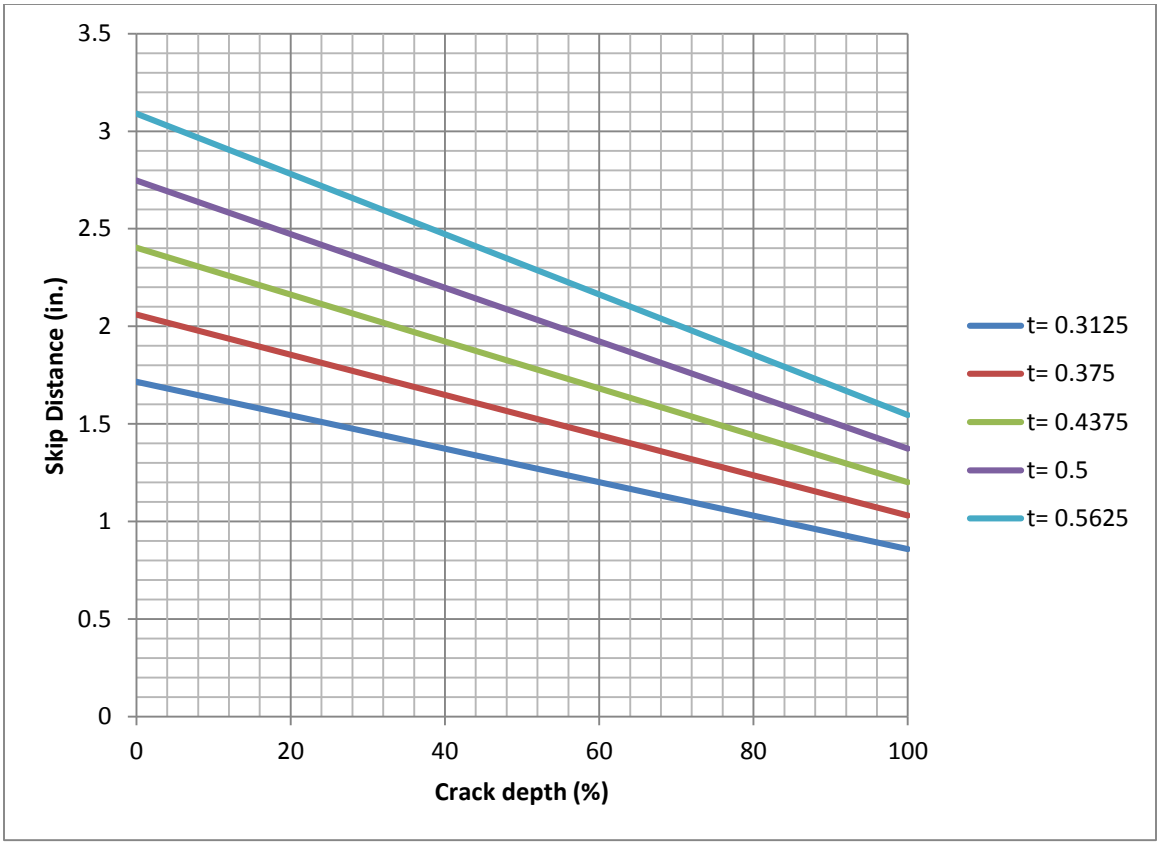

Figure 4.21: Crack depth (%) vs. measured skip distance for different thicknesses - 70^0 probe

The determination of the fatigue crack inclination is a factor that affects the estimation of the remaining fatigue life of the particular structure. As a result, the need of a useful tool that will help in-field measurements of crack depth and inclination is important. In Figure 4.22, it is assumed the crack initiates at the toe of the weld. The two independent variables (φ and x) can only be found if two measurements are taken in-field. The skip distance is automatically calculated by the Ultrasonic Testing equipment and as a result the crack depth can be determined as shown in Figure 4.21. In order to determine the crack inclination, the difference between the skip distance and the distance of the transducer to the toe of the weld needs to be measured. Note that the best testing procedure

is to start testing with the transducer at the minimum skip distance (assuming maximum crack depth) moving it backwards. Measurements have to be made at the location where the first reflection is obtained while moving backwards. As a result, the error is given by the following equation:

	$\Delta e = x \cdot tan\varphi$	Eq. 4-2

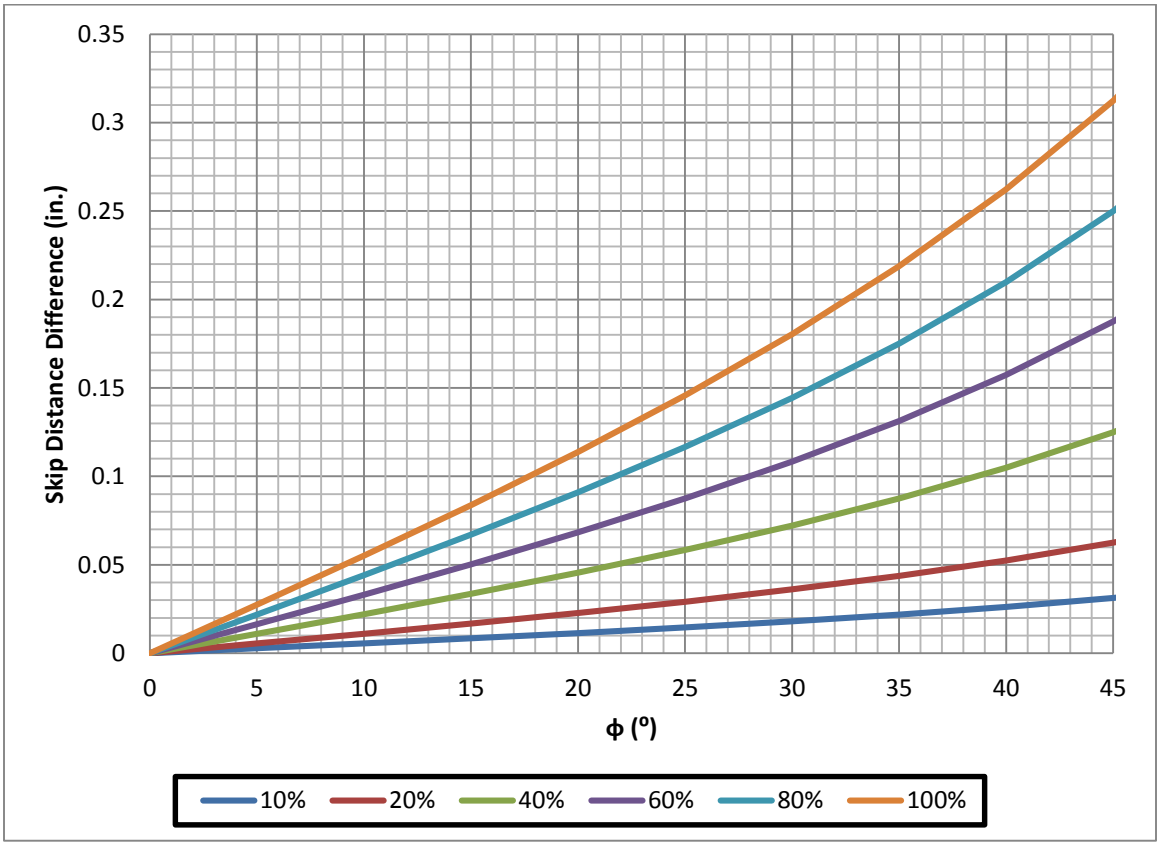

Figure 4.22: Skip Distance Error vs. angle of inclination of crack (t=5/16")

4.5 Destructive testing

During the destructive testing conducted in this phase, all bends were saw-cut from edge to edge of the crack. The locations were indicated by the Ultrasonic Testing procedure

and the pole was subsequently cut at the location were UT indicated that the crack was starting. As some areas of the cross-section did not have fatigue cracks, in some cases the piece of the shaft had to be torn out. As it can be seen in Figure 4.23, at bend #4 the UT didn't perform well in indicating where the crack ended. The reason for the non-agreement is likely due to two main reasons:

1. The location of the crack within the cross-section. The crack was located at a bend with a longitudinal weld seam. As a result, the UT transducer was not able to be placed at the bend, thereby leading to bad readings.

2. The ultrasonic beam spreads as it propagates through the material. This may be the reason of reflections (cracks or defects) coming from lateral sides of the UT target. As a result, difficult or wrong interpretation of the received signals can occur.

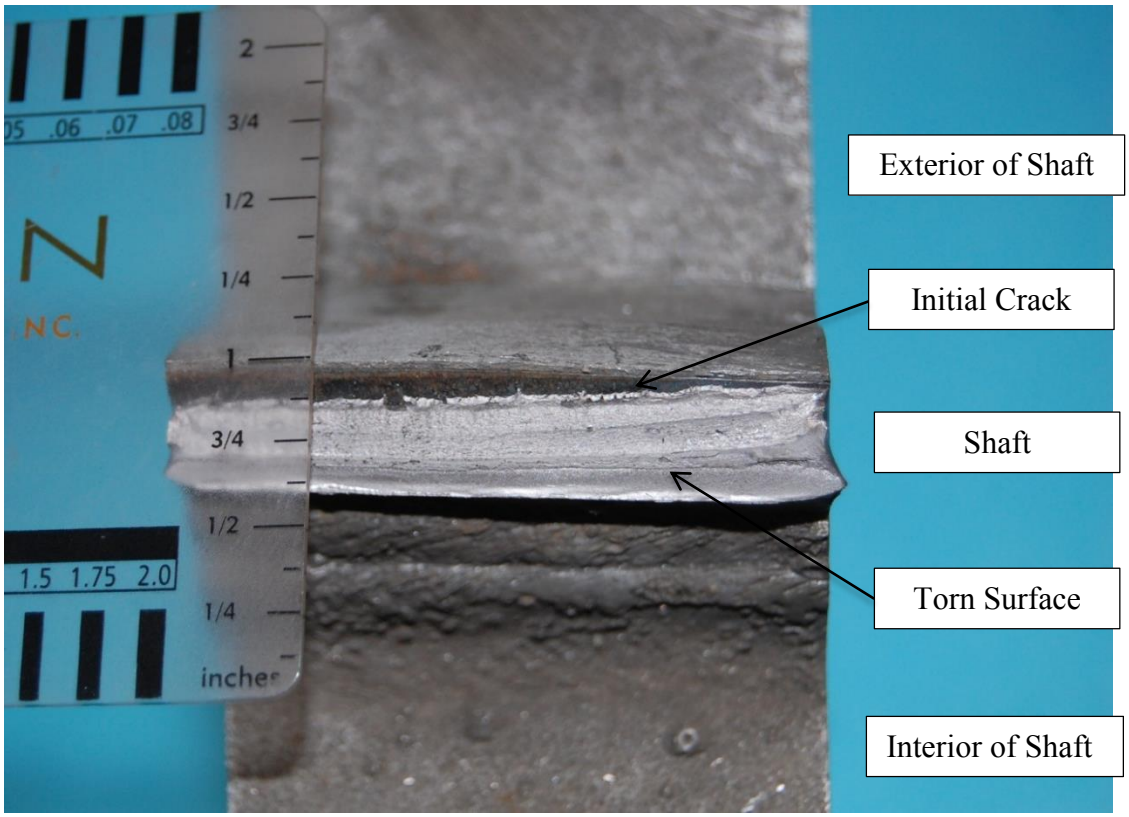

Figure 4.23: Close up of crack at Bend 4

From various crack locations that were opened during the destructive testing the cross-section could be categorized into 4 distinct groups. The first, as seen in Figure 4.24, is the darker area of the cross-section, probably created during the galvanizing process due to the higher concentration of Zn as proven by Scanning Electron Microscope (SEM) images. The second and third areas appear similar, but the difference in their roughness led the researchers to conclude that they are fatigue cracks potentially at different stress range levels, with rougher surface meaning higher stress level. Finally, the fourth area is observed, roughest and caused by the tearing of the cross-section for better inspection.

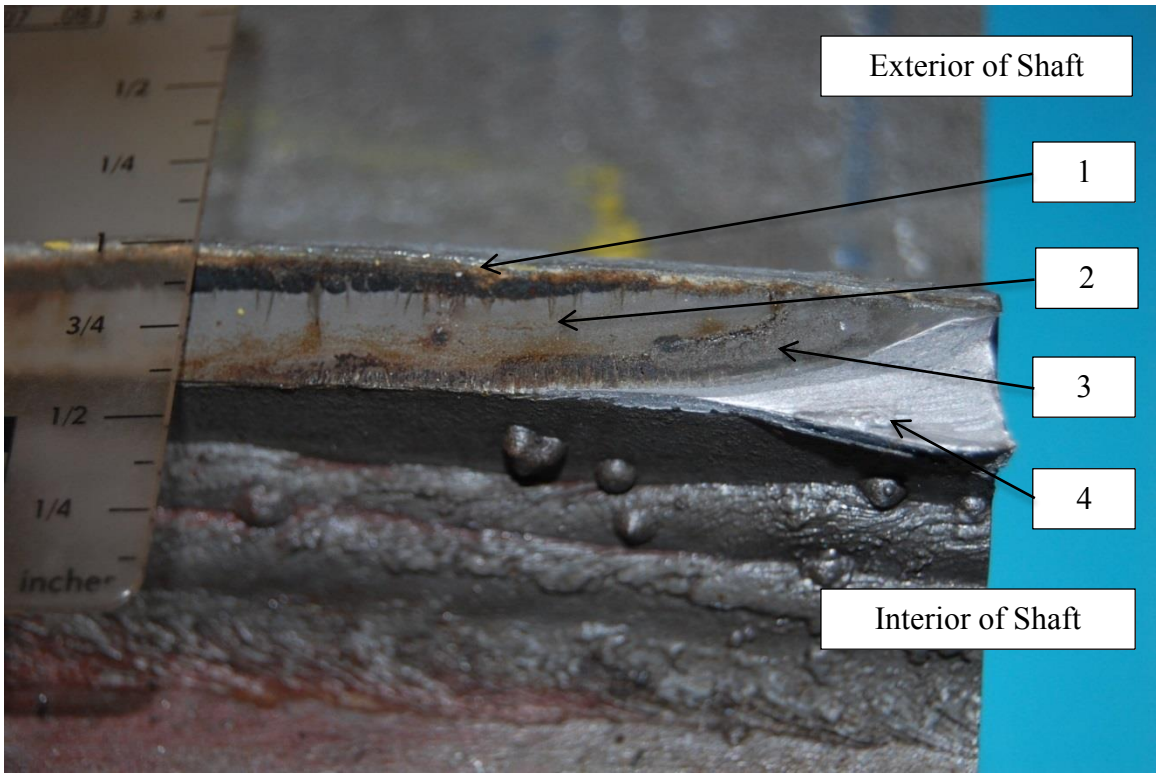

Figure 4.24: Close up of crack at Bend 12

Figure 4.25, Figure 4.26 and Figure 4.27 show the same crack from different perspectives. From a bare eye view to an elemental view, it can be seen that the outer region has a higher concentration in zinc as evidenced by the shiny surface. This shiny surface supports the conclusion that the crack was likely created during galvanization when the molten zinc could flow into the crack. Figure 4.27 is an image of a portion of the crack depth as seen from an electron microscope. The portion is approximately 20% of the cross-section of the exterior portion of the crack. The assumption that the crack might be created during the galvanization process is further confirmed by the higher concentration of zinc in the exterior surface of the crack, and the dominant presence of ferrous elements deeper in the crack cross-section.

Figure 4.25: Close up of crack at Bend 8

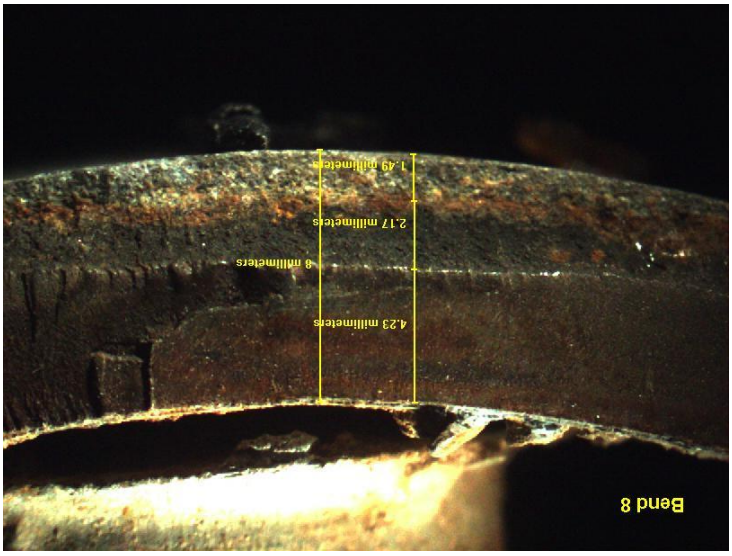

Figure 4.26: Stereoscope image of crack at Bend 8

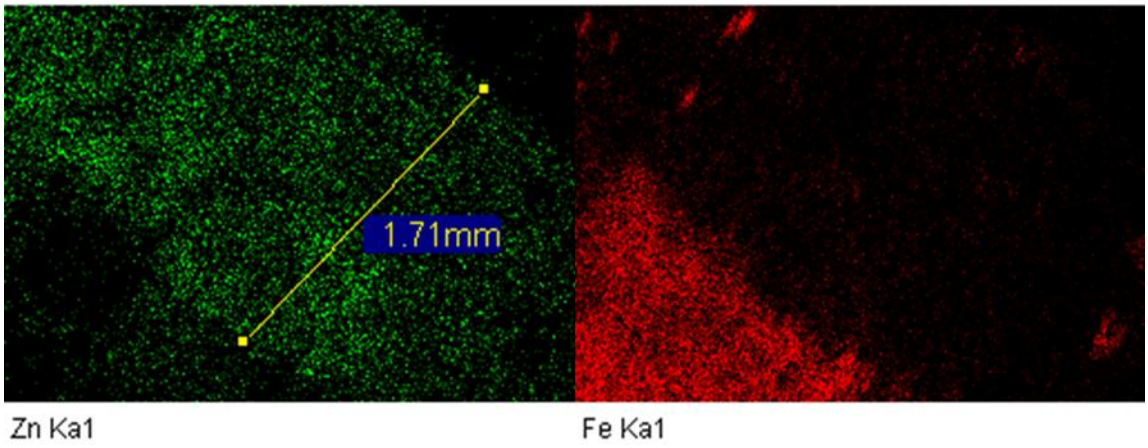

Figure 4.27: Scanning Electron Microscope (SEM) image of outer edge of crack at Bend 8

CHAPTER 5: CONCLUSIONS

5.1 Introduction

This chapter is a summary of the results obtained by the research program described previously. The work presented extends the previous work conducted at The University of Texas on high mast illumination poles and luminaire highway structures. The study discussed in this thesis focused on the evaluation of the remaining fatigue life of damaged high mast illumination poles using laboratory tests. The motivation of the work was to validate methods proposed for estimating the remaining life of HMIPs in-service. Another aspect of the study focused on the evaluation of ultrasonic impact treatment (UIT) on pole repairs. The study made use of ultrasonic tests and magnetic particle testing in evaluating damage in the poles.

5.2 Conclusions

The main outcome of the research is the reasonable agreement of the remaining fatigue life as estimated by the two methods. This can enable the HMIP owners to use results from field monitoring as an aide in making decisions of replacing or repairing damaged HMIPs. Another outcome of this study is that repair with UIT seems to provide an improved fatigue performance of field repairs on the welds between the pole shaft and base plate. Furthermore, during the study, concerns were raised about the localized damage due to the prominent wind directions. Results, showed that such an effect was not observed. On the contrary, all tested areas showed similar fatigue performance in terms of remaining life.

In addition, destructive testing and subsequent scanning in electron microscope (SEM) revealed portions of the cross-section with higher concentrations of zinc, which is

an indication that initial cracking likely occurred during the galvanization process. Lastly, it was observed that the galvanizing thickness in addition to the weld geometry can act be detrimental for crack detection using NDT methods.

5.3 Recommendations and Future Work

In order to produce more reliable fatigue models, fatigue tests of new and in-service poles should be conducted. One of the variables that can yield different results for the remaining fatigue estimates is the constant amplitude fatigue limit (CAFL). Conducting tests in lower stress ranges will provide more insight towards the proper CAFL for HMIP base plate connections.

One potential method of reducing or eliminating cracking in the base plate to shaft connections in the HMIPs may be utilizing localized preheating. The use of pre-heating of the shaft-to-base-plate area or the use of slower dipping speeds may provide a means to minimize the temperature shock this area experiences during galvanizing.

APPENDIX A: REPAIR PROCESS USING ULTRASONIC IMPACT TREATMENT

This section presents thoroughly the process followed to repair the damaged pole. The repair was done by Lamb Star Engineering, LP. The process started with identifying the crack locations with the magnetic particle test and gradually grinding the cross-section until no magnetic evidence of the crack as can be seen in Figure A.1.

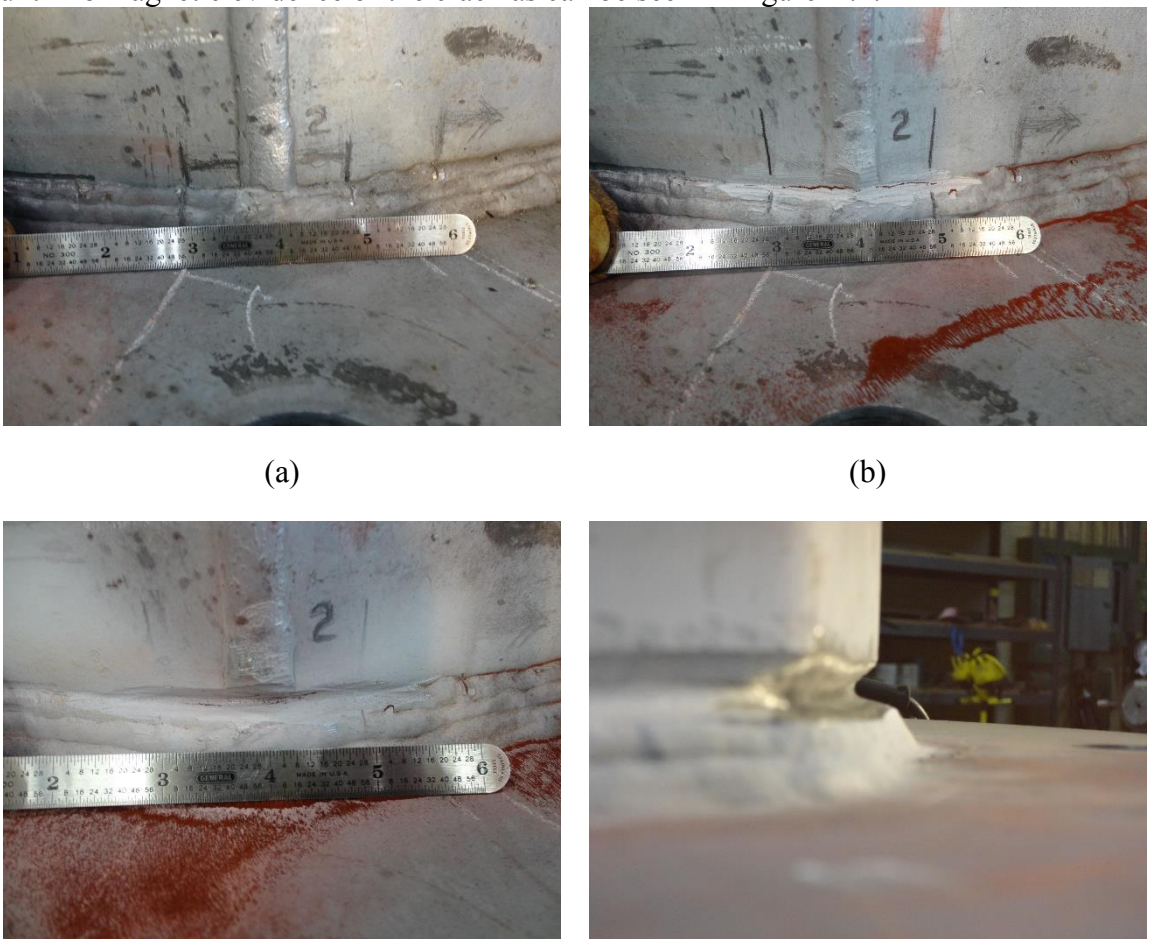

(a) (b)

(c) (d)

Figure A.1: Crack identification and elimination. Identifying the crack (a), grinding the cross-section to expose the crack (b), no magnetic evidence of the crack (c), remaining cross-section (d)

Following this process the groove created, is filled with weld material until the designed geometry is reached. An illustration of the bend after the repair was installed is shown in Figure A.2.

Figure A.2: Bend after the groove was filled

Once the groove was filled, UIT was performed to release the residual stresses at the weld area. The characteristics of the impact treatment for this repair procedure were 26 μm for the amplitude and 27 MHz for the frequency. The procedure and the final result are shown in Figure A.3 and Figure A.4.

Figure A.3: UIT being performed at one bend

Figure A.4: Final result after repair

BIBLIOGRAPHY

AASHTO (2001). Standard Specifications for Structural Supports for Highway Signs, Luminaires and Traffic Signals. Fourth Edition. A. A. o. S. H. a. T. Officials. Washington, D.C.

Anderson, T. H. (2007). Fatigue Life Investigation of Traffic Signal Mast-Arm Connection Details, University of Texas at Austin.

Fasl, J. D. (2013). "Estimating the remaining fatigue life of steel bridges using field measurements."

Kleineck, J. R. (2011). Galvanizing crack formation at base place to shaft welds of high mast illumination poles. Department of Civil Engineering, The University of Texas at Austin. **M.S.**

Magenes, L. (2011). Fatigue assessment of high mast illumination poles using field measurements. Department of Civil Engineering, The University of Texas at Austin. **M.S.**

Miner, M. A. (1945). "Cumulative Damage in Fatigue." Journal of Applied Mechanics **12**(1).

Pool, C. S. (2010). Effect of galvanization on the fatigue strength of high mast illumination poles. Department of Civil Engineering, The University of Texas at Austin. **M.S.**

Rios, C. A. (2007). Fatigue performance of multi-sided high mast illumination towers. Department of Civil Engineering, The University of Texas at Austin. **M.S.**

Stam, A. P. (2009). Fatigue performance of base plate connections used in high mas lighting towers. Department of Civil Engineering, The University of Texas at Austin. **M.S.**

Warpinski, M. K. (2006). "The effect of base connection geometry on the fatigue performance of welded socket connections in multi-sided highmast lighting towers."

VITA

Konstantinos (Kostas) Victor Belivanis was born in Paris, France to Telemachos Belivanis and Gabrielle Georgette Victorine Jeanne Couderc. After graduating from the 3rd high school of Heraklion, Crete he entered the Civil Engineering School of the Aristotle University of Thessaloniki (AUTh), Greece. He received his Diploma in Civil Engineering in October 2010. In August 2011, he entered the Graduate Program of the Cockrell College of Engineering at The University of Texas at Austin to pursue a Master's degree. Upon completion, Kostas will be pursuing his PhD at The University of Texas at Austin conducting research on the behavior and performance of steel-laminated elastomeric bearings.

E-mail: kbelivanis@gmail.com

This thesis as typed by the author.